

Fatigue assessment of offshore tubular structures

Using Dirlik's method to establish the procedure

Pankaj Dheer

Technische Universiteit Delft



Specialization: Transport Engineering and Logistics

Report number: 2017.TEL.8121

Title: **Using Dirlik's method to establish
the procedure for fatigue
assessment of offshore tubular
structures**

Author: P.A. Dheer

Title (in Dutch) De methode van Dirlik gebruiken om de procedure vast te stellen voor het meten van vermoeidheid van offshore buisstructuren.

Assignment: Master thesis

Confidential: Yes

Initiator (university): Dr. Ir. D.L. Schott

Initiator (company): Dr. Ir. Yanrong Yu (Allseas Engineering B.V., Delft)

Chair: Dr. Ir. D.L. Schott

Daily Supervisor: Dr. Ir. X.L. Jiang

Date: November 27, 2017

This report consists of 75 pages and 5 appendices. It may only be reproduced literally and as a whole. For commercial purposes only with written authorization of Delft University of Technology. Requests for consult are only taken into consideration under the condition that the applicant denies all legal rights on liabilities concerning the contents of the advice.

Mekelweg 2
2628 CD Delft
the Netherlands
Phone +31 (0)15-2782889
Fax +31 (0)15-2781397
www.mtt.tudelft.nl

Student:	P.A. Dheer	Assignment type:	Master thesis
Supervisor (TUD):	Dr. Ir. Xiaoli Jiang (TU Delft)	Creditpoints (EC):	35
Supervisor (Company):	Dr. Ir. Yanrong Yu (Company)	Specialization:	TEL
		Report number:	2017.TEL.8121
		Confidential:	Yes
			Indefinite period

Subject: Using Dirlik's method to establish the procedure for fatigue assessment of offshore tubular structures

Structural analysis in frequency domain is preferred over conventional time domain when loads are random in nature, for example, loads due to wind, waves and earthquakes. Computational time involved for frequency analysis is less when compared to equivalent time analysis for larger models and higher periods. Frequency analysis coupled with Dirlik's counting method can offer engineers faster and reliable fatigue damage results. With this in mind, this research is focused on conducting a feasibility study on the application in tubular structures.

Dirlik's method has already been proven to calculate fatigue damage values with good accuracy, compared to rainflow counting algorithm for various structures. With this research, an attempt is made to implement it for tubular structures.

The main objective of the research is to conduct a feasibility study on implementing Dirlik's method to calculate fatigue damage on simple models.

Chair,

Dr. Ir. D.L. Schott

FATIGUE ASSESSMENT OF OFFSHORE TUBULAR STRUCTURES

USING DIRLIK'S METHOD TO ESTABLISH THE PROCEDURE

by

Pankaj Dheer

Master of Science

in Mechanical Engineering

at the Delft University of Technology.

to be defended publicly on , 27th November 2017 at 13:00.

Student number: 4518527
Report Number: 2017.TEL.8121
Project duration: February 6, 2017 – November 27, 2017
Chair: Dr. Ir. D. L. Schott
Thesis committee: Dr. Ir. X. L. Jiang, TU Delft (Daily supervisor)
Dr. Ir. J. M. G. Coenen, TU Delft
Dr. Ir. Y. Yu, Allseas Engineering (Company supervisor)
Dr. Ir. N. Ermolaeva, Allseas Engineering

This thesis is confidential and cannot be made public

CONTENTS

Summary	vii
Summary (In Dutch)	x
Acknowledgement	xi
List of Figures	xiii
List of Tables	xvii
List of Symbols & Acronyms	xx
1 Introduction	1
1.1 <i>Pioneering Spirit</i>	1
1.2 Allseas pipelaying approach	2
1.3 Research Objective	3
1.4 Main Research Question	5
1.5 Methodology	5
1.6 Limitation.	5
2 Fatigue Assessment	7
2.1 Fatigue assessments methods.	7
2.2 Fatigue assessment for Tubular structures	9
2.3 Fatigue assessment according to DNVGL	10
2.3.1 Simple joints.	10
2.3.2 Complex joints.	13
2.4 Fatigue assessment of Solitaire's stinger.	15
2.5 Conclusion	16
3 Proposed Frequency Analysis	19
3.1 Frequency domain analysis	19
3.1.1 Power Spectral Density.	20
3.1.2 Modal frequency response analysis	21
3.1.3 Inputs for the analysis	22
3.2 Fatigue estimation using PSD	25
3.2.1 Time domain fatigue estimation	25
3.2.2 Frequency domain fatigue estimation	25
3.2.3 Counting methods for frequency domain	26

3.3	Dirlik's approach to estimate damage	28
3.4	Conclusion	29
4	Theoretical verification - Frequency analysis	31
4.1	Simple models for verifying application of PSD	32
4.1.1	Cantilever beam with mass attached at free end	33
4.1.2	Cantilever beam model with Single PSD	34
4.1.3	Cantilever beam model with Two PSD	35
4.2	Analysis of verification models	36
4.2.1	Cantilever beam with mass attached at free end	36
4.2.2	Cantilever beam model with Single PSD	37
4.2.3	Cantilever beam model with Two PSD	39
4.3	Results of the verification models	39
4.3.1	Cantilever beam with mass attached at free end	39
4.3.2	Cantilever beam model with single PSD	40
4.3.3	Cantilever beam model with two PSD's	41
4.4	Conclusion	42
5	Damage calculation - Results	43
5.1	Cantilever beam model	44
5.1.1	Application of a Single load	44
5.1.2	Application of two PSD	50
5.2	Frame model	52
5.2.1	Application of single PSD	54
5.3	Detailed analysis of Frame Model	56
5.3.1	Fixed Beam	57
5.3.2	Increasing analysis time	62
5.3.3	Cantilever frame model	64
5.4	Conclusion	67
6	Conclusion and Recommendations	69
	Bibliography	73
A	Research Paper	77
B	Research Flowcharts	87
B.1	Detail research flow	88

C Additional theory	91
C.1 Vibration due to Base excitation	91
C.2 Random process	92
C.3 Fast Fourier Transform	92
C.4 Cross power spectral density	94
D Matlab codes	95
D.1 Dynamic response of SDOF model	95
D.2 Dynamic response of MDOF model.	96
D.3 Time domain to Power spectral density and Cross spectral density	99
D.4 Calculation of SCF and hot spot stress PSD for simple tubular joint.	104
D.5 Dirlik's approach to calculate stress range.	107
E Additional results	111
E.1 Example to calculate stress ranges using Dirlik's method	111
E.2 J-Rain verification.	113
E.3 Additional results for verification models	116
E.4 Additional results of complete analysis	120

SUMMARY

Fatigue assessment for offshore structures has always been important owing to the nature of dynamic loading due to waves and wind. To effectively quantify fatigue damage and design fatigue resistant structures, industrial standards developed by International Association of Classification Societies (IACS) are used all across the world. Two of the classification societies 'Det Norske Veritas' and 'Germanischer Lloyd SE' collaborated together in 2013 to form 'DNV GL AS' [1] which provides recommendations for designing and manufacturing ships and related offshore structures. **Allseas** has been designing ships and offshore structures for a long time and has gained enough experience in fatigue design using the recommendations provided by 'DNV GL AS'. However, with the design of their newest vessel, the *Pioneering Spirit*, they have encountered an additional load case due to the vessel's unique design. The vessel has a cut-out to help it straddle an entire topside in a single operation, but due to its design, the vessel now has two individual bows. The gap between the two bows also accommodates the 'stinger', which helps in laying pipes on the sea bed. The movement of the two bows during operation of the vessel will induce an additional load on any structure fixed in-between them. In this research, we will be considering the dynamic effect of the bows on fatigue damage of stinger. The detail description of the problem along with the research objective is explained in Chapter 1.

The stinger guides the pipes coming out of the vessel onto the sea bed providing support and keeping the strain in the pipes within acceptable limits. Considering the importance of the stinger for pipelaying activities, it is important to consider the additional increase in damage due to the movements of the bows. To quantify the fatigue damage in the tubular joints of the stinger, it is decided to implement Dirlik's method with frequency analysis. Dirlik's method with frequency analysis is computationally faster than equivalent time domain analysis for larger models. Dirlik's method is already proven to achieve comparable fatigue damage results compared to rainflow counting method [2–4]. With these advantages, frequency analysis with Dirlik's method offers engineers an approximate fatigue damage value in the early stages of structural analysis, which can be very helpful in optimizing the overall design.

For fatigue damage calculation, two important factors should be calculated, number of cycles and stress range. This is achieved by a suitable stress cycle counting algorithm for example, the well-established rainflow counting method for time based dynamic analysis. For frequency based analysis, Dirlik gives an effective semi-empirical method to calculate the probability density function of stress range from the dynamic response power spectral density of structure. Chapter 3 explains the basic principles of structure analysis in frequency domain, its advantage and how Dirlik's method can be implemented. Verification of frequency analysis on assumed simple models are done by conducting equivalent time domain analysis and comparing the fatigue damage values calculated from both the analyses. Assuming time domain analysis as the basis of reference, the percentage error in the fatigue damage value calculated using frequency analysis with Dirlik's method is compared for periodic and random loads. For one of the models, good comparison of fatigue damage values are achieved, but similar results could not be achieved for the second model. Detailed analysis on the second model is conducted to pinpoint the major causes for the difference in the damage values.

The research begins with explaining the need and objective of the research, discussed in Chapter 1 and the current state of the art is studied in Chapter 2. The author then proposes and explains in detail the frequency analysis with Dirlik's method in Chapter 3 and introduces the verification models in Chapter 4. In Chapter 5, a complete analysis of verification models is conducted and fatigue damage results are compared with equivalent time domain analysis. The conclusion and future recommendation of the research are discussed in Chapter 6.

Pankaj Dheer
Delft, November 2017

SUMMARY (IN DUTCH)

De taxatie van de vermoeiing van offshore constructies is altijd belangrijk geweest vanwege de natuur van de dynamische krachten van wind en golven. Om effectief de vermoeiingsbeschadiging te bepalen en vermoeiingsresistente constructies te ontwerpen worden industriële standaarden van de International Association of Classification (IACS) over de hele wereld gebruikt. Twee van de classificatie organisaties 'Det Norske Veritas' en 'Germanischer Lloyd SE' werkten samen bij de vorming van 'DNV GLAS' [1] dat aanbevelingen aandroeg voor het ontwerpen en vervaardigen van schepen en andere gerelateerde offshore constructies. **Allseas** ontwerpt al een lange tijd schepen en offshore constructies en heeft al veel ervaring opgedaan met vermoeiingsdesign door gebruik te maken van de aanbevelingen aangedragen door 'DNV GLAS'. Echter, met het ontwerp van hun nieuwste schip, de *Pioneering Spirit* komen ze in aanraking met een extra belasting vanwege het unieke ontwerp van het schip. Het schip heeft een uitsparing om de hele bovenzijde in één bewerking te overbruggen, maar dankzij het ontwerp heeft het schip nu twee afzonderlijke bogen. De opening tussen de twee bogen bevat ook de 'stinger' die helpt bij het leggen van pijpen op de zeebodem. De beweging van de twee bogen tijdens het actief zijn van het schip zal een extra belasting veroorzaken op elke constructie die daartussen is bevestigd. In het onderzoek wordt het dynamisch effect van de bogen op de vermoeiingsschade van de stinger beschouwd. De gedetailleerde omschrijving van het probleem wordt samen met het onderzoeksdoel beschreven in Hoofdstuk 1.

De Stinger geleidt de pijpen die uit het schip komen tot op de zeebodem, zorgt voor ondersteuning en houdt de spanning in de pijpen binnen aanvaardbare grenzen. Gezien het belang van de stinger voor pijplegactiviteiten, is het belangrijk om rekening te houden met de extra toename van schade als gevolg van de bewegingen van de bogen. Om de vermoeiingsschade in de buisvormige koppelingen van de stinger te kwantificeren, is besloten de Dirlik's-methode te implementeren met frequentieanalyse. De Dirlik's methode met frequentieanalyse is wat betreft rekentijd sneller dan equivalente tijdsdomein analyses voor grotere modellen. Vergeleken met de Rainflow Cutting methode heeft de Dirlik's methode al vergelijkbare resultaten opgeleverd voor vermoeiingsschade berekeningen [2-4]. Met deze voordelen biedt frequentieanalyse met de Dirlik's methode, engineers al een geschatte waarde voor vermoeidheidsschade in de vroege stadia van de constructieanalyse, wat zeer nuttig kan zijn bij het optimaliseren van het totale ontwerp.

Voor de berekening van de vermoeidheidsschade moeten twee belangrijke factoren worden berekend: het aantal cycli en de spanningsrange. Dit wordt bereikt door een geschikt algoritme voor het tellen van stresscycli, bijvoorbeeld de goed bekende Rainflow Counting methode voor de op tijd gebaseerde dynamische analyse. Voor de op frequentie gebaseerde analyse geeft Dirlik een effectieve semi-empirische methode voor het berekenen van de kansdichtheidsfunctie van de spanningsrange van de dynamische spectrale krachtdichtheid van de constructie. Hoofdstuk 3 legt de basisprincipes uit van structuuranalyse in frequentiedomein, het voordeel ervan en hoe Dirlik's methode kan worden geïmplementeerd. Verificatie van frequentieanalyse op eenvoudig veronderstelde modellen wordt uitgevoerd door het uitvoeren van een equivalente tijddomeinanalyse en het vergelijken van de waarden voor de schade door vermoeiing die zijn berekend uit beide analyses. Uitgaande van tijdsdomeinanalyse als de referentie, wordt de procentuele fout in de waarde van de vermoeiingsschade berekend met behulp van frequentieanalyse met de methode van Dirlik voor periodieke en willekeurige belastingen. Voor een van de modellen is een goede vergelijking van de waarden van de vermoeiingsleeftijd bereikt, maar voor het tweede model konden vergelijkbare resultaten niet worden bereikt. Gedetailleerde analyse van het tweede model wordt uitgevoerd om de belangrijkste oorzaken voor het verschil in de waarden voor de vermoeiingsschade aan te wijzen.

Het onderzoek begint met het uitleggen van de noodzaak en het doel van het onderzoek, besproken in hoofdstuk 1. De huidige stand van de techniek wordt bestudeerd in hoofdstuk 2. De auteur stelt vervolgens in detail de frequentieanalyse voor met de Dirlik's methode in hoofdstuk 3 en introduceert de verificatiemodellen in hoofdstuk 4. In hoofdstuk 5 wordt een volledige analyse van verificatiemodellen uitgevoerd en resultaten van

de schade door vermoeiing worden vergeleken met een vergelijkbare analyse in het tijdsdomein. De conclusies van het onderzoek en de aanbevelingen voor de toekomst worden besproken in hoofdstuk 6.

Pankaj Dheer
Delft, November 2017

ACKNOWLEDGEMENT

I would first like to thank my thesis advisor, Dr. Xiaoli Jiang and my chair, Dr. Dingena Schott, of the Faculty of Mechanical, Maritime and Materials at Delft University of Technology. The doors to their offices were always open whenever I had troubles or had a question about my research or writing. They consistently allowed this research to be my own work, but steered me in the right direction whenever they thought I needed.

I would also like to thank Dr. Yanrong Yu and Dr. Natalia Ermolaeva who were involved in the research and provide their assistance. Without their passionate participation and input, the research could not have been successfully conducted. I would also like to thank Allseas Engineering B.V in providing the opportunity for me to work on this research.

I would also thank Delft university of technology for the opportunity to attain my Masters. Finally, I must express my very profound gratitude to my parents and my friends for providing me with unfailing support and continuous encouragement throughout my years of study and through the process of researching and writing this thesis. This accomplishment would not have been possible without them.

LIST OF FIGURES

1.1	The <i>Pioneering Spirit</i> [7]	1
1.2	S-lay method [9]	2
1.3	Wave motion [10]	3
1.4	Motion of vessel in sea [11]	3
1.5	Stinger position during pipelaying [8]	4
2.1	Approaches of description of fatigue strength and life [13]	7
2.2	A typical tubular joint [22]	9
2.3	Types of simple joints [22]	10
2.4	Types of loads on tubular joints [22]	11
2.5	Superposition of stresses [1]	11
2.6	Formulae to calculate hot spot stresses [1]	12
2.7	T-curve for tubular joints [1]	12
2.8	Hot spot stress of Multi-planar joint [1]	13
2.9	Linear extrapolation method [1]	14
2.10	Second order polynomial extrapolation method [1]	15
2.11	Fatigue assessment of <i>Solitaire's</i> stinger	16
3.1	Different types of engineering time histories and PSD [24]	21
3.2	Output Frequencies	24
3.3	Additional control on frequency range	24
3.4	Typical time domain fatigue life estimation process [24]	25
3.5	Typical frequency domain fatigue life estimation process [24]	25
4.1	Stinger beam model 2D view [35]	31
4.2	Stinger beam model 3D view [35]	32
4.3	Single degree of freedom model	33
4.4	Inputs for SDOF model	34
4.5	Cantilever beam model with single PSD	34
4.6	Inputs for cantilever beam model with single PSD	35
4.7	Cantilever beam model with two PSD	35
4.8	Inputs for cantilever model with two PSDs	36
4.9	FEMAP SDOF model	37
4.10	FEMAP cantilever beam model	38

4.11 Modal Analysis	40
4.12 Displacement response PSD for sub-case 1 - Single PSD	41
4.13 Displacement response PSD for sub-case 1 - Two PSD	42
5.1 Fatigue damage calculation of cantilever beam - Time domain analysis	43
5.2 Fatigue damage calculation of cantilever beam - Frequency domain analysis	43
5.3 Cantilever beam model	44
5.4 Input acceleration load – Single frequency periodic load	46
5.5 Bending moment PSD – Single frequency periodic load	46
5.6 Bending moment PSD comparison	46
5.7 Bending stress PSD – Single frequency periodic load	47
5.8 Input acceleration load – Standard Deviation = 0.333	48
5.9 Bending moment PSD – Standard Deviation = 0.333	49
5.10 Bending stress PSD – Standard Deviation = 0.333	49
5.11 Input loads for 2 PSDs - Random loads 1	50
5.12 Input loads for 2 PSDs - Random loads 2	51
5.13 Bending moment PSD comparison - 2 PSD (Random loads)	51
5.14 Bending stress PSD comparison - 2 PSD (Random loads)	51
5.15 Frame model	53
5.16 Results of modal analysis of frame	53
5.17 Single sine load on the frame model	54
5.18 Input periodic load	54
5.19 Bending moment PSD comparison - Single sine load	55
5.20 Bending moment - Single sine load - Frame model	56
5.21 Bending moment - Single sine load - Cantilever beam	56
5.22 Single sine load on the fixed beam	57
5.23 Modal analysis on fixed beam	57
5.24 Input sine load for fixed beam	58
5.25 Bending moment - Single sine load - Fixed beam	58
5.26 Bending moment-Single sine load with trend-line - Frame model	59
5.27 Bending moment-Single sine load with trend-line - Fixed beam	59
5.28 Bending moment-Single sine load with new X-axis - Frame model	59
5.29 Bending moment-Single sine load with new X-axis - Fixed beam	60
5.30 Input PSD loads	60
5.31 Bending moment result comparison - Frame model	61
5.32 Bending moment result comparison - Fixed beam	61
5.33 Input periodic load (120 seconds) - Frame model	62
5.34 Input periodic load (120 seconds) - Fixed beam	63

5.35 Bending moment result comparison (120 seconds) - Frame model	63
5.36 Bending moment result comparison (120 seconds) - Fixed beam	63
5.37 Cantilever frame model	64
5.38 Modal analysis for cantilever frame model	65
5.39 Input loads for cantilever frame model	65
5.40 Cross power spectral density input	66
5.41 Bending moment result comparison - Cantilever frame	66
B.1 Overview of Fatigue analysis of stinger	88
B.2 Research flow - Part 1	89
B.3 Research flow - Part 2	90
C.1 Mass with spring-damper system [46]	91
C.2 Dividing a single signal into two [47]	93
C.3 Process of calculating Cross spectral density function	94
C.4 Six cross spectral density for four time series input	94
E.1 Assumed hot spot stress PSD	111
E.2 Probability density function versus Stress range	113
E.3 Graphical User interface of J-Rain [50]	113
E.4 Assumed stress cycle for J-Rain verification	114
E.5 Filtered stress cycle for J-Rain verification	114
E.6 Stress range calculation starting from peak	115
E.7 Stress range calculation starting from valley	115
E.8 Input load for Sub-case 2-Single PSD	117
E.9 Modal analysis - Sub case 3	117
E.10 Displacement response PSD for sub-case 2 - Single PSD	118
E.11 Displacement response PSD for sub-case 3 - Single PSD	118
E.12 Input load for Sub-case 2-Two PSD	119
E.13 Displacement response PSD for sub-case 2 - Two PSD	119
E.14 Displacement response PSD for sub-case 3 - Two PSD	120
E.15 Input acceleration load – Three frequency periodic load	120
E.16 Bending moment PSD – Three frequency periodic load	121
E.17 Bending stress PSD – Three frequency periodic load	121
E.18 Input acceleration load – Standard Deviation = 1	121
E.19 Bending moment PSD – Standard Deviation = 1	122
E.20 Bending stress PSD – Standard Deviation = 1	122
E.21 Input loads for analysis - PSD (Periodic) - 1	122
E.22 Input loads for analysis - PSD (Periodic) - 2	123

E.23 Input loads for analysis - PSD (Periodic) with phase difference	123
E.24 Bending moment PSD comparison - 2 PSD (Periodic)	124
E.25 Bending stress PSD comparison - 2 PSD (Periodic)	124
E.26 Bending moment PSD comparison - 2 PSD (Periodic) with phase difference	124
E.27 Bending stress PSD comparison - 2 PSD (Periodic) with phase difference	125
E.28 Input random load - Frame model	125
E.29 Bending moment PSD comparison - Single random load - Frame model	125
E.30 Bending moment results - Frame model	126
E.31 Input loads - Fixed beam	126
E.32 Bending moment results - Fixed beam	127
E.33 Input loads (3rd mode) - Cantilever frame model	127
E.34 Input loads (7th mode) - Cantilever frame model	127
E.35 Input Cross power spectral density - Cantilever frame model	128
E.36 Output bending moment PSD comparison (3rd mode) - Cantilever frame model	128
E.37 Output bending moment PSD comparison (7th mode) - Cantilever frame model	128

LIST OF TABLES

1.1	Stinger dimensions and features	2
4.1	Material Properties for all the models	33
4.2	Details of SDOF model	33
4.3	Details of MDOF model	35
4.4	Output results of SDOF system	40
4.5	Comparison of Modal analysis for single PSD	40
4.6	Comparison of maximum displacement response PSD - Single PSD	41
4.7	Comparison of maximum displacement response PSD - Two PSD	42
5.1	Basquin constant values for models	44
5.2	Natural frequencies of the model	45
5.3	Bending moment PSD (Periodic load) - Area calculation	47
5.4	Damage calculation – Periodic loads	48
5.5	Bending moment PSD (Random loads) - Area calculation	49
5.6	Damage calculation – Random loads	49
5.7	Bending moment PSD (Two loads) - Area calculation	52
5.8	Damage calculation – 2 PSD	52
5.9	Geometrical dimensions for frame model	53
5.10	Bending moment PSD (Single load) - Area calculation	55
5.11	Bending moment PSD with trend-line (Single sine load) - Area calculation	61
5.12	Damage calculation – Single sine load	62
5.13	Bending moment PSD with trend-line (Single sine load 120 seconds) - Area calculation	64
5.14	Damage calculation (120 seconds) – Single sine load	64
E.1	Dirlik's parameters	112
E.2	Damage fraction calculation	112
E.3	Stress range using hand calculations	115
E.4	Stress range using J-Rain	116
E.5	Results of verification of J-Rain	116
E.6	Details of square cross-section cantilever beam model	116

LIST OF SYMBOLS & ACRONYMS

γ	Bandwidth parameter, function of spectral moments	
∞	Infinity	
ω	Frequency of signal	<i>rad/sec</i>
ϕ	Eigenvector corresponding to mode	
C	Damping matrix of the structure	<i>kg.s/m</i>
D	Displacement vector	<i>meter</i>
E	Young's modulus	<i>N/m²</i>
$E[P]$	Expected number of peaks	
f	Frequency of signal	<i>Hz</i>
F_n	First natural frequency	<i>Hz</i>
G, g	acceleration due to gravity	<i>m/s²</i>
$G(f)$	Output stress power spectral density function	<i>Pa²/Hz</i>
G_{RMS}	Root mean square of acceleration	<i>m/s²</i>
I	Area moment of inertia	<i>m⁴</i>
K	Stiffness matrix of the structure	<i>N/m</i>
L	Length of a cantilever beam	<i>meter</i>
M	Mass matrix of a structure	<i>kg</i>
m_n	n^{th} statistical moment of power spectral density function	
$N(S)$	Number of cycles corresponding to stress range S	
P	Load vector	<i>Newton</i>
$p(S)$	Probability density function of stress range S	
Q	Amplification factor Constant for Dirlik's counting method	
S	Stress range	<i>Pa, MPa</i>
T	Total time	<i>seconds</i>
t	thickness of the brace	<i>meter</i>
t	time	<i>seconds</i>
x_m	Mean frequency, according to Dirlik's method	
Y_{RMS}	Root mean square of displacement	<i>m</i>
Y_{st}	Static deflection of a cantilever beam	<i>meter</i>
Z	Normalized stress range	
z	Independent mode participation factor	
FEM	Finite Element Method	

MFRA	Modal Frequency Response Analysis
PDF	Probability Density Function
PSD	Power Spectral Density
SCF	Stress Concentration Factor
SHF	Stinger Hang-Off
STF	Stinger Transition Frame
TLS	Top-side Lifting System

1

INTRODUCTION

Allseas is a global leader in offshore pipeline installation and sub-sea construction with its head office based in Switzerland. It operates a versatile fleet of specialized heavy-lift, pipeline and support vessels. The company's approach involves supporting their clients early in the conceptualization phase offering them services in the field of project management, engineering and procurement and also provide support with installation and commissioning [5]. The latest vessel developed by the company is called the *Pioneering Spirit*.

1.1. *Pioneering Spirit*

Figure 1.1 shows the aerial view of the vessel with the stinger attached at the front. The vessel is a complete in-house design, with focus on its application for single lift installation, removal of large oil & gas platforms and installation of record weight pipelines [6]. Generally, to perform these two operations, two different types of vessels are required but, due to its unique design *Pioneering Spirit* can complete both jobs efficiently and effectively.



Figure 1.1: The *Pioneering Spirit* [7]

The vessel at the front, has two bows, because of a slot of 122 m long and 59 m wide through which the vessel is able to straddle a platform and install or remove an entire topside. The vessel achieves this by using 16 hydraulic arms mounted on the bows called as the 'Top side lifting system (TLS)'. As a result of this, the vessel significantly reduces the amount of offshore work which is moved to the shore where it is cheaper, safer and more environmental friendly [6]. This slot also serves as the perfect location to mount the stinger and the

'Stinger Transition Frame (STF)', to carry out pipelaying operations when needed. A stinger is a space frame structure which is used to support the pipe as it comes out of the vessel. The stinger is manufactured using hollow circular steel sections welded together to provide rigidity and stiffness. It is supported at four locations on both bows, two are main hinge points and other two are stinger hang-off points as shown in Figure 1.5. Stinger is designed such that its radius can be adjusted depending upon the operating depth allowing it to attain different positions. This change in radius also helps in keeping the strain of the pipes within limits. *Pioneering Spirit* uses S-lay method for pipelaying, this method is explained in Section 1.2. With a S-lay tension capacity of 2000 Tonnes, it is the world's largest pipelaying vessel. The main dimensions and features of the stinger are given below in Table 1.1.

Table 1.1: Stinger dimensions and features

Feature	Value
Total length	145 m
Total length with STF	200 m
Range of radius	110 m – 425 m
Installation range of pipe diameter	6" – 68" (outer diameter)
Top pipe tension capacity	2000 tonnes
Bottom pipe tension capacity	700 tonnes

1.2. ALLSEAS PIPELAYING APPROACH

Pioneering Spirit will be majorly utilized for pipelaying purposes, an estimated 65% of its life will be spent for pipelaying related operations [8]. Stinger is the main equipment which supports the pipeline when it is being installed on the sea bed. There are various lay methods that are used by different companies also the type of lay method has a great influence on the design of the vessel. Allseas have been using the S-lay approach for all their vessels and hence the same is followed for *Pioneering spirit*. S-lay is one of the oldest pipelaying method, it has a faster laying capacity when compared to other methods. Some of the other popular methods are J-lay, Reeling and towing. The S-lay method is discussed below.

S-LAY METHOD

The method has got its name due to the shape that the pipeline forms as it leaves the vessel and touches on the sea bed. Figure 1.2 shows how the pipeline leaves the vessel and is carried by the stinger forming a 'S' shape as it touches on the sea bed.

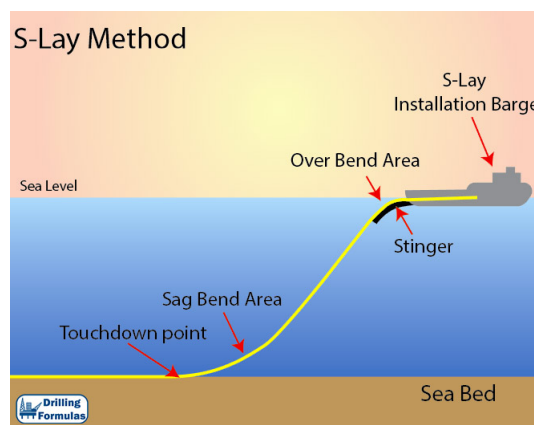


Figure 1.2: S-lay method [9]

The pipes are assembled on a horizontal working plane called as the 'Firing line', on-board the vessel. Pipes are welded together, inspected and then coated at different stations inside the vessel till it moves out and onto the stinger. The stinger supports the pipeline as it moves towards the sea bed, preventing pipe buckling by

providing the support to the pipeline and controlling the curvature of its upper section. The curvature of the lower section is controlled by on-board tensioners which clamps the pipe as it moves onto the sea bed. The amount of tension and stinger length during pipelaying operation, controls the capacity of the S-lay method. The method has following advantages.

Advantages:

1. Installation process is much faster when compared to other methods.
2. The method has good workability over large ranges of water depth.
3. If the stinger radius is adjustable, the same method can be used for shallow to ultra deep water depths.

It is now important to understand the problem which this research will try to solve and decide its main and additional objectives. This is discussed in detail in the next section.

1.3. RESEARCH OBJECTIVE

The motion of the waves is dynamic with alternate crest and trough as seen from Figure 1.3, which causes the vessel to move in six directions with respect of its horizontal and vertical axes. Three of these motions are translation and the other three are rotation as shown in Figures 1.4a and 1.4b respectively.

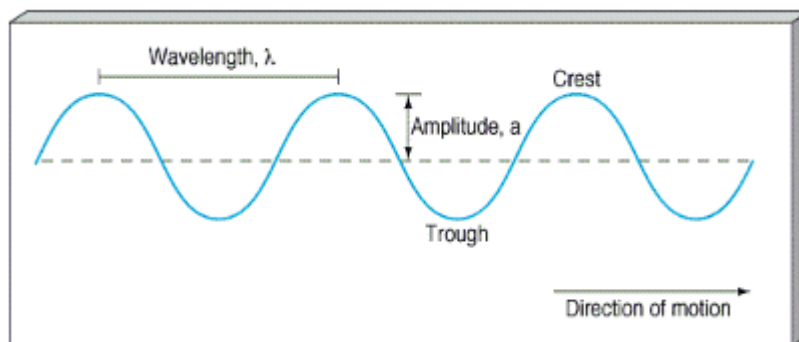
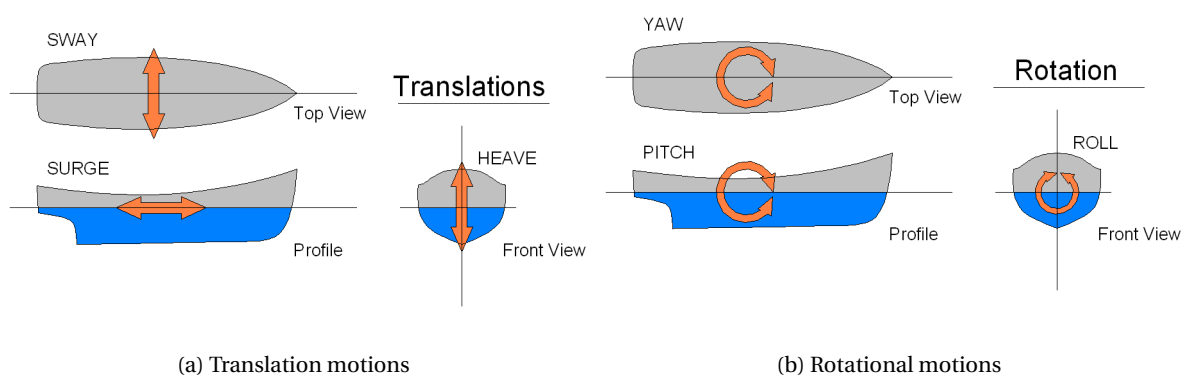


Figure 1.3: Wave motion [10]



(a) Translation motions

(b) Rotational motions

Figure 1.4: Motion of vessel in sea [11]

As the *Pioneering Spirit* has two bows, relative movements between individual bows will occur under different sea conditions (wave height, wave period and wave heading). As the main hinges and supports points of the stinger are connected at the bows, movement of individual bows will cause motion of the stinger during pipelaying operation. This will impart an additional load, called as 'Bow deflection' on the tubular joints of the stinger, leading to increase in fatigue damage. Fatigue damage in tubular joints are also induced various other loads but, the scope of this research is restricted to considering the effect of bow deflection on stinger.

To counter bow deflection effects during sway and roll, the stinger is designed with a swivel connection at the portside hinge. This measure allows a small transverse movement of the stinger during sway and roll motions of the vessel. However, for surge, heave, yaw and pitch motions, the stinger is susceptible to fatigue damage due to bow deflection. Figure 1.5 shows the position of stinger at the bows during pipelaying operations. This image should help in clarifying the problem which will be faced by the stinger during deflection of the bows.

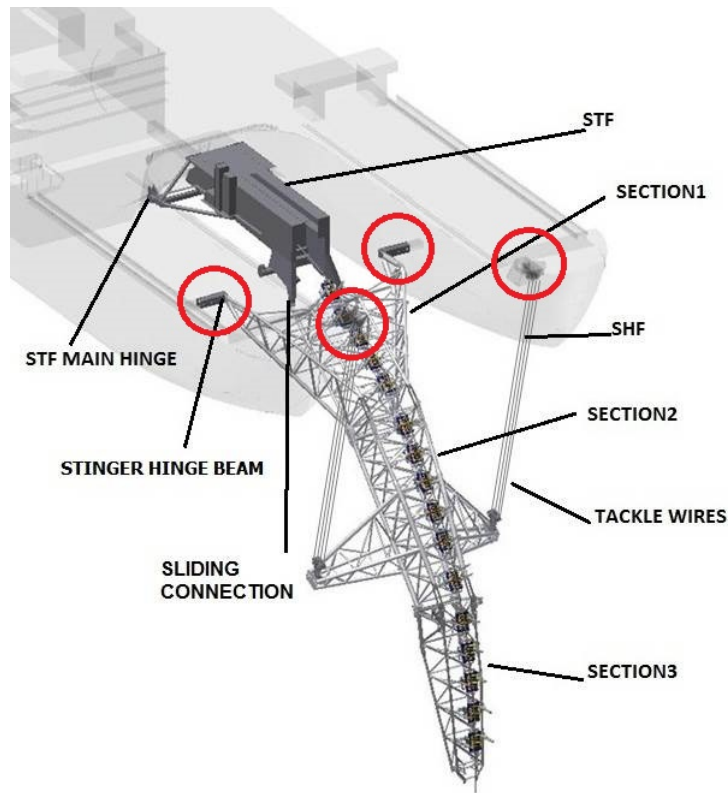


Figure 1.5: Stinger position during pipelaying [8]

In Figure 1.5, we can see the four locations where the stinger is connected with the bows. Two are the main hinge points connected on the inside surface of the bows and the other two are called as the 'Stinger Hang-Off (SHF)' point, connected on the top surface of the bows. In this research, all these four points are termed as 'support points'. It is the movement of these support points during bow deflection, that will induce fatigue damage in the stinger tubular joints. The stinger has five main operational modes namely, Pipelay, Abandonment and Recovery (A&R), Stand-by, Transit and Survival. Fatigue damage has to be calculated considering all operations of the stinger but, based on experience, one can consider 'Pipelay' operation to be the governing load case for bow deflection.

To calculate the fatigue damage, Dirlik's method along with frequency analysis will be implemented in this research, as the method is computationally faster for bigger models and higher time periods [12]. Before the method can be applied to the stinger model, with this research, a feasibility study on the application of frequency analysis with Dirlik's method is verified on simple assumed models. The models chosen are cantilever beam and simple frame models and the verification of the proposed frequency analysis is conducted in two parts. First, the application of loads in FEM (FEMAP) is verified using available literature data. In this part, fatigue damage is neglected and the focus is given to fully understand how input loads are applied in FEM. Second, the overall methodology including fatigue damage results is verified by conducting an equivalent time domain analysis. In this part, fatigue damage results from time analysis (using rainflow counting) and frequency analysis (using Dirlik's method) are compared. For frequency analysis, out of the many available counting methods, Dirlik's method is chosen as its accuracy is comparable with equivalent rainflow counting method [12]. With this information, the main research question is formulated along with additional objective, which are listed in the next section.

1.4. MAIN RESEARCH QUESTION

The main research question is:

Conduct a feasibility study on fatigue damage assessment using Dirlik's method.

In addition to the main objective, with this report following additional objective will also be achieved.

- Incorporating damage calculation using Dirlik's method into the overall procedure of fatigue analysis of the *Pioneering Spirit's* stinger.

To achieve the main and additional objectives, the methodology followed in this research is explained in brief in the next section.

1.5. METHODOLOGY

Structural analysis can be conducted in either time domain or frequency domain. Both the methods have their advantages and disadvantages, but for analyzing structures under random loads like wave, wind and earthquake, frequency domain analysis is preferred. The procedure for analyzing structures in frequency domain, for example, inputs, outputs and methodology are explained in detail in Chapter 3 and the flowchart of the method is shown in Appendix B.2 and B.3. The methodology shown in the flowcharts is verified using simple models and is discussed in detail in Chapters 4 and 5.

The loading in frequency domain analysis is represented in terms of a Power Spectral Density (PSD). A PSD provides information on power of the signal (here 'signal' is the input load in time domain) but does not give its amplitude value. In frequency analysis, the dynamic response (output) of a structure is calculated using modal frequency response analysis in simulation software's, for this research the software used is FEMAP. In modal frequency response analysis, the relevant modes or natural frequency of the structure are analyzed to calculate the output response either in terms of member forces or stress. The stresses calculated from FEM can be directly used to calculate fatigue damage either using nominal stress approach or for tubular joints, hot spot stress approach is recommended [1]. Hot spot stress is calculated by multiplying the nominal stress values by stress concentration factor. Stresses (nominal or hot-spot) are then used to calculate damage using a suitable counting method calculates relevant stress ranges from the response. For frequency domain analysis, Dirlik's method is used across a wide band (sea waves) and narrow band (sinusoidal loads) loads and gives good accuracy when compared to results obtained from equivalent rainflow counting algorithm [3, 4].

Dirlik's method relates the output stress (nominal or hot spot) response PSD of any structure to the Probability Density Function (PDF) of stress ranges. Total damage is calculated by Miner's cumulative damage rule from stress range 'S' and PDF. The statistical moments calculated from the stress response of the structure are used to calculate probability density function of stress ranges given by Dirlik's formula. The main advantage of Dirlik's method is that, it is relatively easy to understand and follows a series of empirical formulae which calculates PDF of stress ranges, and eventually, fatigue damage. More detail on Dirlik's method and its application is discussed in Chapter 3. Overall research procedure also has certain assumptions which leads to limitations, these are addressed below.

1.6. LIMITATION

The main limitations of this research are discussed below.

1. The fatigue damage estimation using Dirlik's method is conducted assuming frame models with simple joints, but in reality simple joints rarely exist, almost every joint is a complicated or multi-planar joint for which the hot spot stress calculation is conducted in FEM and a complete 3D model is required for analyzing multi-planar joint. However, to keep focus on the research objective, it is decided to analyze simple joints assuming simple beam models.

2. All the loads considered in the research are assumed and no reference is considered. This is purely done to keep the simulations in FEMAP faster and easier to understand.

As the methodology and limitations of the research are known, an overview of the fatigue analysis procedure is given in Figure B.1. The figure also shows where exactly this analysis would take place in the overall fatigue design and its contribution in calculating overall fatigue damage. A research paper is also attached in Appendix A, which provides brief details about the work conducted in this research. In Chapter 2, a brief description on the different methods for fatigue evaluation is given and discussion on the current methodology for fatigue assessment in tubular structures.

2

FATIGUE ASSESSMENT

In this chapter, we will discuss on the current methodology used for fatigue assessment in general and also specific for tubular joints. Fatigue has been analyzed throughout the ages and there is an abundance of literature available on the subject including the various implemented methods. Fricke describes these main approaches in his article [13] and the approaches are briefly discussed in Section 2.1. To get a better understanding on the fatigue assessment procedure implemented in Allseas, we will discuss fatigue assessment of stinger of *Solitaire*, the vessel prior *Pioneering Spirit*, in Section 2.4. This will give an idea on how the overall assessment is conducted and where and how how deflection will be included.

2.1. FATIGUE ASSESSMENTS METHODS

Figure 2.1 shows different approaches which are used to calculate fatigue damage along with the important effect considerations in each of the methods.

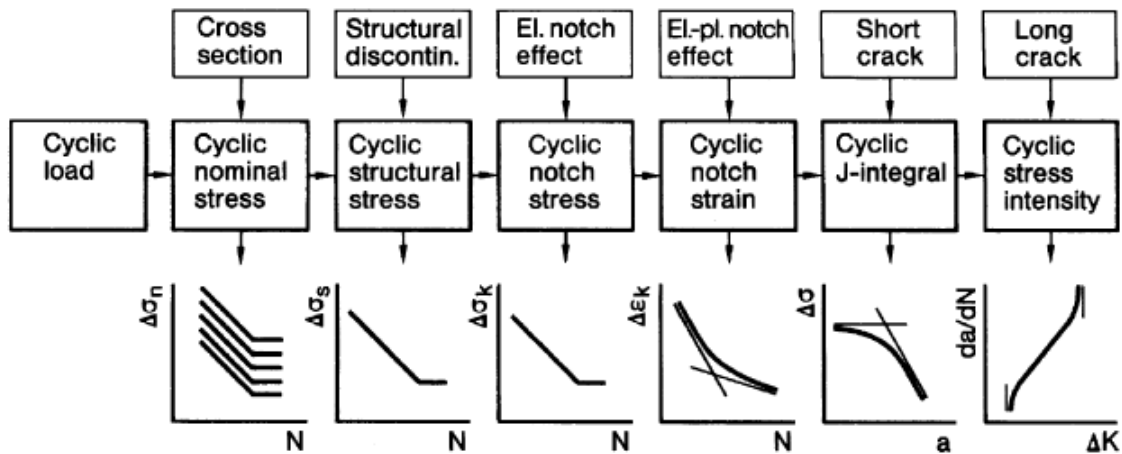


Figure 2.1: Approaches of description of fatigue strength and life [13]

Nominal stress approach:

The nominal stress approach calculates nominal stress in the vicinity of critical cross-section of the welded joint and compares it to S-N curves. For welded components, the S-N curve includes notch effects and weld quality class [14]. These curves are based on statistical evaluation of relevant fatigue tests where uniform scatter bands have been defined. From these, a harmonized set of S-N curves and an associated catalogue of details are agreed upon internationally [13]. Consideration of several influencing factors in fatigue have been investigated such as effect of mean stress and plate thickness effect, which are also being considered in the S-N curve. The acting forces and moments can also be introduced in the curves if it is difficult to calculate

nominal stress [14]. This approach is one of the easiest methods to calculate fatigue damage, but lacks the consideration of local stress raising effects [15]. Bi-axial stresses can also be considered but it requires special attention, more detail can be found in the work of Backstrom and Marquis [16], where they analyzed eight different experiments for both proportional and non-proportional loading. In this research, for the cantilever beam, nominal stress approach is followed to calculate cyclic nominal stress.

Structural or hot-spot stress:

For welded structure it is difficult to calculate nominal stress as the cross-section at the weld is very complicated and hence fatigue damage calculation will never be correct [17]. A different method can be used by calculating hot spot stress near the weld area. Hot spot stress approach considers stress increase due to structural configuration or in other words, the macro-geometry. This approach excludes the local stress concentration effect due to weld toe, instead calculates by extrapolating stress or strain at a distance away from the weld toe. Such a stress evaluation and extrapolation at certain distance away from weld depends upon the thickness of plate or shell. This method was developed in combined effort by classification societies and operators of offshore installation. Various codes and recommendations exist for load assumptions and for stress evaluations and extrapolation, like the parametric formulae of hot-spot stress concentration factors and use of appropriate S-N curve [13]. Although, it can be said that the hot-spot stress is a fictitious value, it corresponds to sum of membrane and bending stress at the weld toe which can be determined either by surface extrapolation or linearisation of stress. This approach however, fails at in-plane notches such as welded edge gussets where plate thickness is no longer a relevant parameter for defining the stress evaluation.

Notch stress approach:

There are limitations to hot spot stress approach while analyzing welded structures as it does not include the notch stress due to weld beads in total stress because of nonlinear stress distribution through the thickness of the plate [18]. The analysis and assessment of elastic notch stress at the weld toe or root faces problems of high or even infinite peaks at sharp notches. The analysis of notch stress can be used either on theory of elasticity or on numerical methods such as FEM. For example, undercuts occurring with different welding processes can be recorded and subsequently assessed. Furthermore, geometry of fillet welded joints can be optimized with respect to fatigue, taking into account all geometrical influence factors [13]. Multi-axial loading and residual stresses have also been included in this approach. Also, good fatigue predictions under out-of-phase loading can be achieved particularly by effective shear stress hypothesis for ductile materials. However, for semi-ductile metals the consideration of the plane with maximum normal/shear stress combination has shown to be superior to others [13].

Notch Intensity approach:

The elastic stress field around sharp notches can alternatively be described by the theoretical solution for V-shaped notches under symmetric and anti-symmetric loading. From observations it is suggested to use notch intensity factor as a parameter describing the crack initiation life of welds including short crack propagation up to a crack depth of approx. 0.5 mm [13]. This approach has the same basis as the fracture mechanics approach except that instead of a crack we have a sharp weld notch [19]. The approach has limitations with respect to the structural stress approach and local strain measurements on weld toes [13]. Good agreement is achieved between prediction and published test data when assuming an initial crack length of 0.3 mm for subsequent crack propagation part [13].

Notch strain approach:

Unlike the above approach, notch strain approach considers the elastic-plastic stress and strain in the notch. This has been successfully applied to notches at base material which include computation of local stress and strain taking into account the elastic effect of surrounding material and cyclic material behavior [13]. This approach can be used to predict the crack initiation life of welded joints for load cycles less than 10^5 . It is also suggested in [20] that the cyclic elastic-plastic stress-strain and strain-life of the parent (base) material, the weld filler material and the heat affected zone material should be used as input to calculate the response. The response is calculated at every notch root of the weld using Ramberg-Osgood's relation between stress

and strain and Seeger-Beste's notch approximation formula [20]. This approach has been further developed to include multi-axial fatigue failure.

Crack propagation approach:

This approach is well established to assess fatigue failure in welded joints, where crack propagation phase is longer than crack initiation phase, for example, a through thickness crack. By measuring the crack length, the assessment of fatigue failure of welded joints can be performed using this approach. The elements of the approach are the crack propagation equations given by Paris and Erdogan in 1963 [21]. This approach can be used to investigate the effect of special geometrical factors of fatigue life, like longitudinal attachment, misalignment of load carrying cruciform joints [13]. One major difficulty in practical situations is the estimation of effective part of cycle which is influenced by plastic wake left behind the crack tip. This approach plays a key role to assess the remaining life and structural redundancy and to establish rational inspection planning.

Having seen the major method which are being used to assess fatigue damage of welded structures, we will now see how tubular structures are analyzed for fatigue. It is important to say that the assessment procedure which will be followed is based on Hot spot stress approach, this is discussed in the next section.

2.2. FATIGUE ASSESSMENT FOR TUBULAR STRUCTURES

Structures for offshore application are typically constructed using 3D tubular frames fabricated from steel. To stiffen the structure, different tubular members are joined together to form tubular joints. Figure 2.2 shows the basic tubular joint and its two most vital parts (members). The members or parts are called *chord* and *brace*. The chord has a larger diameter than the brace and there can be one or more braces attached to the chord. In 2.2 we see a simple tubular joint consisting a chord with a single brace attached to it.

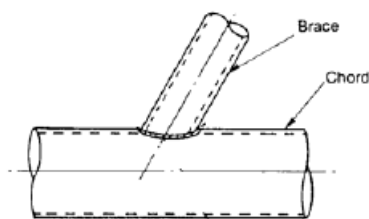


Figure 2.2: A typical tubular joint [22]

Both the structure and the tubular joints should be designed for a higher design life and should be able to sustain ultimate design loads [22]. The design process is divided into two main stages namely, the global design and local design. The analysis should start with the global design which determines the sectional forces and stresses on various elements later serving as boundary conditions for local stress analysis of the joints. These local stresses at the joints are several times higher than nominal stresses and can sometimes be even higher than yield stresses [22]. These high stress regions are called as hot spots and these are normally found at the weld toe of the joint [22]. A detail analysis would result that there are two main places where these hot spots can be found [22]:

1. Weld toe at the brace side.
2. Weld toe at the cord side.

The hot spot stress at these joints are calculated by multiplying nominal stress and stress concentration factors. These hot spot stresses are used to calculate fatigue damage on the joint or joints. To provide a common platform for analyzing offshore structures, classification societies provide recommended practice based on experience and extensive experimental data to calculate hot spot stress. Det Norske Veritas (DNV) and Germanischer Lloyd SE (GL) are two of the biggest classification society which provides recommendations for

designing vessels, offshore structures and mobile offshore units [1] and have combined together to provide a recommended practice for fatigue assessments of different types of joints used in offshore structures. Allseas uses DNVGL recommended practice to design and analyze tubular joints which is discussed in the next section.

2.3. FATIGUE ASSESSMENT ACCORDING TO DNVGL

Fatigue design of tubular joints is conducting as per DNVGL-RP-0005:2014-16, which deals with offshore steel structures. This document provides fatigue damage assessment methodology for high cycle region [1]. Fatigue assessment methodology described in DNVGL differs for plated and tubular joints. For tubular joints, hot spot stress is calculated different for single-plane (simple) and multi-plane (complex) joints. Joints classified as simple tubular joints have chord and the attach brace or braces in the same plane, for example joints like 'Y', 'K' joints, which are shown in Figure 2.3 are simple tubular joints. Multi-planar joints as the name suggests, are joints where the brace and chord are not in the same plane. Keeping in line with the methodology of the research, only simple tubular joints will be analyzed, however, calculation of hot spot stress for both types of joints is discussed in Subsections 2.3.1 2.3.2.

2.3.1. SIMPLE JOINTS

Figure 2.3 shows the various types of simple joints distinguished by [22].

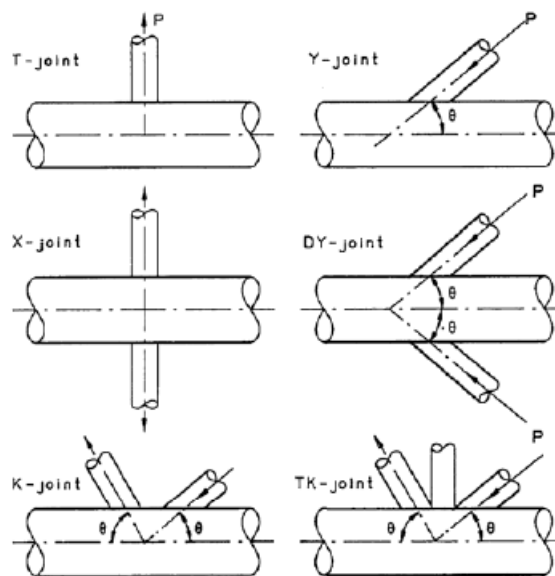


Figure 2.3: Types of simple joints [22]

Although the structures are mostly composed of multi-planar joints rather than simple joints, understanding the procedure for hot spot stress evaluation of these joints is important as it plays an important role in fatigue design [22]. Since only a feasibility study is conducted in this research, simple joints can be analyzed faster and the overall procedure is computationally less expensive. The most important loads acting on a tubular joints are axial load, in-plane bending (IP) and out-plane bending (OP). It is important to know that the loads are calculated at the brace of the joint in joint co-ordinate system. Simple tubular joints can be analyzed using a simple beam element model of the structure in FEM. For a BEAM element, bending moment is calculated in two different planes namely, Plane1 and Plane2. It is important to understand which of these planes give IP bending moment and OP bending moment. Figure 2.4 provides the visual description of the forces acting on a typical simple joint.

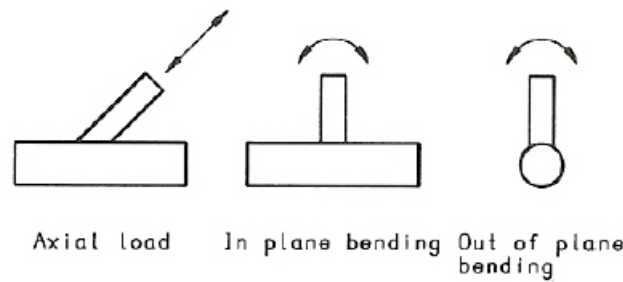


Figure 2.4: Types of loads on tubular joints [22]

For simple tubular joints, nominal stresses are calculated by dividing axial load and bending moments (in-plane and out of plane) at the brace with geometrical dimensions of the brace. For a particular joint, hot spot stresses are calculated by superposition of axial stress, in-plane and out of plane bending stresses multiplied with appropriate stress concentration factors (SCF) as per formulae provided in DNVGL recommended practice [1]. The SCF depend on the type of simple joint (Y, T, K, etc.) and also on the geometrical dimensions of the brace and chord. A total of 16 hot spot stresses are calculated for a joint, 8 on the chord-side and 8 on the brace-side. Figure 2.5 shows the eight location on the chord-side where the hot spot stresses are calculated using the formulae given in Figure 2.6. Using the same superposition formula, hot spot stress is calculated at the brace-side. For calculating hot spot stress on the brace and chord, the only change in the formulae shown in Figure 2.6 is the value of stress concentration factors.

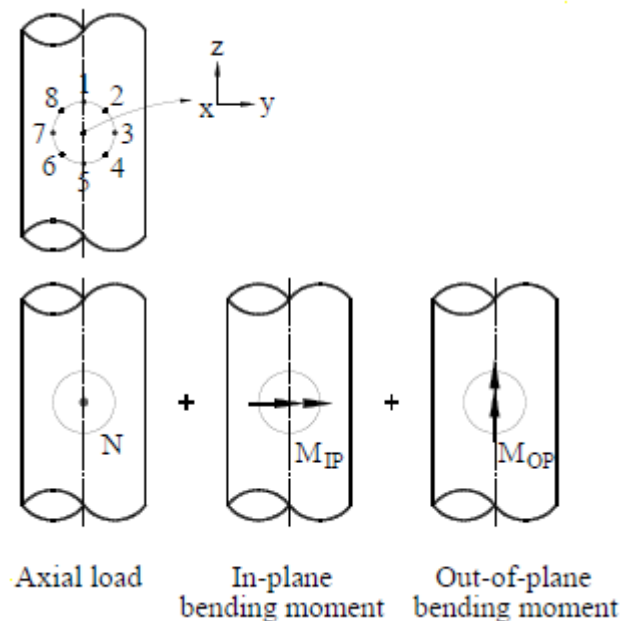


Figure 2.5: Superposition of stresses [1]

In this research, a simple frame model is selected for verifying the frequency analysis, considering a simple ‘T-joint’. The different stress concentration formulae for a ‘T-joint’ are given below in Equation 2.1 [1]. The first four factors are calculated for axial forces, the next two for in-plane bending moment and the last two for out of plane bending moment. All the parameters can be calculated using the geometric details of brace and chord and their formulae can be found in Appendix B of [1].

$$\begin{aligned}
CS &= \gamma\tau^{1.1}(1.11 - 3(\beta - 0.52)^2)\sin\theta^{1.6} \\
CC &= \gamma^{0.2}\tau(2.65 + 5(\beta - 0.65)^2) + \tau\beta(0.25\alpha - 3)\sin\theta \\
BS &= 1.3 + \gamma\tau^{0.52}\alpha^{0.1}(0.187 - 1.25\beta^{1.1}(\beta - 0.96))\sin\theta^{2.7-0.01\alpha} \\
BC &= 3 + \gamma^{1.2}(0.12e^{-4\beta} + 0.011\beta^2 - 0.045) + \beta\tau(0.1\alpha - 1.2) \\
IBMCC &= 1.45\beta\tau^{0.85}\gamma^{(1-0.68\beta)}(\sin\theta)^{0.7} \\
IBMBC &= 1 + 0.65\beta\tau^{0.4}\gamma^{(1.09-0.77\beta)}(\sin\theta)^{(0.06\gamma - 1.16)} \\
OBMCC &= \gamma\tau\beta(1.7 - 1.05\beta^3)(\sin\theta)^{1.6} \\
OBMBC &= \tau^{-0.54}\gamma^{-0.05}(0.99 - 0.47\beta + 0.08\beta^4) OBMCC
\end{aligned} \tag{2.1}$$

A MATLAB code is written in Appendix D.4 to calculate SCFs and hot spot stresses at all 16 sixteen locations of a simple 'T-joint'. For tubular joints, it is suggested in DNVGL [1] to use 'T-curve' for calculating fatigue damage, the S-N curve is shown in Figure 2.7. The two slope S-N curve provided by DNVGL differs for structures working under sea water condition and air condition. For the purpose of this research, a single curve S-N curve for air is used as the stinger is coated to protect rusting and is regularly checked for any abnormalities and damages. For calculating total fatigue damage, damages for each load case is calculated separately and added together using Miner's cumulative rule. While calculating total fatigue damage, percentage of occurrence of a load case should be multiplied by its corresponding damage value to provide an apt estimation of the total fatigue damage of the structure which also gives information on which of the load case is causing the most damage. With this information it is possible to take effective precautions against the load case either by increasing the structural strength or making appropriate maintenance plan.

$$\begin{aligned}
\sigma_1 &= SCF_{AC} \sigma_x + SCF_{MIP} \sigma_{my} \\
\sigma_2 &= \frac{1}{2}(SCF_{AC} + SCF_{AS}) \sigma_x + \frac{1}{2}\sqrt{2} SCF_{MIP} \sigma_{my} - \frac{1}{2}\sqrt{2} SCF_{MOP} \sigma_{mz} \\
\sigma_3 &= SCF_{AS} \sigma_x - SCF_{MOP} \sigma_{mz} \\
\sigma_4 &= \frac{1}{2}(SCF_{AC} + SCF_{AS}) \sigma_x - \frac{1}{2}\sqrt{2} SCF_{MIP} \sigma_{my} - \frac{1}{2}\sqrt{2} SCF_{MOP} \sigma_{mz} \\
\sigma_5 &= SCF_{AC} \sigma_x - SCF_{MIP} \sigma_{my} \\
\sigma_6 &= \frac{1}{2}(SCF_{AC} + SCF_{AS}) \sigma_x - \frac{1}{2}\sqrt{2} SCF_{MIP} \sigma_{my} + \frac{1}{2}\sqrt{2} SCF_{MOP} \sigma_{mz} \\
\sigma_7 &= SCF_{AS} \sigma_x + SCF_{MOP} \sigma_{mz} \\
\sigma_8 &= \frac{1}{2}(SCF_{AC} + SCF_{AS}) \sigma_x + \frac{1}{2}\sqrt{2} SCF_{MIP} \sigma_{my} + \frac{1}{2}\sqrt{2} SCF_{MOP} \sigma_{mz}
\end{aligned}$$

Figure 2.6: Formulae to calculate hot spot stresses [1]

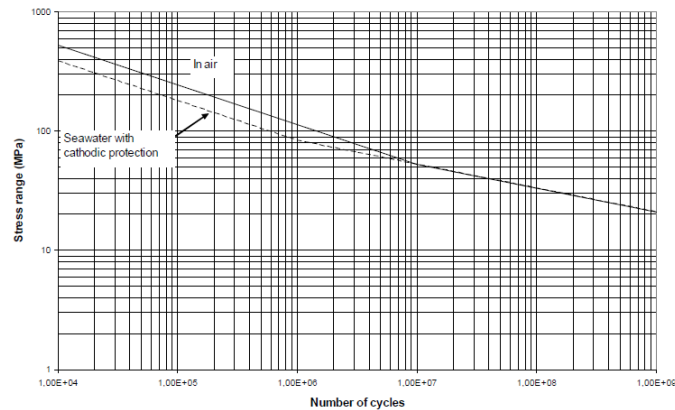


Figure 2.7: T-curve for tubular joints [1]

This is how a simple tubular joint is analyzed using DNVGL recommended practice. To follow the procedure of calculating hot spot stress, it is important to pre-select the critical joint for the analysis. Pre-selection of a joint reduces the amount of computational time required for calculating hot spot stress at the joint. As Allseas has a lot of experience in design of offshore tubular structures, pre-selection is usually done based on experience of the design group. However, each and every joint of the stinger is analyzed for fatigue damage hence the pre-selection of joints is justified. Now we will look at how the multi-planar joints are analyzed as per DNVGL rules.

2.3.2. COMPLEX JOINTS

Unlike simple joints, complex (multi-planar) joints are difficult to analyze because there are no direct formulae available to calculate stress concentration factors. However, it is possible to calculate the hot spot stress using finite element method. Meshing of structure model plays an important role in calculating the hot spot stresses at critical joint locations. It is important to have a continuous and not too steep change in the density of element mesh in the areas where hot spot stress is calculated. Hot spot stresses are calculated assuming linear material behavior and using an idealized structure model with no fabrication related misalignment, which means no weld modelling and no rounding near the joint location. To reduce the overall model size and effectively calculate the stresses at a critical joint, different meshing elements can be used to decrease the total analysis time.

To speed up the procedure of analysis of large structures like stinger, Allseas pre-selects a tubular joint and models it using shell elements while the remaining structure is modelled using beam elements. Iterations are then carried out for every joint of the stinger, analyzing each and every joint. Using this technique, the computational time required for each analysis is reduced significantly. For complex tubular joints without any additional plate stiffeners, the hot spot stress is extrapolated as per recommendation given in DNVGL [1] at specified locations along the chord and brace as shown in the Figure 2.8 below. The locations along brace and chord are found using Equations 2.2 to 2.4 along three different directions of the weld.

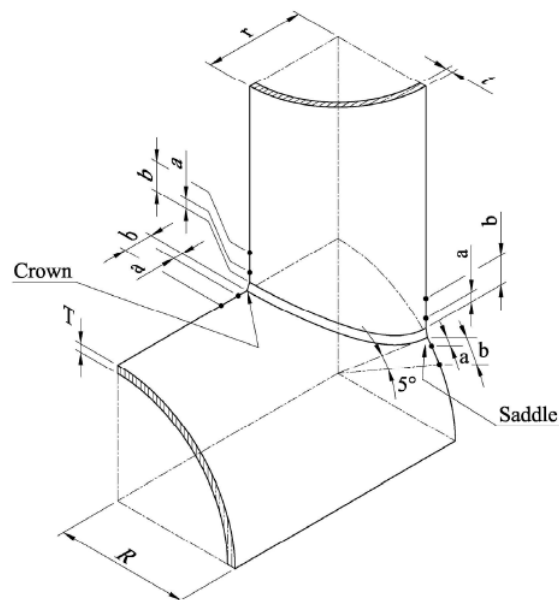


Figure 2.8: Hot spot stress of Multi-planar joint [1]

Equation 2.2 is useful for calculating the location of hot spot stress along the brace surface normal to the weld. Equation 2.3 along the chord surface on the crown side and Equation 2.4 at the saddle side.

$$\begin{aligned} a &= 0.2\sqrt{rt} \\ b &= 0.65\sqrt{rt} \end{aligned} \quad (2.2)$$

$$\begin{aligned} a &= 0.2\sqrt{rt} \\ b &= 0.4\sqrt[4]{rtRT} \end{aligned} \quad (2.3)$$

$$\begin{aligned} a &= 0.2\sqrt{rt} \\ b &= \frac{\pi R}{36} \end{aligned} \quad (2.4)$$

For complex joints with additional plate stiffeners, in addition, hot spot stresses at the connection of plate to tubular section is also calculated using extrapolation methods. To calculate the hot spot stress at such a connection, stress at a distance of $0.5t$ and $1.5t$ are extrapolated to calculate stress at the weld toe, where ' t ' represents the thickness of the chord. The method of extrapolation can be either linear as shown in Figure 2.9 or second order polynomial shown in Figure 2.10 depending upon the type of shell element used to model the pre-selected joint. For second order polynomial, hot spot stress needs more points for extrapolation compared to linear. Selection of extrapolation method depends upon element sizes, for example, element sizes upto txt , linear extrapolation method can be used. Stresses on the mid side nodes along 'AB' can be directly taken as stresses at point $0.5t$ and $1.5t$ and hot spot stress can be calculated using linear extrapolation. For element size higher than txt , depending on the number of node of the shell element used, stresses at $0.5t$ and $1.5t$ are calculated and second order polynomial method shown in Figure 2.10 is used. For 4-node shell element, stresses in the first three elements near the joint are used to calculate stress at $0.5t$ and $1.5t$ as per procedure shown in Figure 2.10. For 8-node shell elements, stresses at the mid-side nodes of the three elements are used to calculate stress at $0.5t$ and $1.5t$ and then second order polynomial is applied to calculate hot spot stresses. The element used for analysis mainly depends on the size of the structure under analysis, using element thickness higher than ' t ' the structure will be analyzed quicker, but second order polynomial extrapolation has to be used.

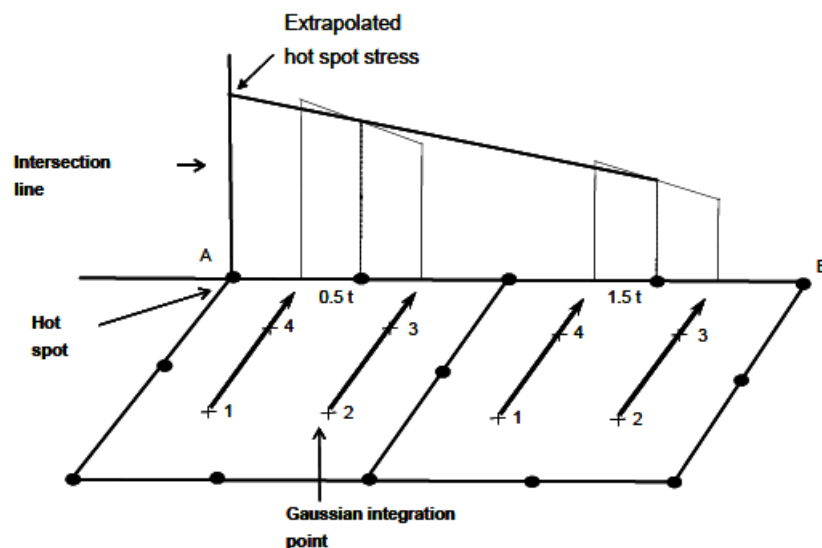


Figure 2.9: Linear extrapolation method [1]

For complex joints it is suggested in DNVGL [1] to use D-curve for calculating fatigue damage instead of T-curve according to the assumption that the stresses in the in-plane direction of the joint gives acceptable results with the hot spot stress concept linked with the D-curve. Depending upon the surrounding environment and pre-treatment of joints, either air or sea-water curve can be used.

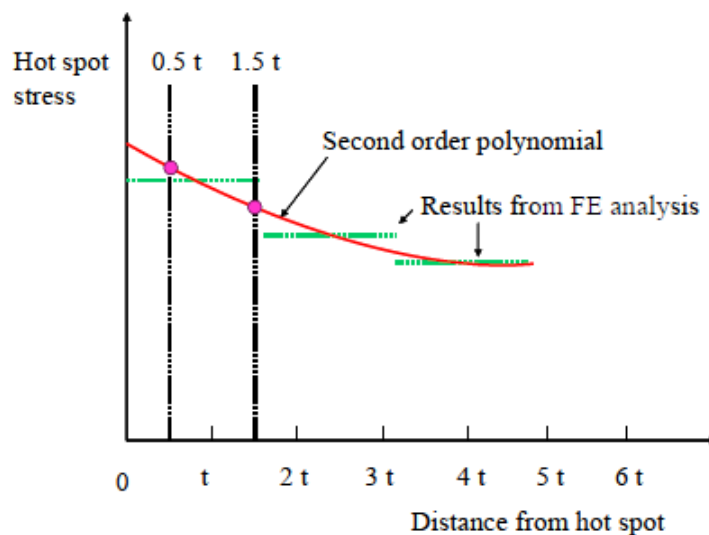


Figure 2.10: Second order polynomial extrapolation method [1]

The main objective of this research, as discussed in Section 1.3 is to check the feasibility of frequency domain analysis for tubular joints, for which analyzing simple joints alone would help in establishing the correct methodology and also save rigorous computational time. Until now we have discussed on fatigue assessment procedure recommended by DNVGL and now we will check its method of application on assessing fatigue damage on stinger of *Solitaire* in next section.

2.4. FATIGUE ASSESSMENT OF SOLITAIRE'S STINGER

Before fatigue assessment is conducted, it is important to calculate the relevant loads cases acting on the stinger and also the number of occurrences of the load cases throughout the life of the stinger. Both are given by 'Life Matrix', a fatigue life matrix is a table giving the number of cycles of each load case acting on the stinger for a year. The load cases are selected depending on the different loads acting on the stinger, main consideration is given to the dynamic load due to sea states. During the life of the stinger it will encounter various sea states and will operate under different positions (depending upon the water depth). Assessing fatigue damage for all these conditions is impractical, hence, different sea state, parameter ranges and step size are considered and the stinger is analyzed only at two extreme positions (extreme shallow and deep water positions). Figure 2.11 shows the major steps involved in assessing fatigue damage of *Solitaire's* stinger.

From the life matrix, total number of loads cases considered for analyses are decided and divided into two types, hydrodynamic and roller box loads. The hydrodynamic loads are due to different sea states acting on the stinger and roller box loads are the reaction forces of roller boxes on the stinger during pipelaying operations. For each load a 3 hour analysis is performed in Ansys AQWA for hydrodynamic loads and in OFFPIPE for roller box loads. After this analysis, for each load case in AQWA, 6 sub-load cases of hydrodynamic loads are calculated as outputs and for each load case in OFFPIPE, 4 sub-load cases are calculated. These sub-load cases are considered as the most relevant sub-load cases that are solved statistically to obtain maximum and minimum stresses at each pre-selected joint.

These load and sub-load cases are then applied on the FEMAP and STAAD model, the joint to be analyzed is pre-selected and modelled using shell elements while the rest of the stinger is modelled using beam elements. Such a modelling technique helps in reducing the computational time as discussed in Subsection 2.3.2. Hot spot stress is then calculated either by using stress concentration factor for simple joints as discussed in Subsection 2.3.1 or by extrapolation techniques for multi-planar joints discussed in Subsection 2.3.2.

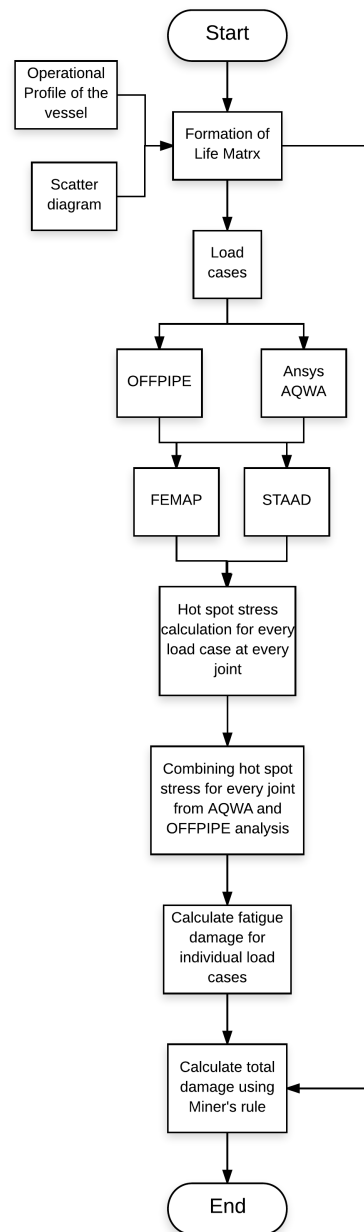


Figure 2.11: Fatigue assessment of *Solitaire's* stinger

The analysis is carried out for each sub-load case and hot spot stress range is calculated from maximum and minimum stress values in each sub-load case. These hot spot stress ranges are then used to calculate damage using S-N curves provided in DNVGL recommendation, T-curve for simple joints and D-curve for multi-planar joints. To calculate total fatigue damage, percentage of occurrences of each load case from the life matrix is used and multiplied by the corresponding damage for each load case. Using this procedure total fatigue damage of a joint is efficiently calculated and the same process is followed for all joints.

2.5. CONCLUSION

In this chapter we have discussed on the current methodology for fatigue assessment of tubular joints used by Allseas as per recommendations provided in DNVGL [1]. Apart from the joints discussed in this chapter, procedure for hot spot stress calculation can be different for other types of joints. For example, joint with web

stiffened cruciform connections or joints with penetrative welds have a different procedure for calculating hot spot stress, discussed in DNVGL [1]. However, these are not included in this report. The procedure for fatigue assessment of *Solitaire's* stinger was discussed as it would help in understanding the general procedure followed in Allseas. But, in case of *Pioneering Spirit*, an additional bow deflection load will impact the damage values for all the joints. Before we can calculate this impact, it is important to check the feasibility of a fatigue assessment procedure. As discussed in Chapter 1, frequency analysis with Dirlik's method is selected and a feasibility study is conducted in this research. The feasibility will be established by verifying the proposed frequency analysis theoretically and also by conducting equivalent time domain analysis with rainflow counting. First, it is important to understand frequency analysis theoretically and its application in estimating fatigue damage with Dirlik's method. This is explained in detail in Chapter 3.

3

PROPOSED FREQUENCY ANALYSIS

The response of a structure can be calculated either in time domain or frequency domain. Structural response due to environmental loads like wave, wind and earthquake are random in nature and hence analysis in frequency domain will provide a better understanding on the structural behavior [23]. Random processes are explained in detail in Appendix C.2. The basic theory behind the type of vibrational analysis which is considered in this research namely, base excitation, is explained in Appendix C.1. This chapter starts with discussing on implementation of frequency analysis for base excitation problems, explained in Section 3.1. Here we will look at the application of Power Spectral density (PSD) functions as input loads in Subsection 3.1.1, followed by other important considerations needed to efficiently carry out the analysis. We will touch upon the various counting methods that can be implemented in frequency domain to calculate stress range and fatigue damage in Subsection 3.2.3 before explaining in detail Dirlik's method which is used in this research in Section 3.3.

3.1. FREQUENCY DOMAIN ANALYSIS

Pioneering Spirit is designed to operate for a minimum of 25 years which means the vessel has to sustain loading cycle during this time. Among these loads, wave loads are assumed to be the most prominent load case. For an efficient design, the vessel should be able to sustain all wave loads acting on it for designed period. To analyze these loads in time domain would lead to huge computational time, however, on the other hand if the time data is converted into frequency domain it will significantly shorten the computational time thereby providing flexibility to optimize the design during the early stages of the design. The load in frequency domain is represented in the form of a *Power spectral density*, which is explained in Subsection 3.1.1. The input values in frequency domain can be calculated using Fourier transform method where a time function can be stated to its reciprocal frequency function as shown in Equation 3.1 [23].

$$f(\omega) = \frac{1}{2\pi} \int_{-\infty}^{\infty} f(t)e^{-i\omega t} dt \quad (3.1)$$

where ω is the frequency of the signal in Hz. Many algorithms are available on how to efficiently convert a time signal to its corresponding frequency signal but the most effective algorithm is Fast Fourier transformation (FFT). FFT decrease the computational time required to convert time signals to frequency signals by discretizing a time signal into various small frequency signals and then combining them. A more detailed explanation on how the FFT algorithm works is given in Appendix C.3. The main advantage of using a frequency dependent approach is the ability to capture small excitation frequencies which could be harmful to the structure. In addition to this, the computational time spent on the analysis is less. For example, in time domain analysis, the model is analyzed at each time history of the input, whereas in frequency domain, the linear transfer function is calculated only once which decreases the time required to compute for different load cases. The transfer function is explained in Subsection 3.1.2 with an assumption that the structures that are analyzed in frequency domain behave linearly. This assumption can be justified as for most engineering solutions, this assumption is reasonable [24].

3.1.1. POWER SPECTRAL DENSITY

Power spectral density (PSD) provides data on the variation of strength of a particular signal with respect to its frequency [25]. This can be in terms of displacement, acceleration, velocity or even force. PSD represents power of a signal, hence it does not directly provide information about the amplitude of a signal but area under the PSD gives mean square power of signal. We can try to further understand PSD by explaining the individual words and their significance [26].

1. Power: It does not represent the physical quantity 'Power' but it represents mean square value of the signal which is analyzed. As power is always related to mean squared value of any quantity like current or voltage, it is also being used here to represent for a particular signal.
2. Spectral: This term is used so point out that the signal which is being assessed is with respect to frequency. In other words, the overall signal representation is done over a spectrum of different frequencies.
3. Density: This term is given as the amplitude values of PSD are always normalized with its frequency. This is seen from the unit of a typical PSD signal. For example, if acceleration of a signal is expressed in terms of PSD, its unit are either G^2/Hz or $(m/s^2)^2/Hz$.

A PSD of a signal is calculated from taking modulus square of the FFT (Fast Fourier Transform) of a time signal. In theory, FFT gives complex number with respect to frequency which define the amplitude and phase for the frequency signal. PSD only contains information on the amplitude of the signal and the phase is neglected. The definition of a PSD can also be explained by Equation 3.2 [24].

$$PSD = \sum \frac{|FFT|^2}{2T} \quad (3.2)$$

where 'FFT' represents the absolute fourier transform of the time signal and 'T' is the total time of the original signal. Following points are important to understand the importance of a PSD signal.

1. PSD only contains the amplitude information from the time signal. This means, when converting a time signal into PSD, all phase information is deleted.
2. The maximum amplitude of a time signal can not be compared to the maximum amplitude of a PSD signal since there is no relation available.
3. With PSD plots, the area under the curve is the most important quantity as we can calculate the RMS (root mean square) of the signal. RMS is defined as the square root of the area under the PSD.
4. The relevant spectral moments can be easily computed for a single sided PSD using Equation 3.3 [24].

$$m_n = \int_0^{\infty} f^n G(f) df = \sum f^n G(f) \delta f \quad (3.3)$$

where ' f ' is the frequency of single sided PSD and ' $G(f)$ ' are values of the PSD. Since in real world we measure data at discrete points, instead of continuous integral, summation is used.

Major engineering processes can be characterized into different types of processes. Figure 3.1 shows the major types of processes. Figure 3.1 (a) represents a 'sine wave' in time domain. When such a process is converted into equivalent PSD, we can find that there is a single spike at the frequency of the sine wave and the area of the spike represents mean square power of the signal [24]. Figure 3.1 (b) represents a 'narrow band' process in time domain. This process is mostly built-up by a series of sine waves covering only a small range of frequency. Figure 3.1 (c) shows a broad band process in time domain. A broad band process constitutes sine waves covering a wide range of frequencies. This process can not be completely identified from its time history and only after converting to PSD, the process can be determined. Figure 3.1 (d) gives a white noise process. This is a special time history process which is built up by sine waves that cover the whole frequency range [24].

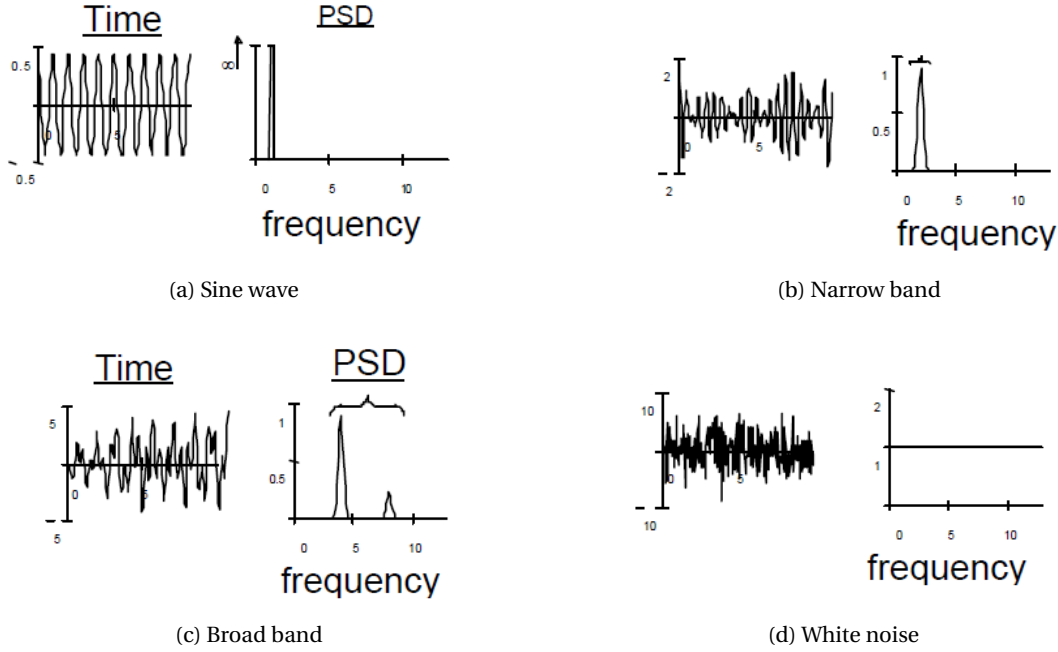


Figure 3.1: Different types of engineering time histories and PSD [24]

Now that we have discussed on what the input of our research is, we will focus on the analysis that will be conducted. Below section talks about the theory behind analyzing a structure in frequency domain.

3.1.2. MODAL FREQUENCY RESPONSE ANALYSIS

Frequency response analysis is used to calculate the structural response of a system due to oscillating excitation. There are two ways in which frequency response analysis can be conducted which are, Direct frequency response analysis and Modal frequency response analysis. Modal frequency response analysis (MFRA) is preferred due to its ability in reducing the problem size by analyzing only the relevant mode shapes of the structure to calculate its dynamic response [23]. Direct frequency response analysis on the other hand, calculates the dynamic response by coupling all the frequencies thereby increasing computational time, however the method gives accurate result [23]. That being said, a trade-off has to be chosen between accuracy and computational time. For this research, MFRA is chosen as its accuracy for larger models is reasonable and can be increased by considering more mode shapes while analyzing the structure. The equilibrium equation for a linear structural system in terms of frequency (ω) is given below in Equation 3.4 [23].

$$([K] + i\omega[C] - \omega^2[M])\{D(\omega)\} = \{P(\omega)\} \quad (3.4)$$

where 'K', 'C' and 'M' are stiffness, damping and mass matrix of the structure and 'D' and 'P' are representing displacement and load vectors in terms of frequency ' ω '. The first term on the left side of Equation 3.4 is the matrix of complex frequency response of the structure also called as structure transfer function which provides the relation between displacement and load vector. This gives a solution for $D(\omega)$ given in Equation 3.5 [23].

$$\{D(\omega)\} = [K]^{-1}P(\omega) + \sum_{j=1}^q z_j(\omega)(\phi_j) \quad (3.5)$$

where 'j' represents number of eigenmodes. $z_j(\omega)$ is frequency dependent participation factor corresponding to the eigenmode and ϕ is the eigenvector corresponding to the eigenmode.

As per the equilibrium equation, for each frequency of the load vector, transfer function and subsequent displacement vector are calculated. To reduce computational time modal frequency response analysis (MFRA) is used. In order to implement MFRA, mode shapes of the structure should be given as an input, therefore modal analysis is conducted prior to MFRA. To further reduce the number of modes for response analysis of the structure mode truncation method can be used [23]. It is specially helpful for higher mode where it uses mode superposition method to reduce the total number of frequencies that are analyzed. This will help to calculate the displacement vector for only chosen frequencies thereby reducing the computational time. However, the correct response of the structure can only be calculated when all modes are considered. To analyze structures using frequency response analysis, the load in the form of PSD's should be given to base nodes. The base nodes are the nodes which are constraint by initial boundary conditions as explained in Section C.1.

A transfer function can be defined as the response per unit input frequency of interest [24]. The concept of transfer function arises from the fact that any increase in amplitude of the input for a linear structure will have a proportional effect on the amplitude of the output. The transfer function is used to predict the output response of the structure by multiplying the amplitude of input with the transfer function at a particular frequency of the input. In FEM analysis, the transfer function is calculated using 'Frequency response analysis'. It could also be calculated from the available data of output response from different tests. In this research, transfer function is directly calculated in FEM by 'Random response analysis' which calculates the output response of the structure by calculating transfer function as a part of the analysis. If needed, the transfer function can be recovered from the input and output responses. However, to get the correct units of the transfer function in the PSD analysis, units of PSD must be squared. This is explained using a simple example where the input PSD is in the form of displacement and output response is calculated in terms of stress. Equation 3.6 gives the correct units of the transfer function.

$$\begin{aligned} \text{Input PSD} * \text{transfer function} &= \text{Output response PSD} \\ \frac{m^2}{Hz} * \frac{MPa^2}{m^2} &= \frac{MPa^2}{Hz} \end{aligned} \quad (3.6)$$

In this research, the input PSD is acceleration and the output PSD is the bending moment and axial force response in the brace of pre-selected joint. Also, since the objective here is to study the application of frequency domain analysis, only simple tubular joints are considered for which hot spot stress can be calculated using defined formulae from DNVGL as discussed in Subsection 2.3.1. In the next subsection we will discuss on the important input data which will be required for the analysis and its importance, considering the scope of this research.

3.1.3. INPUTS FOR THE ANALYSIS

In this subsection we will discuss on the important inputs which will be required for conducting frequency domain analysis and we will also list down the important points which should be considered before and during the analysis.

DAMPING

Analysis of practical model should always include damping to completely consider the effects of loads on the structure and get accurate results. For offshore structures, there are two basic damping namely, Coulomb and viscous damping [27]. Coulomb damping is a result of two surfaces sliding over each other, also called as dry or friction damping [27]. Viscous damping on the other hand is due to the presence of fluid, here water, around the structure providing additional damping during vibrations. Force due to Coulomb damping can be calculated from the normal force and the co-efficient of friction between the two bodies in contact, viscous damping depends on the viscosity of the fluid medium present [27]. Also, viscous damping depends upon the velocity of the motion of the body which is under vibration and is suggested to significantly influence the vibration of the structure [27].

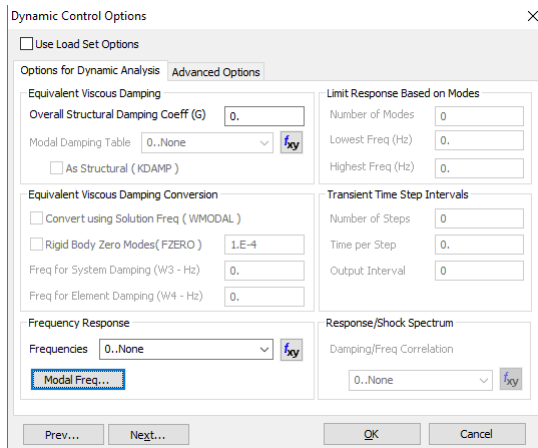
Damping in offshore structures arises due to frictional forces for example, frictional force between structures and their support contact points leads to Coulomb damping. Friction between structure and its surrounding fluid leads to viscous damping and friction between two different structural components lead to structural damping. As these forces are not conservative, it is difficult to derive them from potential energy based on dynamic displacement response of the system. In addition, quantifying the frictional forces is also a difficult task as there are diverse causes for its occurrences for a particular system. These frictional forces are responsible for reducing the response of the system by dissipating the energy or converting the energy from one form to another. The main source of dissipation is in the form of heat, either by conduction or convection to the surrounding fluid.

For the purpose of this research, we will be only considering structural damping for all the models in terms of damping ratio ζ . However, as the application of the method is being verified for offshore structures, it is important to consider an approximate increase in damping ratio due to viscous damping. Considering this, a constant damping ratio of 2% [27] is considered over all the natural frequencies for the models under consideration. With this we assume that the damping ratio remains the same throughout different natural modes of the model.

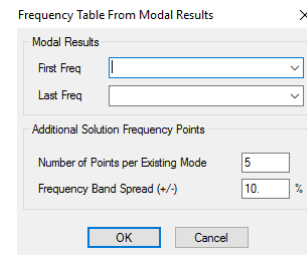
INPUT POWER SPECTRAL DENSITY

In this research, simple models analyzed in frequency domain analysis are verified by conducting an equivalent time domain analysis therefore it is important that the inputs loads used for both the analyses are consistent. In order to verify the models, acceleration (input) values in time domain are assumed and equivalent frequency domain loads are calculated using Fast Fourier transform algorithm using the function 'FFT' in MATLAB. Detail explanation on the Fast Fourier Transform algorithm can be found in Appendix C.3. Two types of loads are considered in this research, sine (periodic) loads and random loads, consisting of Gaussian distributed random numbers. It is important that the conversion of time domain load to frequency domain is performed efficiently and for this, following points need to be consider.

1. **Mass participation factor:** It is important to consider a suitable frequency range for frequency domain analysis. This is achieved by first conducting modal analysis and calculating the number of frequencies which encompass more than 90% of total mass of the system in the direction of load application. This is essential in order to effectively calculate the total dynamic response of the system [28]. In Nastran, it is easy to calculate mass participation factors along with modal analysis and we can decide the maximum number of modes which have to be considered to ensure the dynamic response is correctly calculated.
2. **Sampling frequency:** Sampling frequency is required for converting the time domain loads to frequency domain. Sampling frequency is selected on the basics of frequency range of the model which is analyzed. Frequency range for a structure is selected based on Mass participation factor discussed in the earlier point. It consists of range of frequencies which contain more than 90% of mass of the structure. Sampling frequency should be minimum twice the frequency range of the model. This is done as Fourier transform algorithm converts the time domain series (load values) into frequency series along the sampling frequency containing both positive and negative frequencies as shown in MATLAB code D.3. And since only positive frequencies are chosen, the sampling frequency range is reduced to half.
3. **Output Frequencies:** Importance should also be given in to the output frequency range containing the dynamic response of the structure. It is important to control the output frequency range to achieve comparable results. In FEMAP v11.1, controlling the output frequency range can be achieved in two ways, first method is by adding a specified analysis frequency range in the 'Dynamic Control Option' of 'Random Response analysis'. Figure 3.2a shows the option available under 'Dynamic Control Option'. The frequency range can be specified as shown in Figure 3.2b, where the range can be defined according to the modal analysis allowing the user to control which of the natural frequencies should be analyzed, saving additional computational time. Additional control is achieved by defining the bandwidth in terms of percentage around the selected natural frequencies and the number of points within the selected bandwidth.



(a) Controlling output frequency range - 1



(b) Controlling output frequency range - 2

Figure 3.2: Output Frequencies

The number of points which can be defined in Figure 3.2b is limited to '99'. If additional points are needed around the output frequency range, these can include as shown in Figure 3.3.

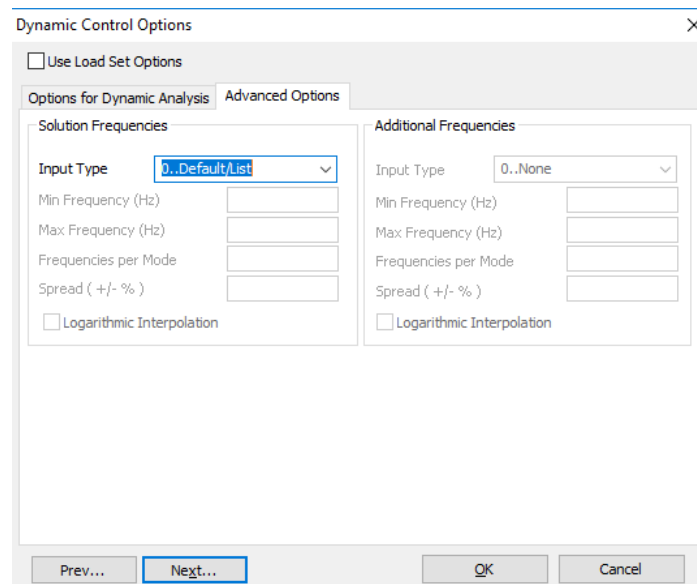


Figure 3.3: Additional control on frequency range

For FEMAP v11.1, there are three options available for 'Input Type', these are 'Frequency range', 'Cluster around modes' and 'Spread around modes'. One or more options can be selected which help in creating additional frequency points around the selected natural frequency/frequencies which we want to analyze. For example, if we select 'Frequency range' option, we can add start frequency, end frequency and number of intervals between them. Nastran will then analyze and present the results for the input number of interval considering the start and end frequency. This helps in achieving accurate results around a frequency range. For analyzing the models in this research, 'Frequency range' is selected for include additional frequencies for analysis.

Now we will look at the method of fatigue damage estimation in frequency domain using Power spectral density function.

3.2. FATIGUE ESTIMATION USING PSD

In this section we will see how fatigue analysis is conducted in frequency domain using PSD's. Before explaining the process for PSD, it will be helpful to highlight the main steps involved in time domain analysis to compare both the processes. For time domain analysis, the traditional nominal stress life approach is discussed in Subsection 3.2.1. The frequency domain approach is explained in Subsection 3.2.2 followed by explanation of different counting methods used in frequency domain analysis in Subsection 3.2.3.

3.2.1. TIME DOMAIN FATIGUE ESTIMATION

The response of the structure in time domain analysis is calculated in the terms of stress or strain time history. If this response contains constant amplitude stress or strain cycles, then the fatigue damage is calculated by referring to a typical S-N curve. However, in reality, constant amplitudes of stress or strain cycles are never achieved. For this purpose empirical algorithms are used to deduce the variable amplitudes into equivalent sets of stress ranges. This is achieved through rainflow counting method which breaks the irregular stress or strain time history into block loading's in the form of a histogram [24]. Figure 3.4 gives an overview of the fatigue estimation process for typical structures.

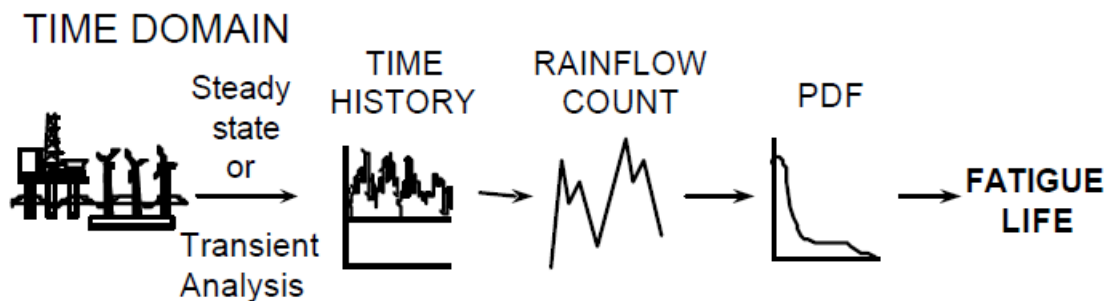


Figure 3.4: Typical time domain fatigue life estimation process [24]

Cycles counted by rainflow counting is used by Palmgren-Miner rule, which assumes a linear relationship between damage in the structure and the stress range. For every stress range from the rainflow counting, a ratio is built for the number of actual cycles for the stress range divided by the number of allowable cycles for the same stress range which is taken from material S-N curve. Summation is done for all the stress ranges to calculate the total damage. If the total damage value is 1, failure is assumed for the structure.

3.2.2. FREQUENCY DOMAIN FATIGUE ESTIMATION

Figure 3.5 highlights the important steps involved in a frequency domain fatigue estimation process.

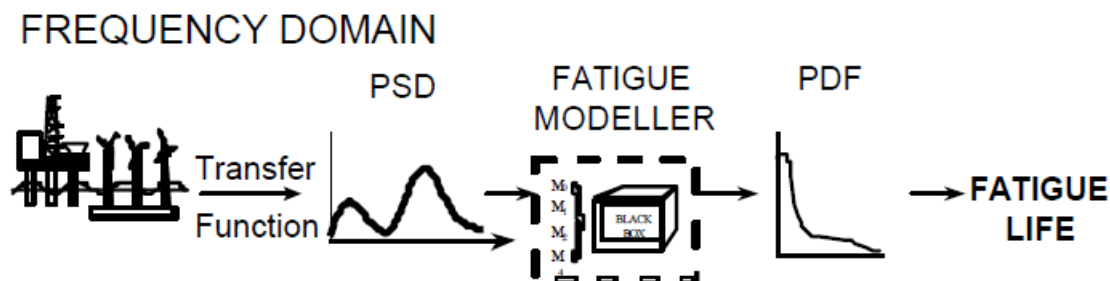


Figure 3.5: Typical frequency domain fatigue life estimation process [24]

For a frequency domain, major computational time is spent on the calculation of transfer function of the model. This transfer function are calculated completely from the parameter of the model and has no depen-

dency on the input loading. The PSD output response is then calculated by multiplying the transfer function by corresponding input PSD. If additional PSDs are acting on the same structure, no additional computational time is needed to calculate the overall output response, as the transfer function has to be calculated only once. Once the output response PSD is calculated, the only part left is the fatigue calculation. For this part of the procedure there are various counting methods available which are explained in Subsection 3.2.3 along with their limitations.

3.2.3. COUNTING METHODS FOR FREQUENCY DOMAIN

As the analysis is being carried out in frequency domain, like the inputs the outputs are also power spectral density functions representing power of the output signal. For example, input displacement or acceleration PSD's will have units as m^2/Hz and $m^2/s^4/Hz$, which after analysis will give outputs with units N^2/Hz for force, $(Nm)^2/Hz$ for moment and Pa^2/Hz for stress. To calculate the fatigue damage, it is important to have an established relation between output response PSD and damage. For time domain analysis, rainflow counting method is utilized to establish a histogram giving information about the stress ranges and their cycle counts. If the histogram is normalized such that the height of each bin is equal to '1', a continuous curve in the form of a probability density function is formed which represent same information. The area under this continuous curve can then be used to calculate fatigue damage by using an elegant and efficient expression given in Equation 3.7 [24].

$$E[D] = \frac{E[P] * T}{C} \int_0^{\infty} S^m p(S) dS \quad (3.7)$$

where 'T' is the total lifetime over which damage is calculated, 'C' and 'm' are material constants defined from the S-N data. $p(S)$ is the probability density function of stress range 'S' and $E[P]$ is the expected number of positive crossings per second. Using this information, estimated damage $E[D]$ can be calculated for time 'T'. If the damage is greater than 1.0, the structure is assumed to have failed. Also by setting the damage value to 1.0, the fatigue life of the structure 'T' in seconds can be calculated [24]. In 1954, S.O. Rice developed a important relationship to calculate $E[P]$ from output response spectral moments of the PSD [4]. The relationship is given in Equation 3.8 [4].

$$\begin{aligned} E[P] &= \sqrt{\frac{m_4}{m_2}} \\ E[0] &= \sqrt{\frac{m_2}{m_0}} \end{aligned} \quad (3.8)$$

where $E[0]$ is the number of peaks per second. Using this information, the irregularity factor (γ) can be calculated as shown in Equation 3.9 [4].

$$\gamma = \frac{E[P]}{E[0]} \quad (3.9)$$

The irregularity factor always has a value between 0 and 1. The irregularity factor gives information on whether the process under analysis is narrow or broad. The value is closer to 1 for narrow band processes and closer to 0 for broad band processes [24]. In Equation 3.7, there is one important parameter that needs calculating, which is $p(S)$. For calculating $p(S)$, different approaches are available which will be discussed briefly in this section. The applications and limitations of every method is also discussed.

NARROW BAND METHOD

Bendat in 1964 proposed the first frequency domain method to estimate fatigue damage for narrow band processes by proposing that the probability density function of stress range of a narrow band process tend to follow Rayleigh distribution [29]. The estimated damage according to Equation 3.7 for a narrow band process can be calculated using Equation 3.10 [24].

$$E[D] = \frac{E[P] * T}{C} \int S^m * \left[\frac{S * e^{\frac{-S^2}{8 * m_0}}}{4 * m_0} \right] dS \quad (3.10)$$

It is clearly seen from the above equation that the probability density function $p(S)$ is represented as a Rayleigh distribution of stress range 'S'. m_0 is the first spectral moment calculated from stress PSD of the system. However, the method is only suited for narrow band process as its main assumption is that, for every positive peak there always be an equivalent negative trough. This is not true for broad band processes and hence this method gives conservative result [2] for broad band processes.

BROAD BAND METHOD

Bendat's narrow band method was calculating conservative for broad band processes because of the assumption positive and negative peaks explained in previous subsection. For broad band process, Steinberg [30] proposed that, the probability density function of peaks is the same as the probability density function of rainflow range and also has a Gaussian distribution and provided at solution in the form of discrete multiples RMS value of amplitudes [31]. The expression to calculate the total number of load cycles given by below expression [31].

$$N(S) = E[P] * T * \begin{cases} 0.683 * 2RMS \\ 0.271 * 4RMS \\ 0.043 * 6RMS \end{cases}$$

This is same as assuming that the number of cycles will fall 68.3% times between $2 * RMS$, 27.1% between $4 * RMS$ and the remaining 4.3% between $6 * RMS$. However, the assumption regarding the rainflow range probability density function being the same as the peaks was later proven to be incorrect by Dirlik in [32]. This method did provide a vital information that stress ranges greater than 8 to 10 times the RMS will not occur in any process [29].

LALANNE/RICE APPROACH

In support of the Steinberg's method, Lalanne proposed that for longer time histories the probability density function of number of stress cycles is the same as the probability density function of peaks. Lalanne used Rice's original formulae on weighted sum of Rayleigh and Gaussian distribution was enough to predict the number of stress cycles [31]. The expression is given in Equation 3.11 [31].

$$N(S) = \frac{\sqrt{1-\gamma^2} e^{\frac{-S^2}{2rms^2(1-\gamma^2)}}}{\sqrt{2\pi}rms} + \frac{S\gamma}{2rms} \left[1 + erf \left(\frac{S\gamma}{rms\sqrt{2(1-\gamma^2)}} \right) \right] \quad (3.11)$$

where S is the stress range, γ is the irregularity factor explained in Subsection 3.2.3. rms is the square root of the zeroth moment (m_0) and erf is the error function given by Equation 3.12 [31].

$$erf(x) = \frac{2}{\sqrt{\pi}} \int_0^x e^{-t^2} dt \quad (3.12)$$

This method, even with the assumption, gives good accuracy when compared to Dirlik's method according to analysis presented in the Article [31]. However, this method is not suitable for both broad band and narrow band processes. When compared to Dirlik's method for broad band processes, there is advantage in terms of computational time required to calculate $p(S)$ and $N(S)$ [31].

Other approaches are also developed with provide correction factors for narrow band approach given by Wirching and Light in 1980, followed by new equation of calculation probability density function for a narrow band by Tunna in 1986. There also have been approaches like Steinberg's to calculate equivalent stress (S_{eq})

by CK Chaudhuery in 1985 and WD Dover in 1988. Brief descriptions on all of the above procedure is available in [4]. However, when results of all of these methods were never comparable to the results obtained from equivalent rainflow counting for larger number of samples. For these reasons, in 1985, Dirlik proposed a semi-empirical method which provided the probability density function for rainflow stress ranges, applicable for narrow and broad band processes. Bishop in his Article [33] in 1990 gave the theoretical background on how rainflow ranges can be calculated from power spectral density data. However, his proposed method was not only computationally expensive but also did not improve the accuracy of the results significantly. After understanding the various counting methods, it was decided to proceed with Dirlik's approach, considering its wide range of application and its accuracy compared to rainflow counting methods as per results given in Articles [3, 4, 29, 31]. The Dirlik's method is explained in detail in the next section.

3.3. DIRLIK'S APPROACH TO ESTIMATE DAMAGE

In 1985, Dirlik proposed a semi-empirical formulae to calculate the probability density function of stress ranges 'S' from PSD response of the structure [12]. It calculates statistical moments from the structural response and uses empirical formulae to determine stress ranges which can then be used to calculate damage. It is a counting method like rainflow, range-pair or Wetzell, that uses structural response in frequency domain to determine stress range. The formula of different parameters used to calculate the probability density function are developed through extensive Monte-Carlo simulations using thousands of test data [12]. As the method is based on empirical formulae, it is easily programmable and hence can be easily used to for different applications. In this section, application of Dirlik's method for this research is discussed.

For this research, the output PSD's are hot spot stresses calculated at 16 location as discussed in Subsection 2.3.1. Each of the 16 hot spot stresses will be used to calculate fatigue damage at 16 locations of a joint. The method has been proven to be as accurate as rainflow counting method [2]. We will now be discussing how the method calculates stress range and number of cycles. Let S be the stress range in MPa and N(S) be the number of cycles corresponding to stress range S. The first step is to determine the frequency step size 'df' which can be either variable or constant depending on the output PSD signal. Using below formula we can calculate the moments m_0 , m_1 , m_2 and m_4 [2].

$$m_n = \int f^n G(f) df \quad (3.13)$$

G(f) is the output PSD in terms of stress amplitude, f is the frequency ranges along which G(f) is calculated. Four moments with n = 0, 1, 2, 4 are calculated which help in calculating of N(S) according to Equation 3.14 [2].

$$N(S) = E[P] T p(S) \quad (3.14)$$

where T is the total time period considered for calculating fatigue damage in seconds, E[P] is the expected number of peaks calculated using Equation 3.15 and p(S) is the probability of stress range S calculated using Equation 3.16 [2].

$$E[P] = \sqrt{\frac{m_4}{m_2}} \quad (3.15)$$

$$p(S) = \frac{\frac{D_1 e^{-Z/Q}}{Q} + \frac{D_2 Z e^{-Z^2/2R^2}}{R^2} + D_3 Z e^{-Z^2/2}}{2\sqrt{m_0}} \quad (3.16)$$

Equation 3.16 consists of a exponential function and two Rayleigh functions. The parameters in Equation 3.16 can be calculated from moments m_0 , m_1 , m_2 and m_4 shown below from Equations 3.17 to 3.24 [2].

$$x_m = \frac{m_1}{m_0} \sqrt{\frac{m_2}{m_4}} \quad (3.17)$$

$$\gamma = \frac{m_2}{\sqrt{m_0 m_4}} \quad (3.18)$$

$$D_1 = \frac{2(x_m - \gamma^2)}{1 + \gamma^2} \quad (3.19)$$

$$R = \frac{\gamma - x_m - D_1^2}{1 - \gamma - D_1 + D_1^2} \quad (3.20)$$

$$D_2 = \frac{1 - \gamma - D_1 + D_1^2}{1 - R} \quad (3.21)$$

$$D_3 = 1 - D_1 - D_2 \quad (3.22)$$

$$Q = \frac{1.25(\gamma - D_3 - D_2 - R)}{D_1} \quad (3.23)$$

$$Z = \frac{S}{2\sqrt{m_0}} \quad (3.24)$$

where x_m is the mean frequency, γ is the irregularity factor and Z is the normalized stress range and other parameters are constants [2]. Once the number of cycles $[N(S)]$ are calculated as per Equation 3.14 and probability density function $p(S)$ using Equation 3.16, a graph can be plotted with values of Stress range (S) and probability density function $[p(S)]$. A simple example to calculate stress ranges using this method is given in Appendix E.1 assuming one of the sixteen hypothetical hot spot stress response at a joint. The total fatigue damage is estimated by calculating the total area under the stress range versus probability density function curve. The method is easy to program in MATLAB and can perform multiple analysis quickly, but has some limitations which are discussed below.

1. Dirlik's counting method is only applicable for power spectral density function of stationary and ergodic processes [32]. Fortunately, most engineering processes including wave loading are in general stationary and ergodic in nature [24].
2. The parameters from Equation 3.19 to 3.24 are calculated using empirical formulae and hence the stress ranges and number of cycles calculated using Dirlik's method may not always be same as rainflow counting method [12]. However, these empirical formulae are developed from extensive sets of data using Monte Carlo simulations to find the best fit values for all the parameters, which gives good confidence in these formulae [32].
3. A study conducted in [34] on wind turbine fatigue loads has also shown that Dirlik's method is more suitable for fatigue estimation involving Gaussian load cases or random loads which follow Gaussian distribution compared to periodic loads. With this research, we are also able to conclude that Dirlik's method gave relatively poor results for periodic (sinusoidal) loads. Fortunately, wave loads are assumed to be Gaussian distributed and hence Dirlik's method can be implemented for this research.

3.4. CONCLUSION

In this chapter we have seen the basic theory behind frequency analysis and the suitable counting method to calculate fatigue damage. Dirlik's method is the most suitable counting method with its simplicity and good accuracy will be used in this research. Up till now, we have discussed the methodology that will be used to calculate fatigue damage. However, an important part of this methodology is the calculation of stress response PSD of structure due to loading conditions, this will be discussed in the next chapter. The analysis on the models will be conducted in FEMAP with Nastran as the main solver. As the loads are in terms of frequency, its application in FEM (FEMAP) is studied by verifying cantilever beam with available theoretical literature, this is explained in detail in Chapter 4.

4

THEORETICAL VERIFICATION - FREQUENCY ANALYSIS

In this chapter we will verify simple models using available theoretical literature. Cantilever beam is selected for conducting theoretical verification on the application of PSD load in FEM due to availability of formula of transfer function. An additional simple frame model is also selected for analysis to represent the main stinger. Stinger model is available in the form of a beam model as shown in Figures 4.1 and 4.2 below.

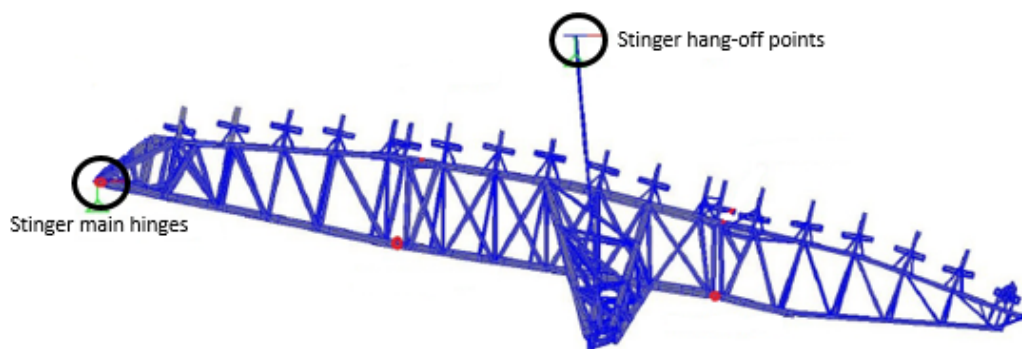


Figure 4.1: Stinger beam model 2D view [35]

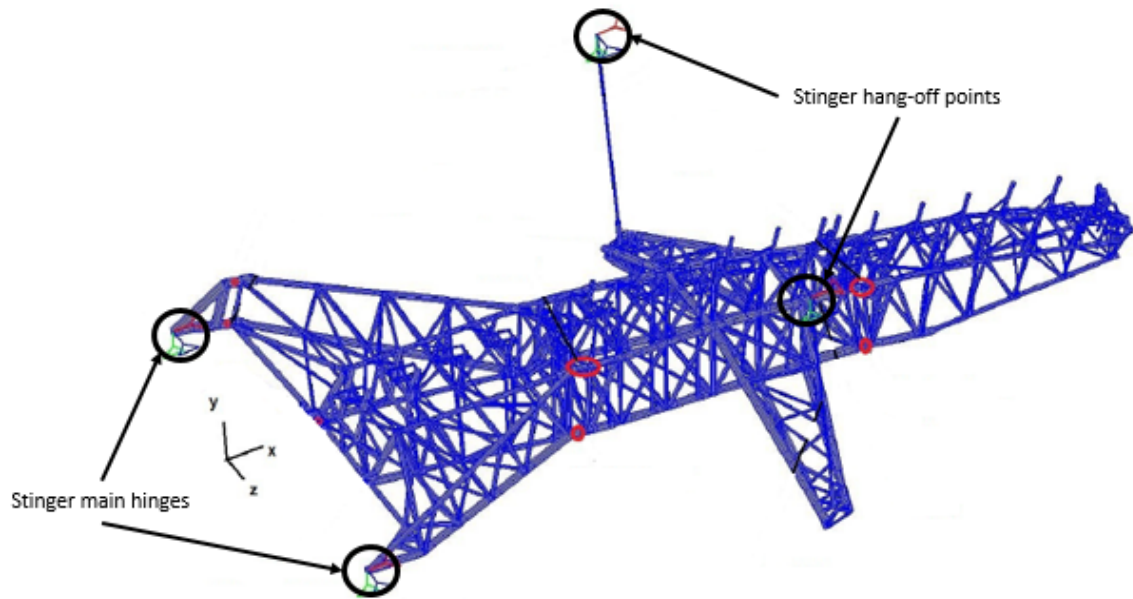


Figure 4.2: Stinger beam model 3D view [35]

The four connection points are clearly shown in Figures 4.1 and 4.2. Although the stinger model is available, it is not used for analysis as it is important to first understand the application of PSD loads on simpler models before analyzing the main stinger model. Considering this, simple models like cantilever beam and frame are used for verification of frequency domain analysis in FEM. Similar to stinger model, a frame model with four boundary condition is selected, this is discussed in detail in Chapter 5. The verification of frequency domain analysis is conducted in two parts. First, analysis of cantilever beam model in FEM (FEMAP) is verified using available formula for transfer function which calculates displacement response PSD at the free end of the beam due to input acceleration PSD load at the base. This is explained in detail in this chapter, starting with a cantilever beam with mass attached at the free end. Cantilever beam with single and also two loads are verified by comparing FEMAP output displacement response PSD with theoretical calculated values using formula for transfer function as stated before. The description of models, input acceleration PSD loads, their geometrical and material properties are discussed in Section 4.1. The formulae for transfer function for cantilever beam and the procedure to calculate the output displacement response PSD is discussed in Section 4.2, along with the FEMAP analysis. Additional analysis on the models are also conducted using sub-cases to further establish the verification, these are discussed in Section 4.1. The results for all the analyses are discussed in Section 4.3 and FEMAP output displacement PSD values are compared with theoretical values. Percentage Relative errors are calculated for all the cases and sub-cases considering theoretical results as the base and errors less than 10% are acceptable, as discussed with Allseas.

4.1. SIMPLE MODELS FOR VERIFYING APPLICATION OF PSD

In this section we will discuss on the various model which are used to verify the PSD application in FEMAP. The material properties used of all models is listed in Table 4.1 [36]. The geometrical properties (cross-sections) will be individually listed for each model. The inputs and assumptions involved in the analyses are also discussed. All the inputs used for verification are assumed based on engineering judgment and available literature. Important consideration for input acceleration PSD load is that, the loads should at least resonant with one of the natural frequencies of the selected model.

Table 4.1: Material Properties for all the models

Property	Value	Units
Young's modulus	$2.1 * 10^{11}$	N/m^2
Poison's ratio	0.3	-
Density	7850	kg/m^3

As stated above, we will be broadly be considering two models, one single degree of freedom model and other cantilever beam model. Given below are the three different cases which will be considered for analysis. These cases are listed considering the possibility of single and two loads acting on the model.

1. Cantilever beam with mass attached at free end with a single PSD load.
2. Cantilever beam model with a single PSD load.
3. Cantilever beam model with two PSD loads.

Loads are applied in the form of Acceleration PSD at the constraint node, the fixed end of the cantilever beam. As discussed in Section C.1, such type of analysis are distinguished as base excitation problems in which load or loads are applied on the constraint nodes (nodes with specified boundary conditions). Next, we will look into the models which are used for the verification.

4.1.1.1. CANTILEVER BEAM WITH MASS ATTACHED AT FREE END

The model is shown in Figure 4.3 and the geometrical properties are listed in Table 4.2. We will also discuss the assumptions for the analysis followed by the input parameters required for the model.

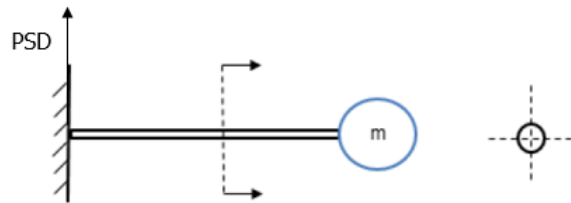


Figure 4.3: Single degree of freedom model

Table 4.2: Details of SDOF model

Property	Value	Units
Outer Diameter	$2 * 10^{-3}$	m
Thickness	$1 * 10^{-5}$	m
Cross-sectional Area	$6.25 * 10^{-8}$	m^2
Moment of inertia	$3.09 * 10^{-14}$	m^4
Length of beam	3	m
Mass at the end of beam	0.5	kg
Gravity	9.81	m/s^2

The assumptions involved in the theoretical calculations are discussed below.

ASSUMPTIONS

1. The model can be considered as a SDOF system, as the mass of the beam is very small when compared to the attached mass.
2. A flat Acceleration Power Spectral Density (ASD) is used for this analysis due to limitation of Miles equation, which is used for verification purposes.

INPUTS FOR SDOF MODEL

As per assumption discussed above, the input PSD is considered to be constant throughout the frequency range. Also damping ratio is also considered as constant to simplify the analysis. The damping ratio of 0.02 throughout the frequency range is considered [37].

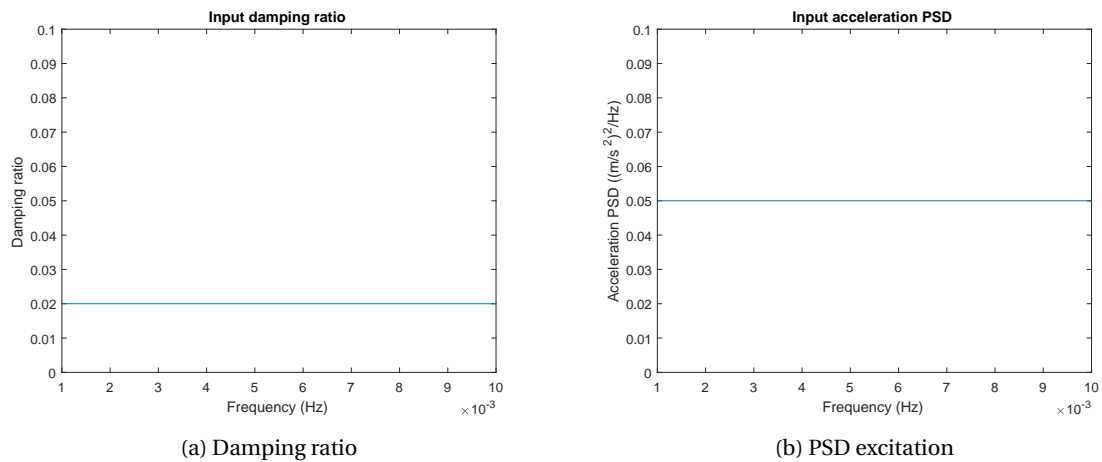


Figure 4.4: Inputs for SDOF model

An additional input required for this analysis is a factor 'Q', which is called as the amplification or quality factor. Q provides information on how much the system is damped. It is calculated using Equation 4.1 [38].

$$Q = \frac{1}{2\zeta} \quad (4.1)$$

where ζ is the damping ratio of the system. The higher the value of Q, the less damping in the system and system will achieve higher response during resonance. The theoretical calculation will be discussed in Section 4.2 and the results will be compared in Section 4.3.

4.1.2. CANTILEVER BEAM MODEL WITH SINGLE PSD

The cantilever beam model used for the verification is shown in Figure 4.5. The geometric details are listed in Table 4.3 below. The analysis of cantilever beam model with single PSD is further divided into three sub cases which are listed below.

1. Cantilever beam with circular cross-section and constant PSD load.
2. Cantilever beam with circular cross-section and varying PSD load.
3. Cantilever beam with square cross-section and constant PSD load.

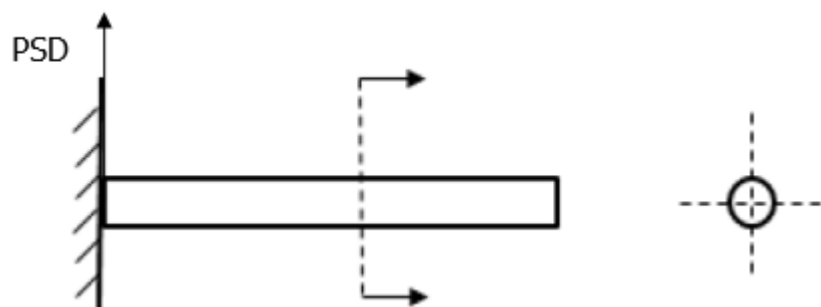


Figure 4.5: Cantilever beam model with single PSD

Table 4.3: Details of MDOF model

Property	Value	Units
Outer Diameter	$1 * 10^{-1}$	<i>m</i>
Thickness	$8 * 10^{-3}$	<i>m</i>
Cross-sectional Area	$2.31 * 10^{-3}$	m^2
Moment of inertia	$2.46 * 10^{-6}$	m^4
Length of beam	3	<i>m</i>
Mass of the beam	54.45	<i>kg</i>
Gravity	9.81	m/s^2
Mass per length	18.15	kg/m

The sub-cases are considered to fully understand how different loading conditions and change in cross-section affect the behavior of the system. In this chapter, theoretical and FEM analysis will be shown for only sub-case 1. However, results will be compared for all the three sub-cases in Section 4.3. Appendix E.3 contains the individual loads and results for sub-cases 2 and 3. Next, in Figure 4.6 we will see the loads acting on sub-case 1.

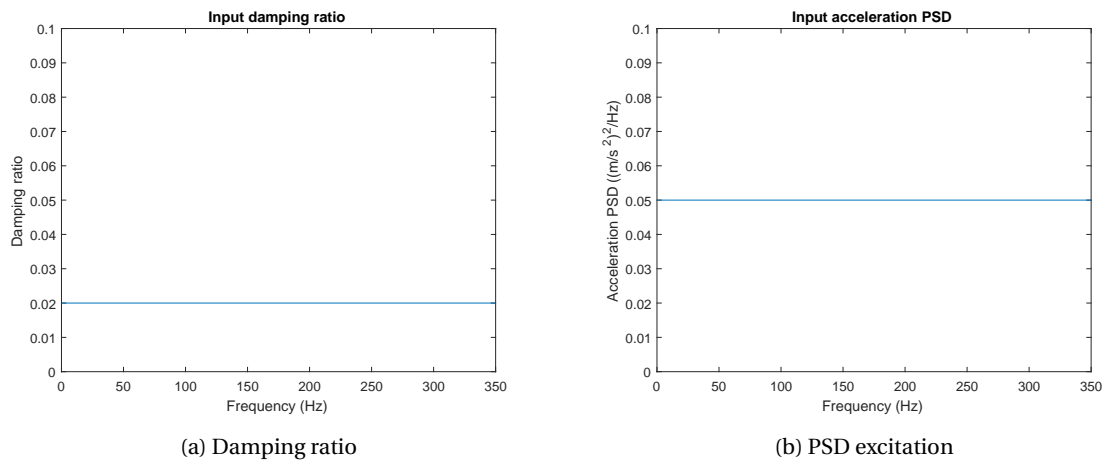


Figure 4.6: Inputs for cantilever beam model with single PSD

Additional inputs required for theoretical calculations will be discussed in the Section 4.2.

4.1.3. CANTILEVER BEAM MODEL WITH TWO PSD

The cantilever beam model used for the verification is shown in Figure 4.7. The geometric details are the same as listed in Table 4.3.

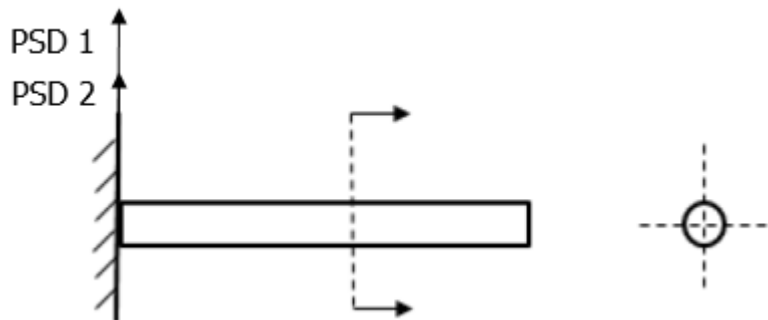


Figure 4.7: Cantilever beam model with two PSD

Similar to previous case with single PSD, case 3 is also further divided into similar three sub cases listed below.

1. Cantilever beam with circular cross-section and constant PSD load.
2. Cantilever beam with circular cross-section and varying PSD load.
3. Cantilever beam with square cross-section and constant PSD load.

Only sub-case 1 will be discussed in this section and loads and result for remaining two sub-cases are shown in Appendix E.3. Figure 4.8 shows the inputs required for the analysis.

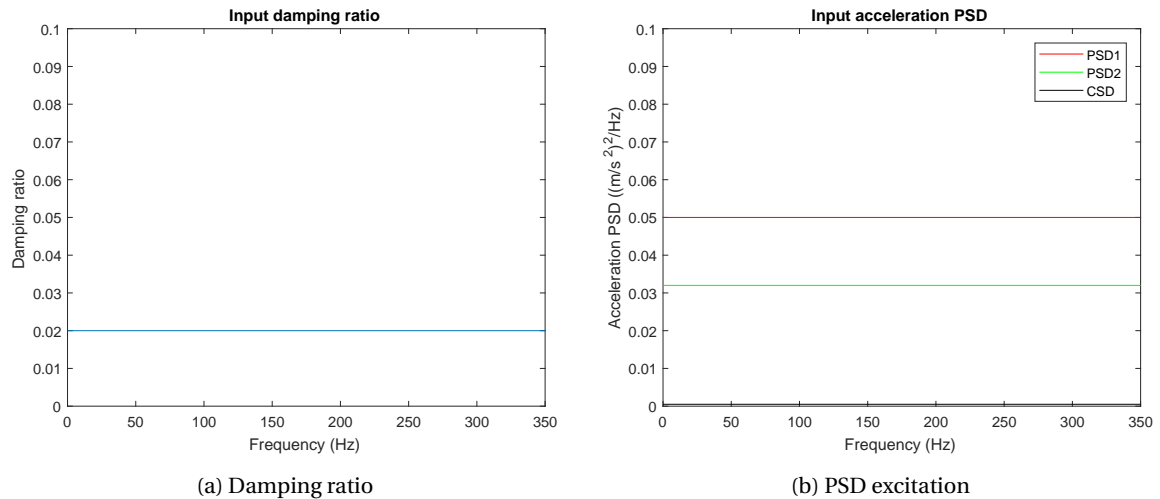


Figure 4.8: Inputs for cantilever model with two PSDs

When two different PSDs acts on the system at the same time, a relation between these two PSDs also has to be provided as an additional input to the FEM analysis. Cross Spectral density (CSD) provides this relation in terms of amplitudes and phase difference at each frequency between the two PSDs. Cross Spectral density is explained in detail in Appendix C.4. The models and the loads acting on them have been discussed and in the next section will deal with the application of these loads for calculating the response of the models using theoretical calculations and FEM.

4.2. ANALYSIS OF VERIFICATION MODELS

In this section we will discuss on how all the models are analyzed, both using theoretical calculations and in FEM environment using Nastran. For theoretical analysis, all the relevant calculations will be discussed in the section along with FEMAP models. Individual model results and their comparison are listed in Section 4.3.

4.2.1. CANTILEVER BEAM WITH MASS ATTACHED AT FREE END

The research methodology has been discussed in detail in Section 3.1 and it is important to first calculate natural frequency of the model. Since the model here is a simple mass spring-damper system, only the first natural frequency is enough to efficiently compute the effective dynamic response. The model is a cantilever beam with a load attached at it free end, and to calculate the first natural frequency, formula for static deflection can be used given in Equation 4.2 [39].

$$Y_{st} = \frac{WL^3}{3EI} \quad (4.2)$$

Where Y_{st} is the static deflection, W is the weight at the free end, L is the beam length and E & I are Young's

modulus and moment of inertia of the beam. Using the static deflection, the first natural frequency is calculated using Equation 4.3.

$$F_n = \frac{1}{2\pi} \sqrt{\frac{g}{Y_{st}}} \quad (4.3)$$

Where F_n is the first natural frequency and g is the acceleration due to gravity. The dynamic response of a SDOF model can be estimated using Mile's equation presented by John. W Miles in 1954 [40]. Although the formula has some assumptions, it can be used to estimate the value of RMS acceleration and RMS displacement at the free end using formulae 4.4 and 4.5 respectively [40].

$$G_{RMS} = \sqrt{\frac{\pi F_n Q ASD_{input}}{2}} \quad (4.4)$$

Where, G_{RMS} is the RMS acceleration output in terms of G at the free end, Q is transmissibility at F_n (depends upon critical damping ratio) and ASD is the input acceleration PSD given to the system in terms of g^2/Hz .

$$Y_{RMS} = \sqrt{\frac{Q ASD_{input}}{32 \pi^3 f_n^3}} \quad (4.5)$$

Where Y_{RMS} is the RMS displacement output, here the unit of ASD input is $(m/s^2)^2/Hz$. The G_{RMS} , Y_{RMS} and F_n are calculated as per Equations 4.4, 4.5 and 4.3 and these are compared with the Nastran results. Matlab code is used for calculating the output RMS values is attached in Appendix D.1.

Next we will look at the equivalent FEMAP model as shown in Figure 4.9.

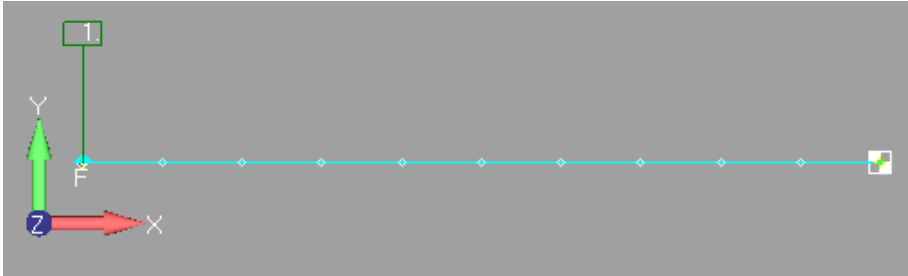


Figure 4.9: FEMAP SDOF model

Figure show the cantilever model with a mass attached at free end, this is achieved by adding a mass property and assigning the property at the node. The mass property requires only one input which is the mass in kg. A fix constraint is given at the other end and acceleration PSD load is applied at the node. The G_{RMS} and Y_{RMS} values are calculated at the free end in FEMAP and the results are compared with theoretical results shown in Section 4.3.

4.2.2. CANTILEVER BEAM MODEL WITH SINGLE PSD

For all the sub-cases, the dynamic displacement response PSD at the free end of the cantilever beam is calculated using available theoretical formula and compared with the results obtained from FEMAP. A MATLAB code written for theoretical calculation attached in Appendix D.2. Again, the first task is to calculate the natural frequencies of the cantilever beam model. For a cantilever beam, natural frequencies can be calculating using theoretical formula shown in Equation 4.6 [41]. For verifying the results, natural frequencies at first four modes are calculated both in and used for calculating dynamic response of the beam.

$$\omega_n = \beta_n^2 \sqrt{\frac{EI}{\rho}} \quad (4.6)$$

Where, ω_n are the natural frequencies of the system, E is the Young's modulus, I is area moment of inertia, ρ is the mass per unit length and β_n is a constant whose values depend upon the mode number and are provided in [41]. The value of β_n for first four modes are 1.875, 4.694, 7.854 and 10.995 [41]. The second output which is calculated is the maximum value of dynamic displacement response PSD at the free end of the beam. For frequency analysis the output response PSD is related to the input PSD using relation shown in Equation 4.7 [37].

$$PSD_{response}(\omega) = |H(\omega)|^2 \times PSD_{input}(\omega) \quad (4.7)$$

Where $H(\omega)$ is the complex transfer function relating the input PSD to the output response PSD of the system, explained in Subsection 3.1.2. In this case, the input PSD is acceleration and the output response is displacement. The formula to calculate the transfer function for this particular input-output relation is shown in Equation 4.8. This equation is derived in [41] and for the purpose of this research, is directly used.

$$H(\omega) = \sum_{n=1}^m \frac{-\Gamma_n Y_n}{(\omega_n^2 - \omega^2) + 2i \zeta \omega_n \omega} \quad (4.8)$$

Where m is the total number of natural frequencies (here $m = 3$), Γ_n is the participation factor of ω_n , Y_n is the eigenvector corresponding to ω_n and ζ is the damping ratio (here, $\zeta = 0.02$). Γ_n and Y_n are calculated using Equations 4.9 and 4.10 respectively [41].

$$\begin{aligned} \Gamma_1 &= 0.783 \sqrt{\rho L} \\ \Gamma_2 &= 0.4339 \sqrt{\rho L} \\ \Gamma_3 &= 0.2544 \sqrt{\rho L} \\ \Gamma_4 &= 0.1818 \sqrt{\rho L} \end{aligned} \quad (4.9)$$

$$Y_n = ((\cosh(\beta_n) - \cos(\beta_n)) - 0.7341(\sinh(\beta_n) - \sin(\beta_n))) \sqrt{\rho L} \quad (4.10)$$

For Y_n , β_n values are the same as used in Equation 4.6. Maximum displacement response is calculated and the results are compared with FEMAP results. Figures 4.10 shows the cantilever beam model in Nastran modelled using beam elements.



Figure 4.10: FEMAP cantilever beam model

In FEMAP, the dynamic displacement response is calculate using 'Random response analysis' which automatically calculates the transfer function and multiplies it by the input PSD load to calculate the output response PSD. From the nature of loading, which is an assumed flat acceleration PSD, the maximum expected response should be achieved at the first natural frequency of the cantilever beam. Also, the output displacement response at all other frequencies will be zero or close to zero as frequency analysis provides output only around the natural frequency of the system.

4.2.3. CANTILEVER BEAM MODEL WITH TWO PSD

When more than one PSD are applied on a structure, it is important to understand the relation between two PSDs. The relation between two PSDs can be expressed as the ‘Correlation coefficient (ρ)’, which has values between ‘1’ and ‘-1’ [42]. Correlation in physical terms can be explained by considering two separate signals ‘x’ and ‘y’, depending upon how each of the signals vary with respect to time ‘t’, the correlation coefficient between the two signals ρ_{xy} will always have values between ‘1’ and ‘-1’. When $\rho_{xy} = 1$, it means that both the signals are completely correlated. A complete correlation means that both the signals increase and decrease at the same time and have the same amplitude for the entire cycle. If two signals are applied in the same axis, there will always be correlation between them. The value of correlation will depend on the amplitude and nature of the two signals. On the other hand when $\rho_{xy} = 0$, signals are uncorrelated, this can only happen when signals are applied in different axes. For example, if signal ‘x(t)’ is applied in X-direction of the structure and ‘y(t)’ is applied in Y-direction, there is no chance for either of the signals to influence each others outcome, and then the signals are said to be uncorrelated. Completely uncorrelated signals can be analyzed by applying one signal at a time and calculate output [42]. Signals having ρ between ‘0’ and ‘+1’ are positively correlated or the relation between them is direct and for values between ‘-1’ and ‘0’, signals are negatively correlated and the relation between them is indirect or inverse. For this research, considering the research objective, completely correlated signals having $\rho = 1$ are used.

There is no available literature which explains theoretically the behavior of a cantilever beam subjected to two different power spectral densities. However, after carrying out some trial analysis, it was clear that a certain behavior pattern is followed when the model was subjected to two different PSD’s. When two PSD’s acts on a model, the resultant response was a combination of PSD’s acts independently according to below expression.

$$PSD_{response}(Total) = PSD_{response}(PSD1) + PSD_{response}(PSD2) + 2 * PSD_{response}(CSD) \quad (4.11)$$

where $PSD_{response}(Total)$ is the total response of the structure when subjected to two PSD’s. $PSD_{response}(PSD 1)$ and $PSD_{response}(PSD 2)$ is the response of the structure due to PSD 1 and PSD 2 respectively. $PSD_{response}(CSD)$ is the response due to cross-spectral density which gives the relation between PSD 1 and PSD 2. Simply explained, it provides details on how two different PSD’s are related to each other across the frequency domain in terms of amplitude and phase difference. More literature on cross-spectral density is available in Appendix C.4, but for the purpose of verification the input values are assumed. All the three values, PSD 1, PSD 2 and CSD are provided as inputs to FEMAP to calculate the dynamic displacement response PSD at the free end of the cantilever beam. The theoretical displacement response is calculated for individual load (PSD1, PSD2 and CSD) separately and then combined together using the relation in Equation 4.11 and in FEMAP the total PSD displacement response ($PSD_{response}(Total)$) is directly calculated. Like the analysis with single PSD load, the result of maximum displacement response at the first natural frequency of the cantilever beam calculated from FEMAP and theory are compared in Section 4.3. In the next section we will compare results from theoretical analysis with FEMAP outputs and discuss on the findings.

4.3. RESULTS OF THE VERIFICATION MODELS

In this section, results for all the verification models will be compared and discussed. Relative error for each of the output results for the models will also be calculated considering theoretical results calculated as the basis and using the formula in Equation 4.12.

$$\% \text{ RelativeError} = \frac{\text{Output}_{theoretical} - \text{Output}_{Nastran}}{\text{Output}_{theoretical}} \times 100 \quad (4.12)$$

Relative errors within 10% are assumed to be reasonable as discussed with Allseas and the verification can be said to be successful.

4.3.1. CANTILEVER BEAM WITH MASS ATTACHED AT FREE END

The outputs are calculated as discussed in Section 4.2 and the results are compared in Table 4.4.

Table 4.4: Output results of SDOF system

Output	Theory	Nastran	% error
Natural Frequency (Hz)	0.006	0.006	-
$G_{RMS}(m/s^2)$	0.1089	0.1088	0.09
$Y_{RMS}(m)$	75.61	75.9	0.3

From the above results we can concluded that the application of PSD input in Nastran for a SDOF model is correct as the percentage error is well below 10%. Next we will look at the output results for cantilever model with single PSD load.

4.3.2. CANTILEVER BEAM MODEL WITH SINGLE PSD

First, the results of modal analysis will be shown. Natural frequencies for sub-case 1 and 2 are going to be same as the boundary conditions and geometric properties are the same. The results of first three modes are calculated from theoretical formula and Nastran and are shown in Figure 4.11.

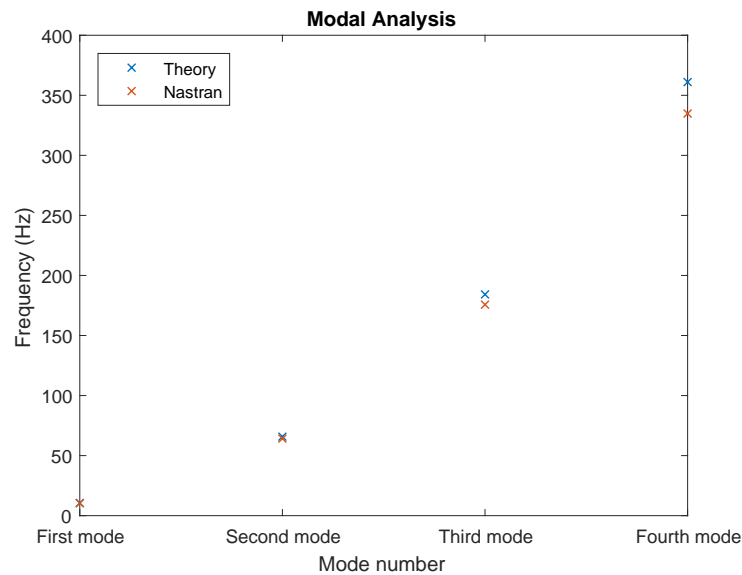


Figure 4.11: Modal Analysis

Table 4.5: Comparison of Modal analysis for single PSD

Circular cross-section	
Mode Number	% error
1	0.65
2	2.46
3	4.61
4	7.38
Square cross-section	
Mode Number	% error
1	0.5
2	1.8
3	3.19
4	4.79

The results of first three modes for sub-case 3 calculated from theory and Nastran is shown in Appendix, Fig-

ure E.9. Table 4.5 shows the comparison of results of natural frequencies calculated using theoretical formula and Nastran for all the sub-cases along with the relative error between them. Next, the maximum displacement response PSD at the free end of the cantilever beam for sub-case 1 is shown in Figure 4.12. The results for sub-case 2 and 3 are shown in Appendix E.3.

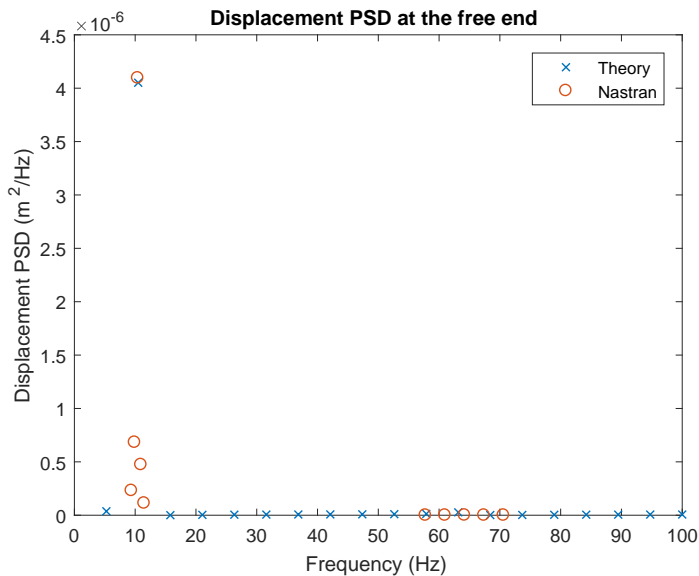


Figure 4.12: Displacement response PSD for sub-case 1 - Single PSD

The theoretical results are calculated at the input frequencies, however, in Nastran, to improve results, more frequencies around the first natural frequency are added. The maximum displacement response is compared in Table 4.6.

Table 4.6: Comparison of maximum displacement response PSD - Single PSD

Maximum response PSD	Theory (m^2/Hz)	Nastran (m^2/Hz)	% error
Sub-case 1	$4.05 * 10^{-6}$	$4.1 * 10^{-6}$	1.09
Sub-case 2	$1.2 * 10^{-6}$	$1.3 * 10^{-6}$	8.47
Sub-case 3	$4.98 * 10^{-5}$	$5 * 10^{-5}$	0.42

Comparing the results in Tables 4.5 and 4.6, we can concluded that the PSD application for a cantilever beam model with single PSD is correct as the percentage error is within 10%. Now, we will look at the results of cantilever beam with two PSD's.

4.3.3. CANTILEVER BEAM MODEL WITH TWO PSD'S

For this case, the results of modal analysis are the same as that shown in Table 4.5 as the boundary conditions and geometrical properties are the same for all the sub-cases. We can therefore directly compare the results of maximum displacement response PSD at the free end of the cantilever beam. For the sub-case 1, the displacement response PSD is shown in Figure 4.13, for remaining two sub-cases, the results are shown in Appendix E.3.

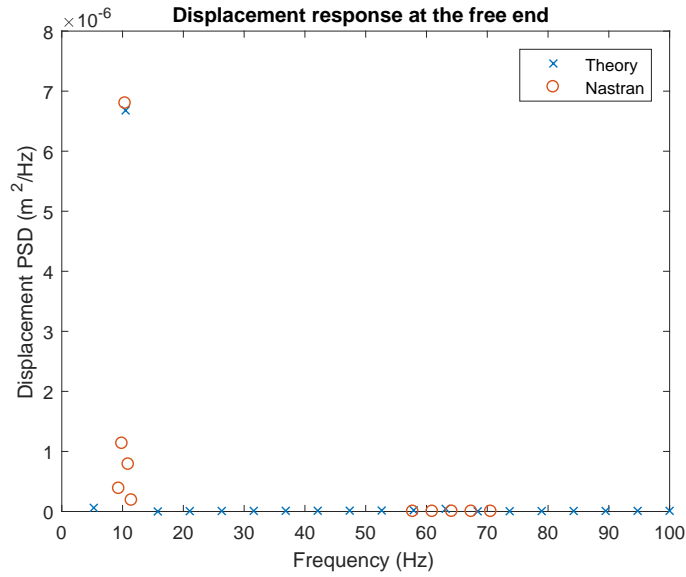


Figure 4.13: Displacement response PSD for sub-case 1 - Two PSD

Table 4.7 shows the comparison of maximum displacement response at the free end for all the three sub-cases.

Table 4.7: Comparison of maximum displacement response PSD - Two PSD

Maximum response PSD	Theory (m^2/Hz)	Nastran (m^2/Hz)	% error
Sub-case 1	$6.68 * 10^{-6}$	$6.8 * 10^{-6}$	1.8
Sub-case 2	$6.42 * 10^{-6}$	$6.73 * 10^{-6}$	4.81
Sub-case 3	$8.49 * 10^{-5}$	$8.29 * 10^{-5}$	1.29

As seen from the above results, the percentage error is within acceptable limits of 10%, hence, it can be concluded that application of PSD on cantilever model with two PSD is correct and successful.

4.4. CONCLUSION

From the comparison of the results in previous section, it is clear that the application of single and two PSD in FEMAP is correct. However, the results for varying loads (sub-case 2) for cantilever beam model with single PSD is having a higher error percentage than other sub-cases. The reason for this is unknown as the analysis follows the same procedure for all the sub-cases, so technically FEMAP results should match the theoretical results. Also, additional analysis were also conducted by changing the loads, but error more than 6% were still observed. The expression used to calculate total displacement response PSD for cantilever beam with two PSD's shown in Equation 4.11 has no theoretical background and is only based on logic. However, when the results were compared with FEMAP, good accuracy is observed. Having said that, the author feels that the expression should be verified through experiments if it has to be used for actual analysis on the stinger model. Up till now, the models are analyzed in FEM with no verification of fatigue damage calculation using Dirlik's method. In the next chapter, we will analyze the models completely (including damage calculation) and verify the damage results with equivalent time domain analysis.

5

DAMAGE CALCULATION - RESULTS

As discussed at the end of Chapter 4, this chapter will discuss on the application of the overall methodology described in Chapter 3 on cantilever beam and simple frame model. Damage value results calculated using frequency analysis is verified by conducting equivalent time domain analysis with rainflow counting method. Figures 5.1 and 5.2 below shown the overall process flow which is followed for time and frequency domain analyses.

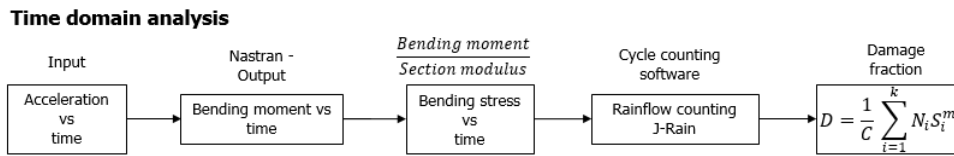


Figure 5.1: Fatigue damage calculation of cantilever beam - Time domain analysis

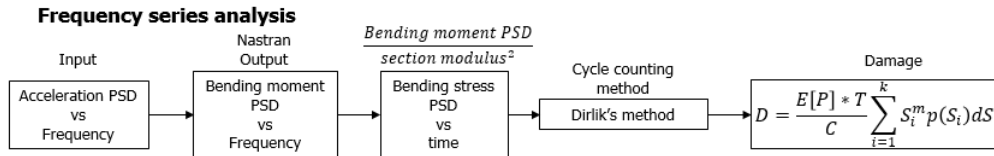


Figure 5.2: Fatigue damage calculation of cantilever beam - Frequency domain analysis

The analysis in time and frequency domain is conducted in FEMAP and the damage values are calculated in both the analysis for comparison. As seen from Figure 5.1, rainflow counting is conducted using an open source software called as 'J-Rain'. To establish its feasibility, the results from J-Rain is compared with hand calculation for a simple stress cycle shown in Appendix E.2. The output of J-Rain is number of cycles and stress ranges, however, the number of cycles calculated using Dirlik's method are rarely equal to the values obtained from rainflow counting method [34]. Thus, the comparison of time and frequency domain analysis will be based on the damage calculation using Equations 5.1 and 5.2 respectively.

$$D = \frac{1}{C} \sum_{i=1}^k N S_i^m \quad (5.1)$$

$$D = \frac{E[P] T}{C} \sum_{i=1}^k p(S_i) S_i^m ds \quad (5.2)$$

where k is the number of divisions of stress range S , N is the number of cycles of stress ranges calculated using rainflow counting method. $E[P]$ is the expected number of peaks calculated using spectral moments shown in Equation 3.8 and T is the total time in seconds. $p(S)$ is the probability density function of stress range calculated using Dirlik's method given in Equation 3.16, dS is the stress range increment. m is the Basquin exponent of the S-N curve and for steel and single slope S-N curve, it is equal to '3'. Basquin constant C is a constant based on selected S-N curve and its value for both the models is different as listed in Table 5.1.

Table 5.1: Basquin constant values for models

Models	Value
Cantilever beam	$10^{14.88}$
Frame	$10^{12.48}$

For cantilever beam model, there are no welded joints and hence, the value of C is taken from Eurocode EN-1993:1:9 [43] for weld category 140, the selected S-N curve is approximately equal to 'B2' S-n curve from DNVGL [1]. For frame model, welded tubular joints are analyzed and hence, the value of C is selected from T-curve in DNVGL-RP-C203 [1] for tubular joints in air. We will start with the analysis and discussion on the results of cantilever beam.

5.1. CANTILEVER BEAM MODEL

The cantilever beam model is shown in Figure 5.3, it has the same material and cross-sectional properties as listed in Tables 4.1 and 4.3 respectively. To verify the overall frequency domain approach suggested in this research, we will first analyze the cantilever model using a single load in Subsection 5.1.1 and then applying two loads in Subsection 5.1.2.

5.1.1. APPLICATION OF A SINGLE LOAD

In this subsection we will discuss the results of application of a single acceleration load at the fixed location of a cantilever beam model both in time and frequency domain and compare the damage results. In order to fully understand the proposed methodology, the cantilever beam is subject to two different loading conditions which are listed below.

1. Periodic load (sine load).
2. Random load (Gaussian distributed).

Different loading conditions are selected to take into account for both the narrow band (sine loads) and broad band (random loads) processes. Using this approach, we will be able to analyze and compare results of Dirlik's method for different types of loads. Next, we will look at the model of the cantilever beam followed by the analysis and results for different loading conditions.

MODEL:

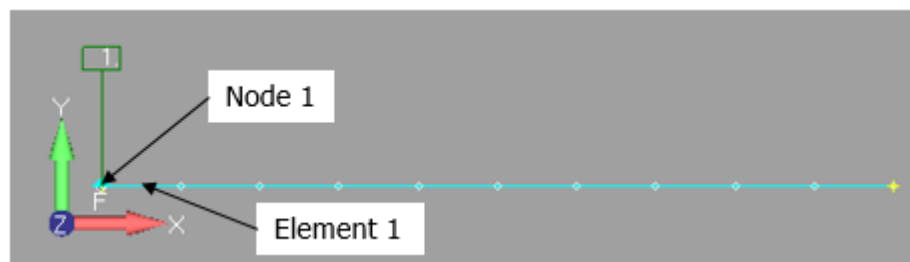


Figure 5.3: Cantilever beam model

Figure 5.3 shows the cantilever model fixed at Node 1. All the loads are applied at Node 1 in Y direction. Bending moment is calculated for Element 1, EndA and will be used to calculate nominal bending stress. Damage is calculated based on nominal stress approach in both time and frequency analysis using Equations 5.1 and 5.2. First, it is important to calculate the natural frequencies of the cantilever beam. Natural frequencies are calculated in FEMAP and a list of Natural frequencies are given below.

Table 5.2: Natural frequencies of the model

Number	Value (Hz)
1	10.43
2	64.18
3	175.7
4	334.38

The theoretical calculation of natural frequencies of cantilever beam has already conducted in Section 4.2 and the results were compared in Section 4.3. The above four natural frequencies are chosen as they together contribute more than 90% of mass of the beam in Y direction. This is an important parameter to be considered to obtain accurate dynamic results of the structure [28], as discussed in Subsection 3.1.3. All time history acceleration loads are assumed and are calculated for different load cases for total period of 60 seconds. Equivalent acceleration power spectral density (PSD) loads are calculated using Fast Fourier transform (FFT) for a frequency range of 0 Hz to 350 Hz , to accommodate all the four natural frequencies. A MATLAB code is available in Appendix D.3 which converts time series into equivalent PSD series. We will start with the analysis of periodic loads. A damping ratio of 0.02 is assumed across the frequency range [27] for all analyses.

PERIODIC LOAD

For this load case, two sub-cases are analyzed, only one of the analysis is discussed here and the inputs and results of the other is shown in Appendix E.4. The first sub-case involves a sine load in time domain consisting of a single frequency (10.43 Hz). The second sub-case involves a sine load combining first three natural frequencies of the beam model and its loads and the results are shown in Appendix E.4. Sine waves with frequencies close to the natural frequencies of the beam are selected for both the sub-cases purposely in order to resonant the model and calculate the response effectively. Figure 5.4 shows acceleration load in time and frequency domain which will be used for the analysis with a single dominant frequency. Time domain sine load with single frequency is mathematically given by Equation 5.3.

$$load = A \sin(2\pi f t) \quad (5.3)$$

Using above equation, a sine load is created having amplitude 'A', frequency 'f' and total time 't'. For periodic load with a single sine load, frequency is equal to 10.43 Hz and total time is 60 seconds. In Figure 5.4, only a part of acceleration vs time load shown, for acceleration PSD vs frequency, it is seen that only one frequency is dominant throughout the range. These two loads along with a constant damping ratio of 0.02 throughout the frequency range are given as input to the model and analyzed using two different analysis. 'Transient time history analysis' is used for acceleration vs time load and 'Random response analysis' is used for acceleration PSD vs frequency load. As discussed earlier, bending moment at element 1 is calculated for both the analyses. Figure 5.5 shows the output bending moment calculated for both time and frequency analyses.

Bending moment results shown for frequency analysis in Figure 5.5 contain a lot of points around the dominant natural frequency. This is intentionally done as per suggestion mentioned in Subsection 3.1.3, to achieve good accuracy in the results. Figure 5.6 shows the impact of considering less number of points around the interested frequency. In Figure 5.6, a comparison is shown on the impact of bending moment PSD results by considering less and more number of output frequencies.

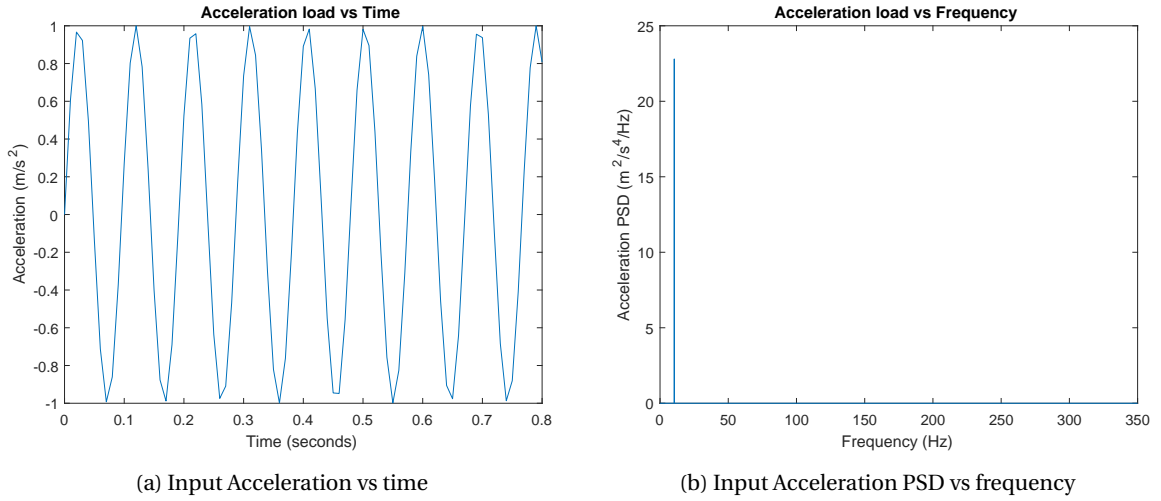


Figure 5.4: Input acceleration load – Single frequency periodic load

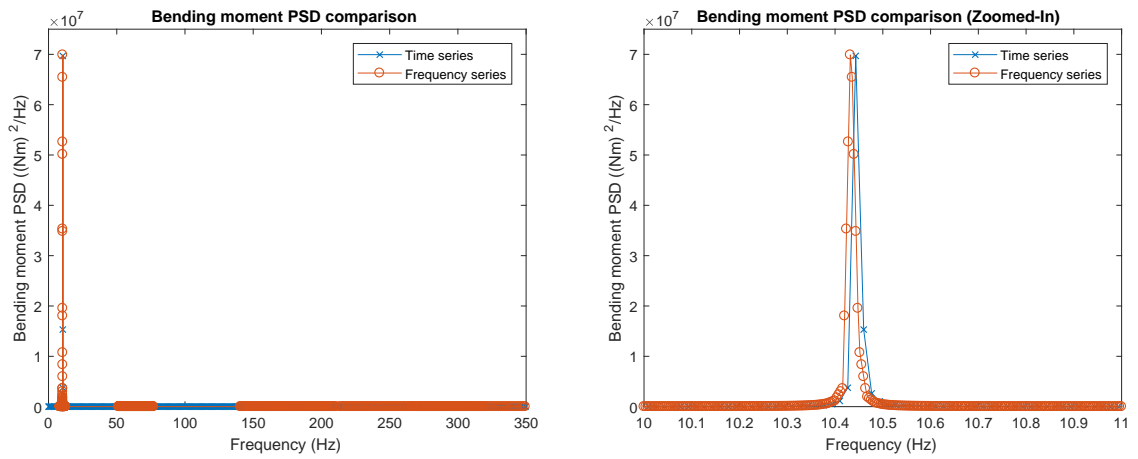


Figure 5.5: Bending moment PSD – Single frequency periodic load

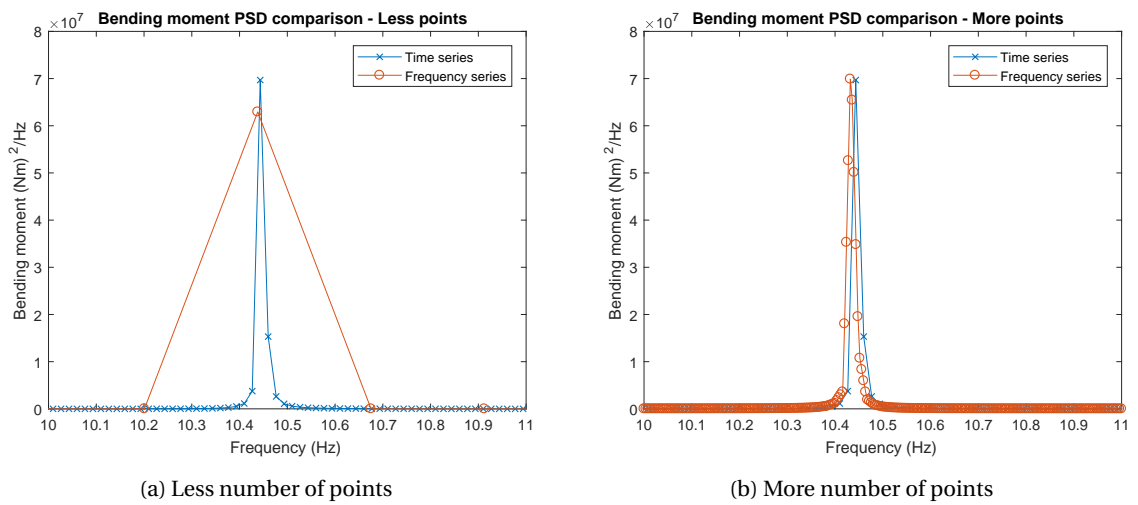


Figure 5.6: Bending moment PSD comparison

In Figure 5.6 (left), the total number of points surrounding the peak frequency is ‘3’, and in Figure 5.6 (right), the number of points have been increased to ‘126’. The difference in the results is quite high and as we know for PSDs, the area under the curve is an important parameter, selecting appropriate number of output points around the expected peak is essential. This is one of the reasons we conduct modal analysis before structural analysis for frequency domain. Modal analysis gives us information on which frequencies will be critical for the analysis, so that we can suitably chose enough output points surrounding it.

In Figure 5.5, time series bending moment result obtained from transient time history analysis is converted to equivalent frequency domain using Fast Fourier transform. This is done for suitable comparison of bending moment results. As there are a lot of uncertainties involved in converting frequency domain results into time domain due to absence of phase information in PSD results, time domain results are converted. Form the graphs it is clear that the results match well, hence it can be concluded that the analysis conducted in Nastran is correct. Additional, a check can be performed at this stage of the analysis to further verify the bending moment PSD results calculated in time domain and frequency domain. This can be done by calculating the area under both the bending moment PSD results, which should almost be equal to each other. The main reason behind this is, analyses in time and frequency domain are essentially the same but conducted under different domains, so the value of output bending moment results should also be very close. Since, we are comparing PSD results, area under the two PSD curves is more important than the peak amplitude values as discussed in Subsection 3.1.1. The results of area under PSD for both the sub-cases is listed in Table 5.3.

Table 5.3: Bending moment PSD (Periodic load) - Area calculation

Sub-case	Area under PSD $(Nm)^2$	
	Time series	Frequency series
One frequency	$1.621 * 10^{06}$	$1.629 * 10^{06}$
Three frequencies	$1.81 * 10^{05}$	$1.83 * 10^{05}$

Results in Table 5.3 show good comparison and hence we can proceed with calculating fatigue damage using Dirlik’s method. This check will now be performed on each of the analyses conducted in this chapter, as it avoids any additional calculations if the outputs of FEMAP do not match. In Figure 5.7, similar comparison is conducted for bending stress but without calculating the area. Time series bending stress is converted to frequency series and compared with bending stress PSD calculated by diving bending moment PSD with square of sectional modulus, the resulting bending stress PSD is shown in Figure 5.7.

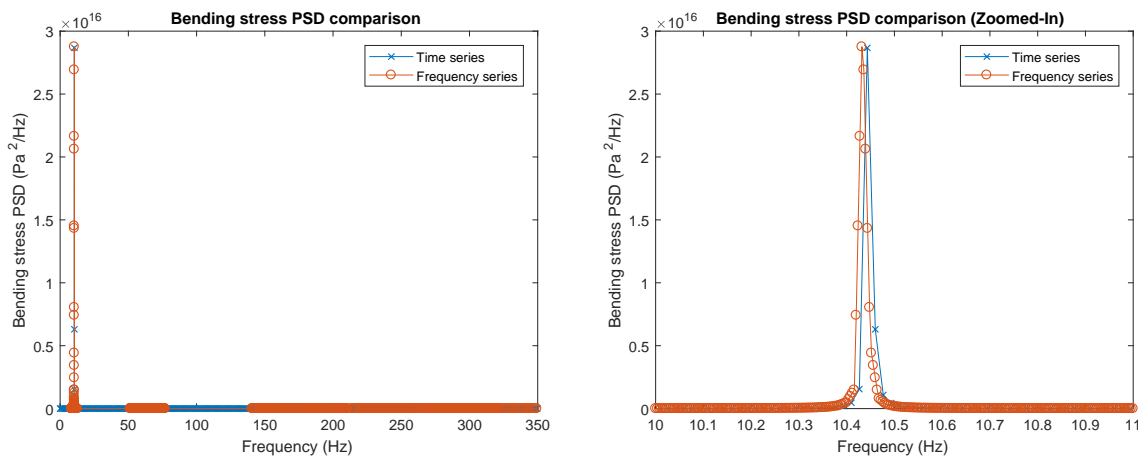


Figure 5.7: Bending stress PSD – Single frequency periodic load

As seen from Figure 5.7, bending stress values also match. From bending stress values, damage is calculated using Rainflow counting (RF) for time domain analysis and using Dirlik’s method for frequency domain analysis and the values are compared in Table 5.4 for both the sub-cases.

Table 5.4: Damage calculation – Periodic loads

Analysis	Damage	% error (RF)
One frequency		
Time domain analysis	$3.23 * 10^{-07}$	-
Frequency domain analysis	$4.31 * 10^{-07}$	33.31
Three frequencies		
Time domain analysis	$1.39 * 10^{-08}$	-
Frequency domain analysis	$1.85 * 10^{-08}$	32.88

From the Table 5.4, percentages error are calculated with respect to results of time domain analysis. From the results we can see that, the difference between time analysis and frequency analysis is 33.31% and 32.88%, which is on a higher side. Similar results have been achieved in literature [34] where difference in damage fraction ($D * C$) result of time domain and frequency domain analysis is more than 30%. In the paper [34], comparison is conducted on the damage fraction ($D * C$) calculated for sum of sine waves (in-phase and out of phase), both yielding results with difference above 30% when compared to rainflow counting results. In conclusion, I agree with the author of [34], that Dirlik's method is not suitable for calculating damage of periodic loads. The main reason for such a difference is, the Dirlik's method was never meant to calculate damage for periodic loads [34]. Dirlik's method was specifically formulated to calculate damage due to stationary ergodic random processes [32]. However, the fatigue damage predicted from Dirlik's method is conservative for both periodic loads and the results can still be used to as reference during early stages of design. To verify Dirlik's method with rainflow counting, stationary ergodic process have to be used consisting of random numbers following Gaussian distribution.

RANDOM LOADS

Random loads with Gaussian distribution with mean equal to zero and standard deviation values of 0.333 and 1 are considered for analysis as sub-case 1 and sub-case 2 respectively. A standard deviation of 0.333 is selected to achieve 99.7% of values within the range of $[-11]$ and standard deviation of 1 is selected randomly. The random number are converted to equivalent Gaussian white noise using MATLAB code given in Appendix D.3. A Gaussian white noise frequency load is selected for the analysis as the results can be compared with the results found in literature [34]. Figure 5.8 shows the input load in time and frequency domain analysis for sub-case 1. Similar to analysis for periodic loads, bending moment at Element 1 is calculated and results are compared as shown in Figure 5.9. For sub-case 2, the loads and the results are shown in Appendix E.4. A check is performed by comparing area under bending moment PSD results from time and frequency domain analyses shown in Table 5.5. As the values of area under bending moment PSDs are comparable, bending stress PSD is calculated and compared for time and frequency analyses shown in Figure 5.10 and damage values are calculated are compared in Table 5.6

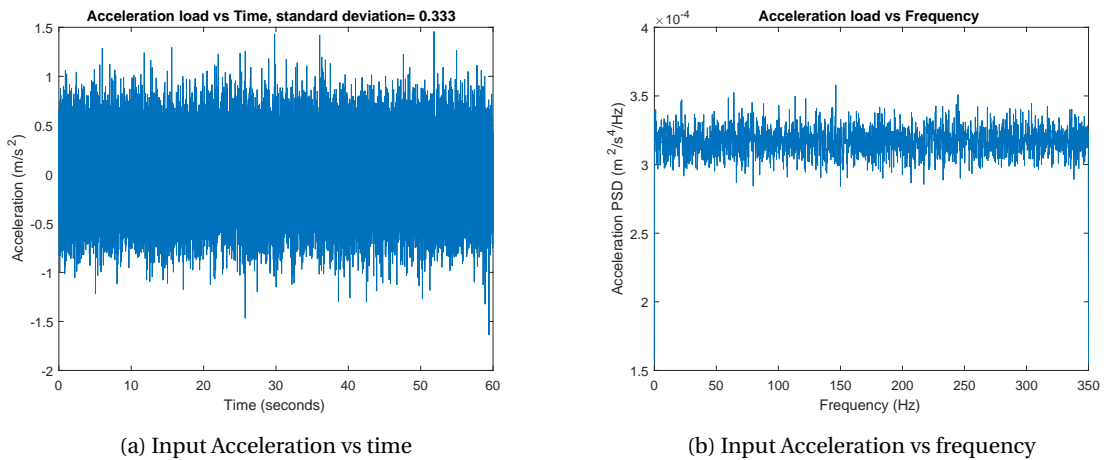


Figure 5.8: Input acceleration load – Standard Deviation = 0.333

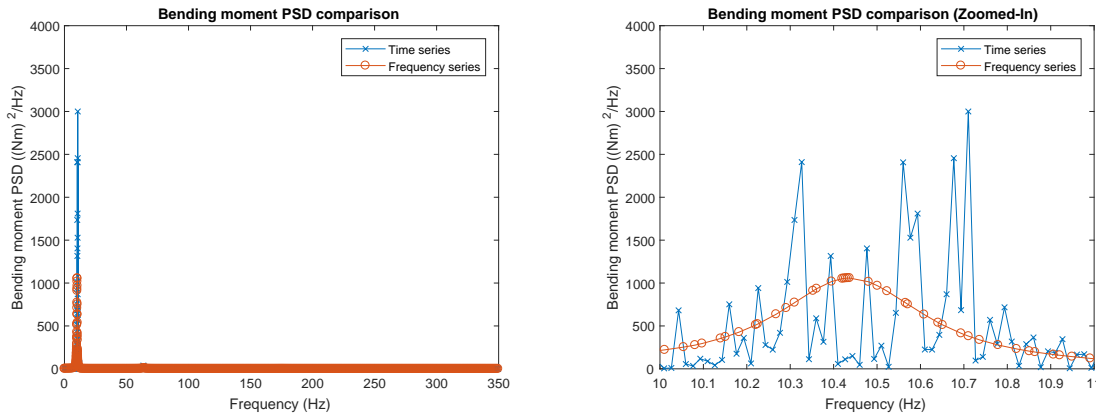


Figure 5.9: Bending moment PSD – Standard Deviation = 0.333

Table 5.5: Bending moment PSD (Random loads) - Area calculation

Sub-case	Area under PSD $(Nm)^2$	
	Time series	Frequency series
Standard Deviation = 0.333	744.44	732.85
Standard Deviation = 1	6.13×10^3	6.57×10^3

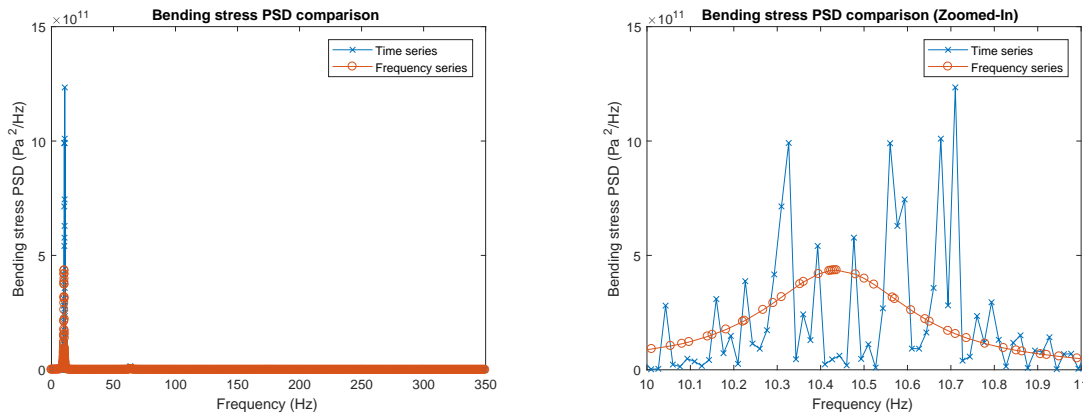


Figure 5.10: Bending stress PSD – Standard Deviation = 0.333

Table 5.6: Damage calculation – Random loads

Analysis	Damage	% error (RF)
Standard deviation = 0.333		
Time domain analysis	5.55×10^{-12}	-
Frequency domain analysis	5.34×10^{-12}	3.81
Standard deviation = 1		
Time domain analysis	1.33×10^{-10}	-
Frequency domain analysis	1.43×10^{-10}	7.49

From Figure 5.9(b) we can see that the, the bending moment from time series around the natural frequency are higher than those calculated from frequency series but, the area comparison shown in Table 5.5 are very close to each other. Since the area of both the time domain and frequency domain results are almost equal, the resulting fatigue damage fraction shown in Table 5.6 lies within acceptable error limits. Similar results

are also obtained for sub-case 2 with standard deviation of 1. This results are in-line with the results shown in the paper [34], which can help us in concluding that the analysis is valid and verified for Gaussian white noise. With this, we can conclude the application of single PSD on a structure and analyze the cantilever beam model with two PSDs.

5.1.2. APPLICATION OF TWO PSD

In this subsection, we will discuss the results of application of two loads at the base of a cantilever beam in time and frequency domain and compare the resultant damage values. As seen from the results in previous subsection, the damage values for random loads are found to be comparable hence, in this subsection we will first apply random loads on the cantilever model. Analysis will follow the procedure described in flowcharts shown in Figures 5.1 and 5.2 for time and frequency analysis. The material and cross-sectional properties is same as used in previous subsection including the natural frequency result shown in Table 5.2.

Similar to the analysis in previous subsection, both loads are applied at Node 1 of the model and bending moment in Element 1 is calculated for both time and frequency domain analysis, bending stress is calculated using nominal stress approach. Damage results are calculated and compared using rainflow counting (J-Rain) for time domain analysis and Dirlik's method for frequency domain analysis. Similar to analysis with single PSD, a frequency range from 0 to 350 Hz is considered and a constant damping ratio of 0.02 across the frequency range is also considered. Two additional analyses using periodic (sine) loads, one in which the two sine loads are in-phase with each other (completely correlated) and the other with a phase difference of $\pi/2$ (partially correlated) is also carried out, loads and results for the additional analyses are shown in Appendix E.4. Comparison of damage values is shown in Table 5.8 at the end of this subsection.

When more than one PSD is applied on a structure at the same time, an additional input is also provided which is cross power spectral density, more information on cross power spectral density is available in Appendix C.4. For random loads the inputs acceleration and cross spectral density are calculated using the MATLAB code attached in Appendix D.3. The inputs for sub-case 1 (two random loads) are shown in Figures 5.11 and 5.12.

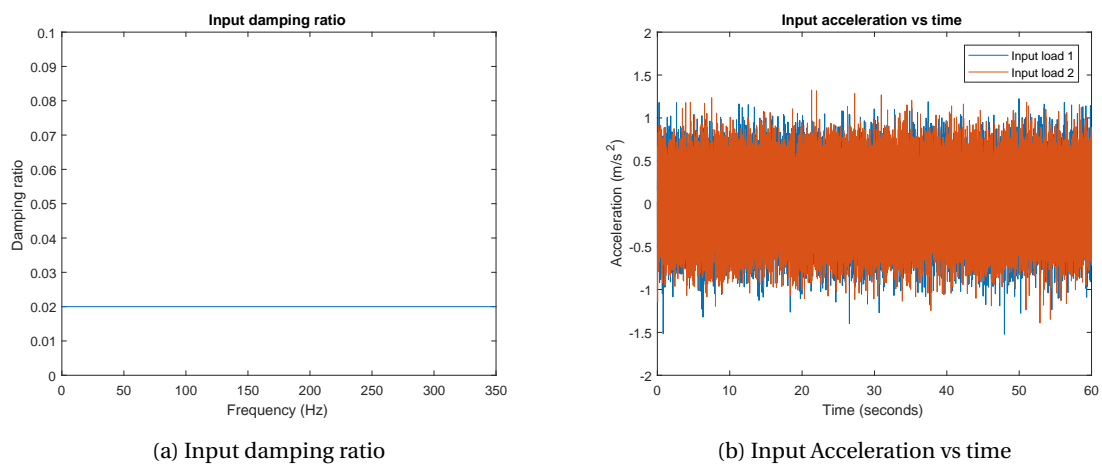
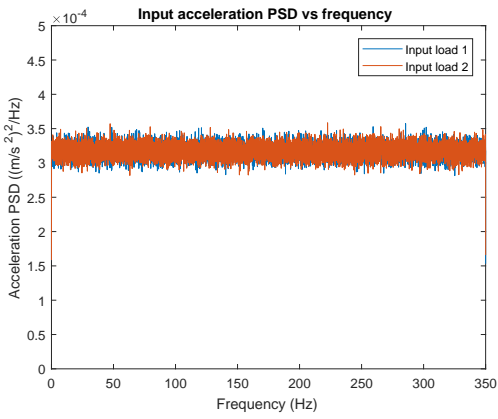
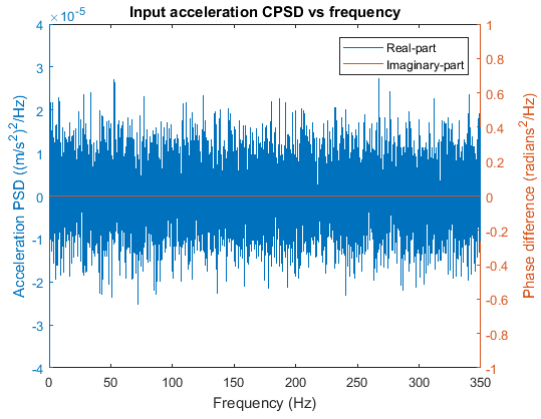


Figure 5.11: Input loads for 2 PSDs - Random loads 1

Similar to analysis in previous subsection, bending moment calculated in time domain analysis is converted to equivalent frequency series using FFT algorithm and compared with the results of obtained from frequency domain analysis. Figure 5.13 shows the comparison between bending moment results of time and frequency domain analysis. An additional check is performed by calculating the area under the bending moment PSD curve for both time and frequency series, similar to previous analysis and the comparison is shown in Table 5.7. As the areas are comparable, bending stresses are calculated and compared as shown in Figure 5.14.



(a) Input acceleration PSD vs frequency



(b) Input cross spectral density

Figure 5.12: Input loads for 2 PSDs - Random loads 2

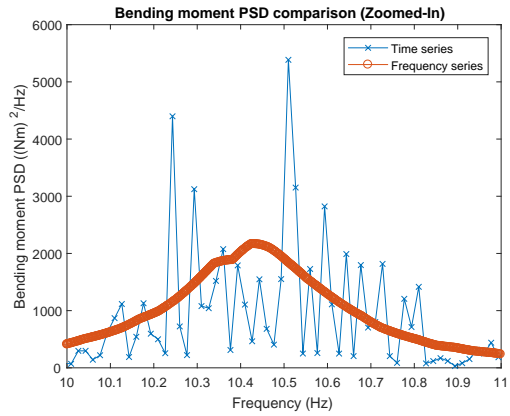
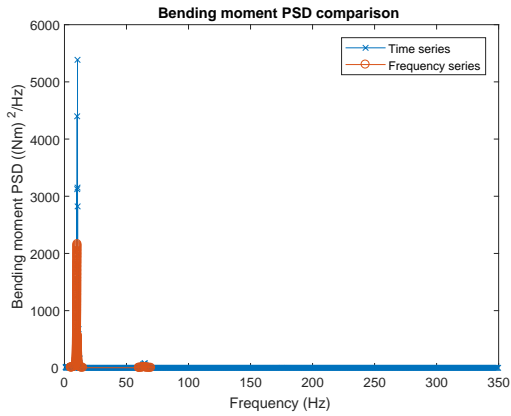


Figure 5.13: Bending moment PSD comparison - 2 PSD (Random loads)

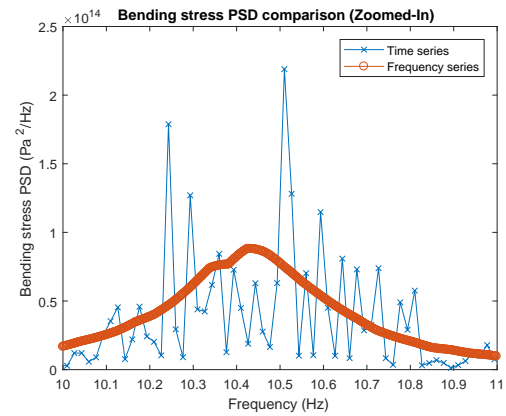
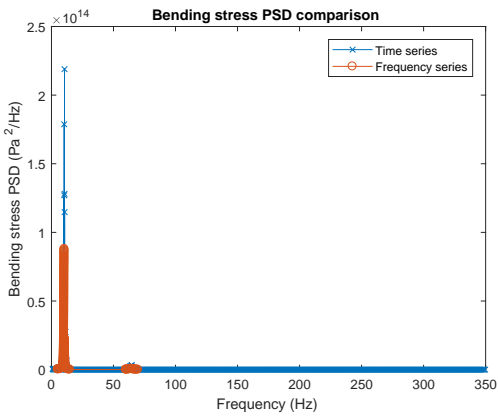


Figure 5.14: Bending stress PSD comparison - 2 PSD (Random loads)

Table 5.7: Bending moment PSD (Two loads) - Area calculation

Sub-case	Area under PSD $(Nm)^2$	
	Time series	Frequency series
Two random loads	$1.378 * 10^{03}$	$1.48 * 10^{03}$
Two periodic loads (in-phase)	$6.48 * 10^{06}$	$6.56 * 10^{06}$
Two periodic loads (out of phase)	$3.24 * 10^{06}$	$3.26 * 10^{06}$

As seen from above Figure 5.14, the peak have different values but as discussed earlier, the value of area under the PSD curve are quite similar, which is important for damage calculation. The fatigue damage results are presented in Table 5.8.

Table 5.8: Damage calculation – 2 PSD

Analysis	Damage	% error (RF)
Random loads		
Time domain analysis	$1.39 * 10^{-08}$	-
Frequency domain analysis	$1.54 * 10^{-08}$	10.76
Periodic loads		
Time domain analysis	$2.54 * 10^{-03}$	-
Frequency domain analysis	$3.43 * 10^{-03}$	34.97
Periodic loads with phase difference		
Time domain analysis	$1.22 * 10^{-04}$	-
Frequency domain analysis	$1.63 * 10^{-04}$	33.38

The percentage error in damage values calculated for random loads using frequency domain analysis is slightly higher than 10%, but it is acceptable as the analysis is only carried out for 60 seconds, which is a small period. If the analysis is conducted for longer time, the results will be much closer. Percentage error for periodic loads is above 30%, similar to what we have seen in all our analyses, confirming that Dirlik's method maybe unsuitable to calculate damage for periodic loads. However, for each analysis, the predicted damage is conservative with respect to rainflow counting and can be useful as a reference during early stages of design. With the results of the different analyses on cantilever beam, we can conclude that, the proposed frequency analysis is successfully verified for cantilever beam. Next, we implement the same analysis procedure on the frame model.

5.2. FRAME MODEL

A line diagram of the frame model selected for the analysis is shown in Figure 5.15a. The frame model is selected, as it is assumed to represent the main stinger model. In Figure 5.15a, the red lines represent the chord and the yellow lines represent brace of the frame model with all free ends constrained using a fixed constraint. Fatigue damage will be calculated in the joint highlighted by the green circle and for the purpose of distinguishing different locations of load applications, the two sides of the model are labeled as 'Port Side' and 'Starboard Side'. Figure 5.15b shows the dimensions of the model, these values are selected after consultation with the company as these are typical found on the stinger of the *Pioneering Spirit*. The material properties required for the analysis is listed in Table 4.1. The cross-sections selected for chord and brace are based on typical values used on the stinger, the geometrical properties of chord and brace are listed in Table 5.9.

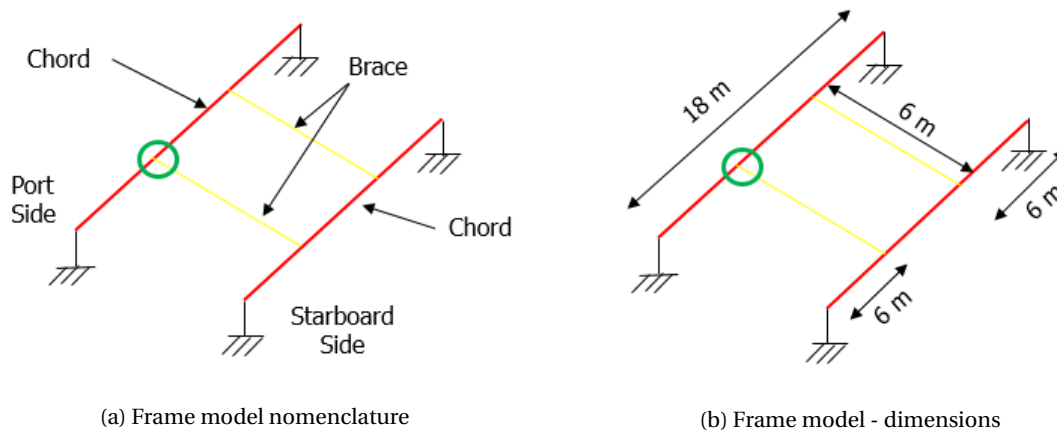


Figure 5.15: Frame model

Table 5.9: Geometrical dimensions for frame model

Property	Chord	Brace
Outer diameter (<i>m</i>)	1.016	0.61
Thickness (<i>m</i>)	0.05	0.0397
Cross-sectional Area (<i>m</i> ²)	0.151	0.071
Moment of Inertia (<i>m</i> ⁴)	0.0175	0.0029

The procedure for analyzing the frame model is similar to the cantilever beam model, which starts with conducting modal analysis to calculate the natural frequencies of the model in FEMAP. With the natural frequencies, the mass participation factors are also calculated which are used to select the frequency range for further analysis. As discussed for the cantilever beam, frequencies considering more than 90% of the mass of the model in the load direction are selected. Similar to the cantilever beam, the loads in frame model are applied in upward Y-direction. Figure 5.16 shows the results of the modal analysis, the first 30 modes are considered which give a frequency range 0 Hz to 210 Hz. A constant damping ratio of 0.02 is assumed [27] across the frequency range.

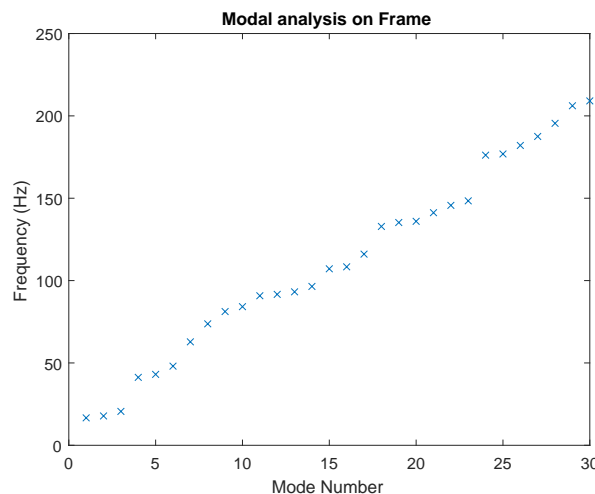


Figure 5.16: Results of modal analysis of frame

From the frequency range, the sampling frequency of 420 Hz is used for converting time domain loads to equivalent frequency domain PSD load using the MATLAB code given in Appendix D.3. Next, we will start

with the analysis of frame model, starting with single PSD load.

5.2.1. APPLICATION OF SINGLE PSD

Like the cantilever beam, the frame model is first analyzed by applying a single sine (periodic) load on the port side as shown in Figure 5.17. The input acceleration load for time and frequency analysis is shown in Figure 5.18, the frequency of the sine load is 20.57 Hz, which is the third mode. This mode is selected as it will have the maximum effect on the pre-selected brace element for bending. This conclusion is made based of experience by observing the mode shape. Total loading time is assumed to be 60 seconds.

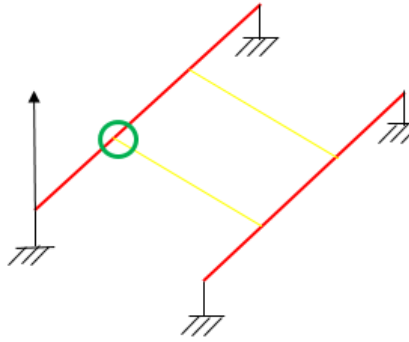


Figure 5.17: Single sine load on the frame model

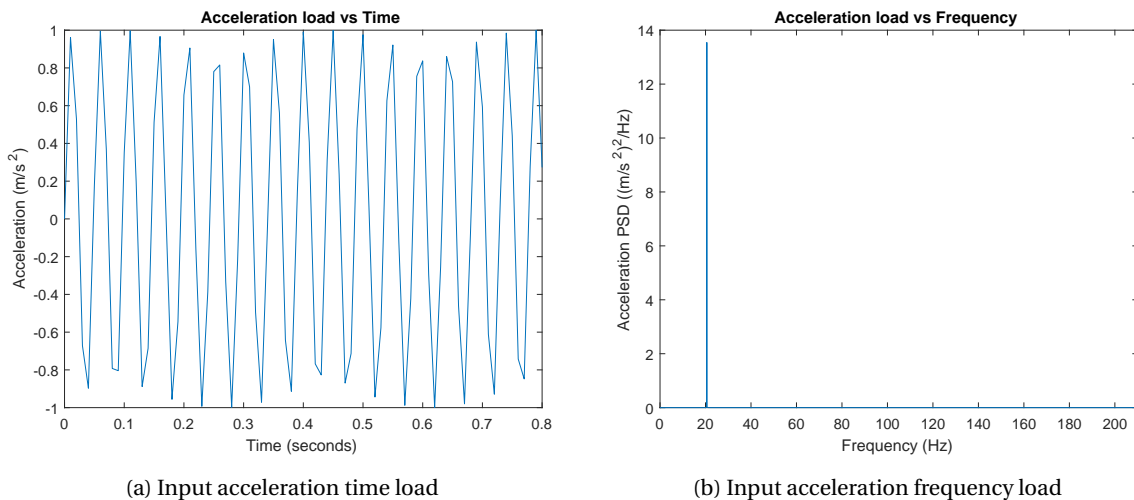


Figure 5.18: Input periodic load

Along with the periodic load, a single random load is also applied at the same location in the same direction consisting of random numbers having mean equal to 0 and standard deviation equal to 0.333, the input loads and the results are shown in Appendix E.4. Using the input periodic loads, the analysis is conducted in time and frequency domain in FEMAP bending moment at the brace of the pre-selected joint is calculated. Bending moment calculated in time domain is converted to equivalent frequency domain using Fast Fourier transform and compared with the bending moment PSD result calculated in frequency analysis, as conducted on cantilever beam. For a simple tubular joint, there are three loads that have to be calculated at the brace as discussed in Section 2.3. However, due to the direction of load, the axial force and in-plane bending moment in the brace are zero for both the analyses, therefore results of out of plane bending moment are compared as shown in Figure 5.19.

For frame analysis, it is suggested by the software support group [44], to neglect frequencies which are less than 1 Hz, so as to avoid any peak structural response at low frequencies. Loads below 1 Hz are created when Fourier transform of acceleration load from time domain to equivalent frequency domain is done. A suitable windowing method can be used to decrease the amplitude at low frequencies. In this research, hanning window is used, which is one of the most effective methods for reducing the signal strength at low frequencies, thereby forcing the structure to resonant around the main frequency. As discussed in Subsection 3.1.3, output response PSD of a structure at required frequencies can be calculated in FEMAP. To avoid any incorrect results, suggestion from support group [44] are taken into consideration and responses below 1 Hz are neglected.

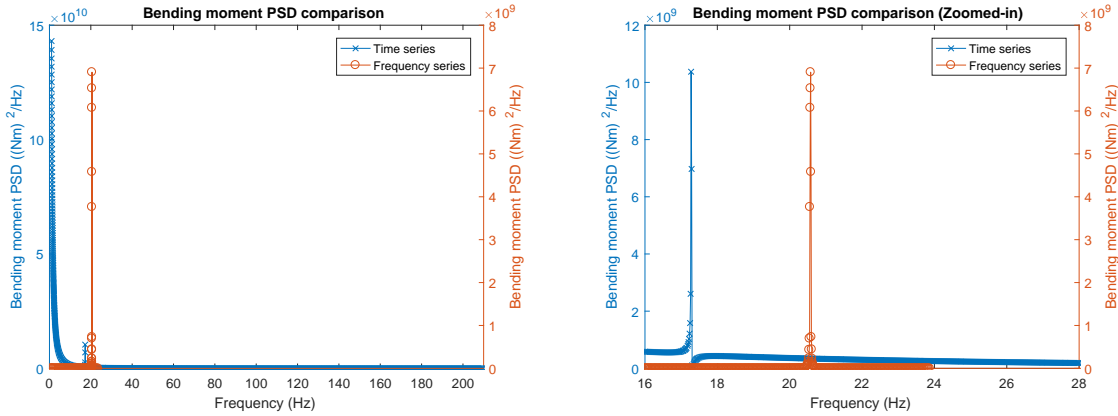


Figure 5.19: Bending moment PSD comparison - Single sine load

From the bending moment results shown in Figures 5.19 and E.29, two important observations are:

1. For periodic loads, peak frequency achieved for time analysis is very different from frequency analysis and there is also a huge difference in the peak amplitude. For time series, two distinguished peaks are observed at 1 Hz and at 17.28 Hz, whereas for equivalent frequency analysis only single peak is observed at 20.57 Hz. As the loading is periodic, response as at single peak is expected, this means, results calculating in time analysis are incorrect and further investigation should be done.
2. For random loads shown in Appendix E.4, multiple peaks are achieved in frequency analysis, however the first peak is achieved at 1 Hz. Whereas for time analysis, only single peak is achieved at 1 Hz. For random loads, multiple peaks around the natural frequencies are expected but, peaks achieved below the first natural frequency gives the impression of incorrect calculations. With this we can conclude that for random loads, both the analyses are calculating incorrect results.

Results of modal analysis in Figure 5.16 shows that, the first natural frequency occurs at 16.65 Hz, so a peak achieved at 1 Hz is incorrect. For periodic load, a peak in the bending moment PSD result was expected to be at 20.57 Hz for both the analyses, however, for time series the peak was achieved at 1 Hz. With the conclusion that the time analysis is giving incorrect results, the area under the bending moment PSD result was calculated to check the difference in the results between the analyses.

Table 5.10: Bending moment PSD (Single load) - Area calculation

Sub-case	Area under PSD (Nm)²	
	Time series	Frequency series
Single sine load	$1.45 * 10^{11}$	$2.55 * 10^{08}$
Single random load	$6.55 * 10^{12}$	$1.12 * 10^{08}$

As observed from Table 5.10, there is a big difference ($> 10^3$) in the results for periodic loads and even bigger difference (10^4) is observed for random loads. The analyses on frame model follows the same procedure as the cantilever beam model, but the results obtained from both the model are very different. As the area under bending moment PSD for frame model are not matching for time and frequency analysis, further calculation

and comparison of bending stress PSD and fatigue damage will not be conducted and the remaining part of this research will be focused on finding the source of the problem.

5.3. DETAILED ANALYSIS OF FRAME MODEL

According to the results shown in Figure 5.19, the peak bending moment PSD response for frequency domain analysis is achieved correctly at the third mode (20.57 Hz) but, for time domain analysis, there are two peaks achieved. Having concluded that the time analysis is giving incorrect bending moment result, the output bending moment result from time analysis is plotted in Figure 5.20.

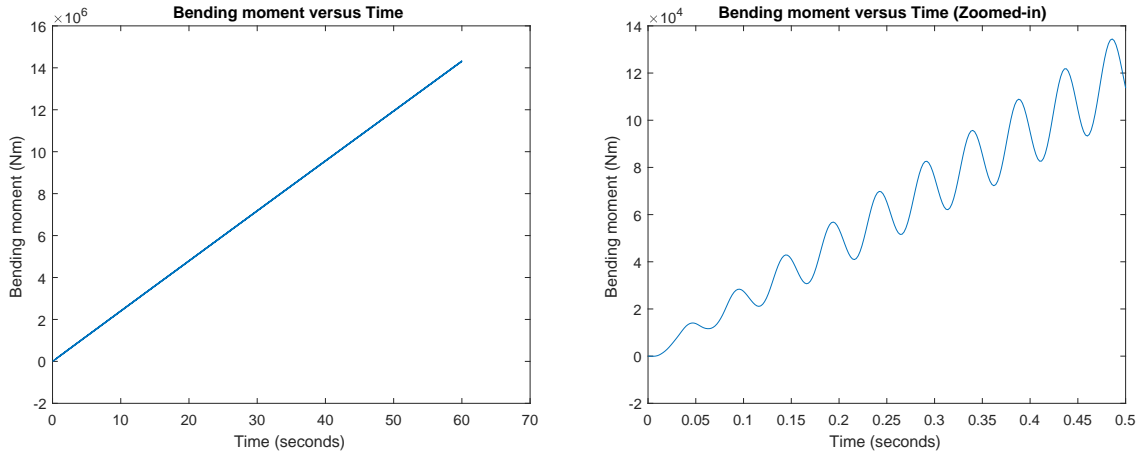


Figure 5.20: Bending moment - Single sine load - Frame model

The graphs in Figure 5.20 show the distribution of out of plane bending moment with respect to time, as given by FEMAP. From the figure, we can see that, the curve has periodicity but it is diagonally increasing with respect to time. In Figure 5.21 we see the bending moment results for the cantilever beam analyzed in Section 5.1.

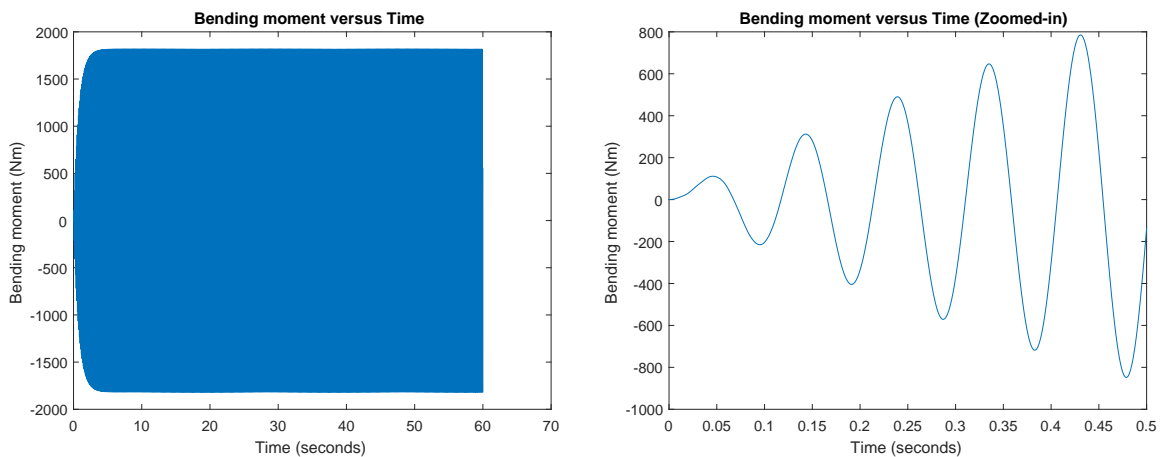


Figure 5.21: Bending moment - Single sine load - Cantilever beam

When the distribution of bending moment with respect to time for frame model shown in Figure 5.20 is compared to cantilever beam model in Figure 5.21, we can see that, for the frame model, the bending moment results are oscillating but not respect to the horizontal X-axis, like the cantilever beam results. Since the oscillation are not symmetrical with respect to time axis, two distinct peak frequencies are achieved for the frame

model when bending moment results are converted to equivalent bending moment PSD (compared in Figure ??). The diagonal increase in bending moment results, could be one of the reasons for achieving peak at 1 Hz. The increasing pattern of bending moment result for the frame model is quite unusual and the issue was forwarded to the support group [44] to which the reply was, the applied acceleration load at the base node is converted to displacement by double integration. Double integration of a function adds two integration constants to the final result. This might be the reason for a diagonal increase in bending moment result observed for frame model. Similar pattern for displacement result is also seen in cantilever beam, but it does not effect the bending moment result. The reason for this was never fully explained by the support group and hence, further investigation on the effect of double integration was done by analyzing a different model.

5.3.1. FIXED BEAM

It's decided to test the hypothesis of double integration on a different model having similar boundary condition. A fixed beam with both ends fixed is analyzed with the model shown in Figure 5.22.

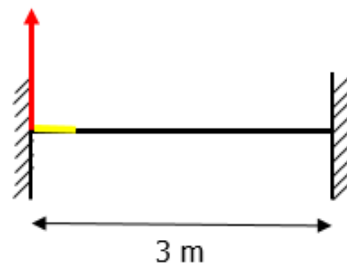


Figure 5.22: Single sine load on the fixed beam

The material and geometrical properties are the same as for the cantilever beam model listed in Tables 4.1 and 4.3. The red arrow shows the location and direction of application of load and the yellow line shows the element where bending moment is calculated in FEMAP for time and frequency analysis. First modal analysis is conducted and the results are shown in Figure 5.23.

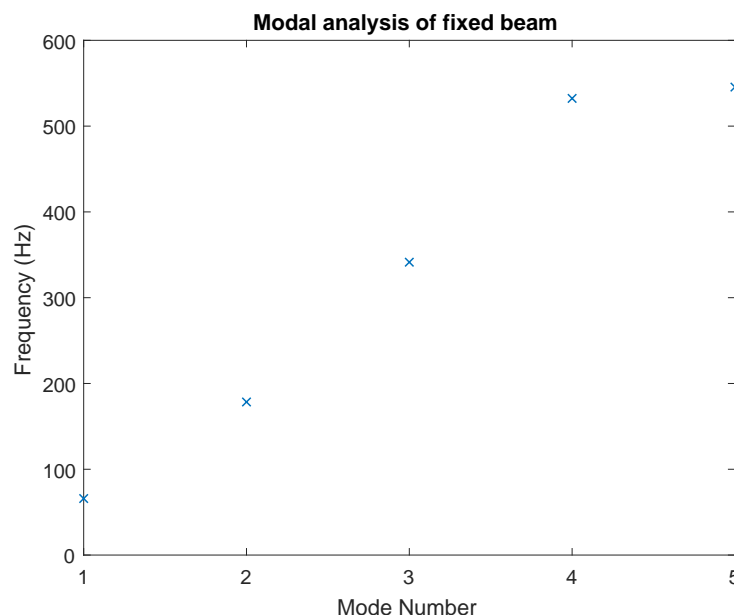


Figure 5.23: Modal analysis on fixed beam

After modal analysis, frequency range from 0 Hz to 550 Hz is selected for the analysis. First, only time domain

analysis is conducted to and bending moment at the chosen element is calculated. A sine load with single frequency of 65.87 Hz is applied at one of the fixed end in FEMAP. The input sine load is shown in Figure 5.24 is applied for total time of 60 seconds and the output bending moment calculated in time domain analysis is shown in Figure 5.25.

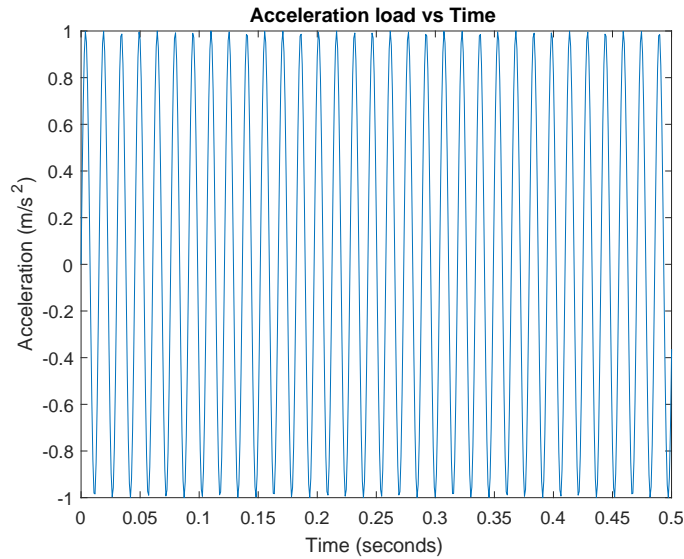


Figure 5.24: Input sine load for fixed beam

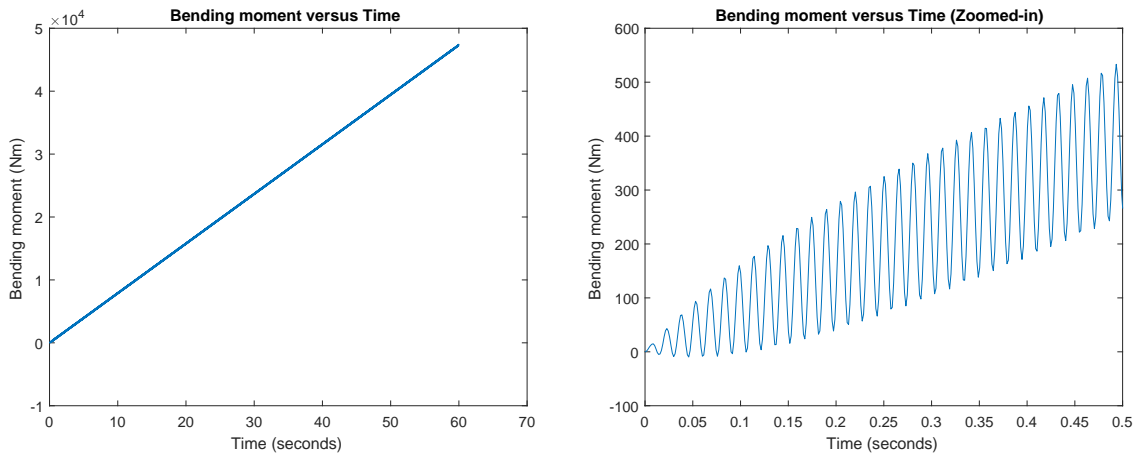


Figure 5.25: Bending moment - Single sine load - Fixed beam

From the output bending moment shown in Figure 5.25, it is observed that, similar pattern seen in the results of frame model is calculated for fixed beam. From the results we can conclude that double integration of acceleration loads, do effect the output bending moment result. Another reason could be the boundary conditions of both the models (frame and fixed beam). First, we will further investigate the effects of double integration. For this, let us assume that the diagonal increase of bending moment results for the frame and fixed beam models due to periodic loads is linear. With this assumption, a linear line can be constructed called as 'trend-line', which can be treated as the new horizontal time axis. This would theoretically eliminate effects of the constants of double integration. It has to be noted that, using a trend-line is based on the assumption that the increase in bending moment results is linear and the assumption is made in order to investigate time domain analysis for frame and fixed beam. Figures 5.26 and 5.27 show the FEMAP bending moment result with a newly constructed linear trend-line for frame and fixed beam model respectively.

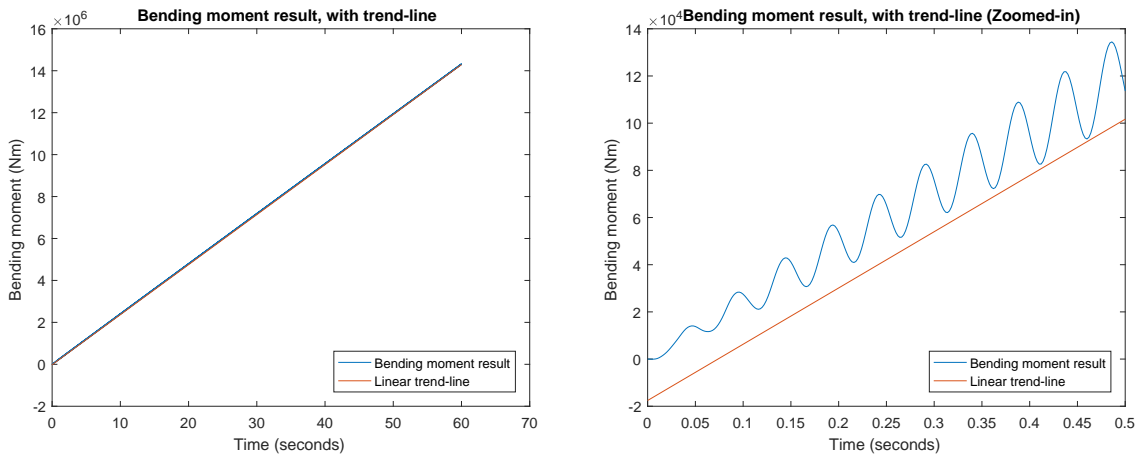


Figure 5.26: Bending moment-Single sine load with trend-line - Frame model

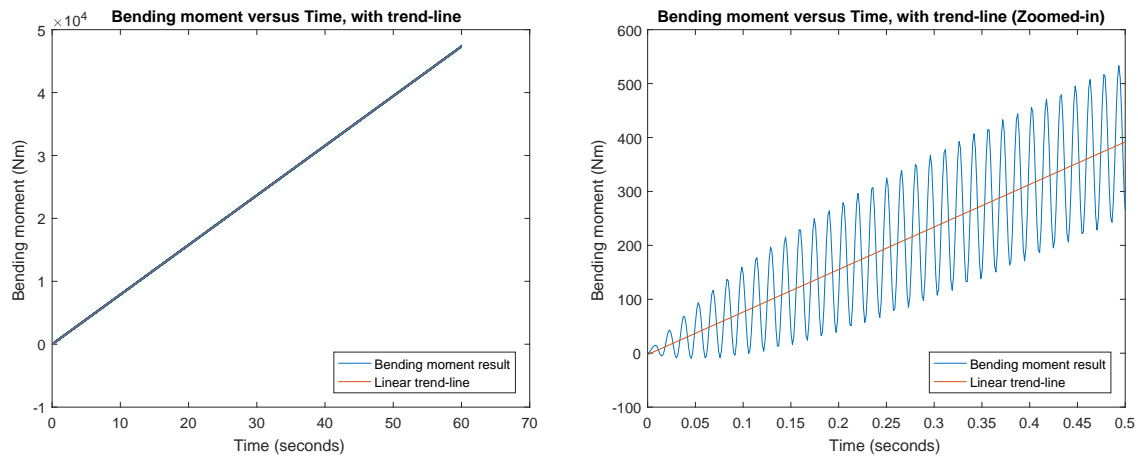


Figure 5.27: Bending moment-Single sine load with trend-line - Fixed beam

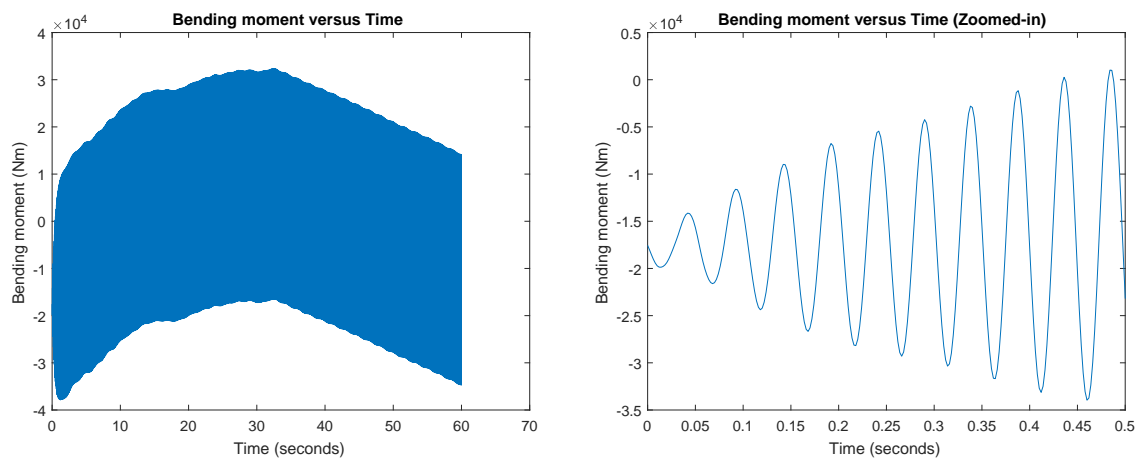


Figure 5.28: Bending moment-Single sine load with new X-axis - Frame model

As discussed, the trend-line is assumed as the new horizontal time X-axis and Figures 5.28 and 5.29 shown the bending moment results with respect to trend-line.

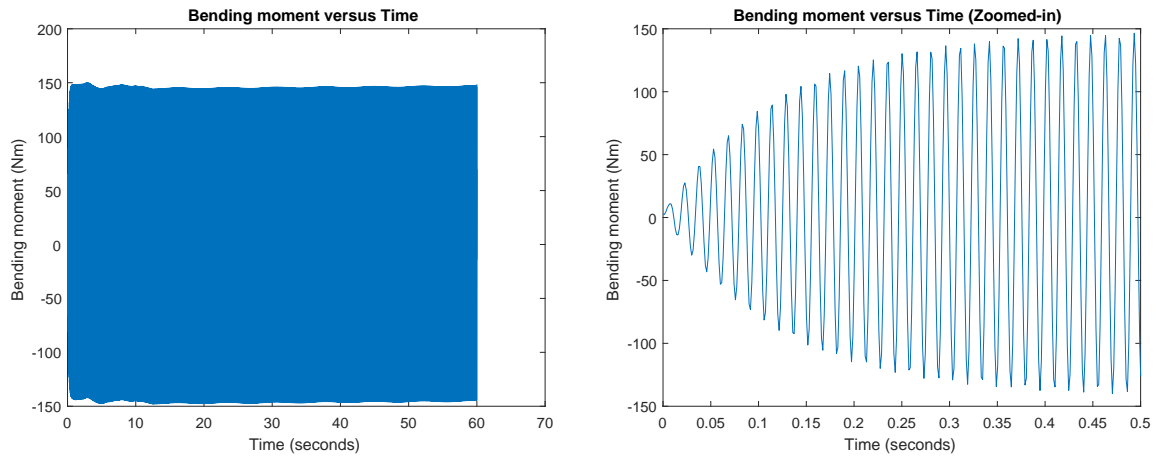
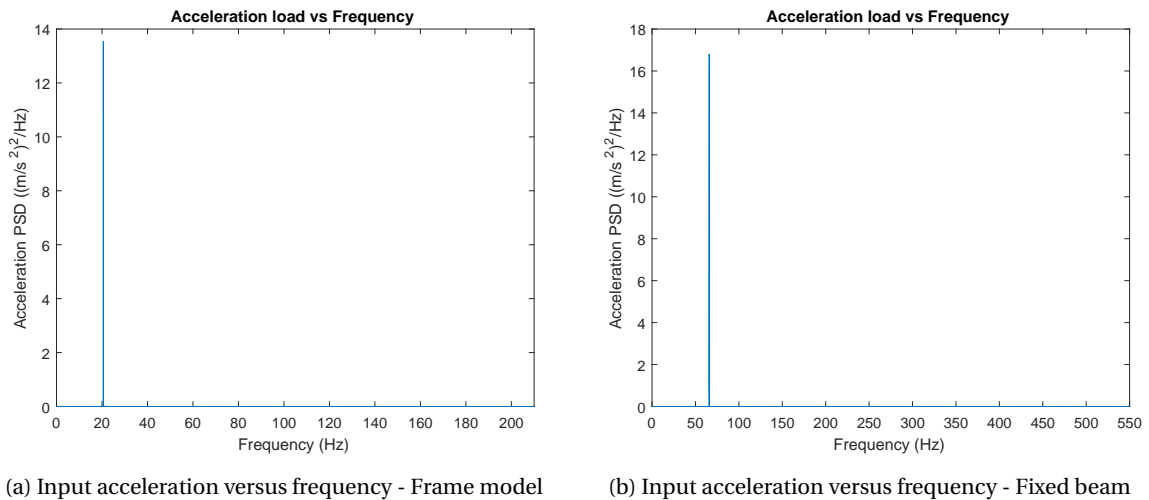


Figure 5.29: Bending moment-Single sine load with new X-axis - Fixed beam

From Figure 5.29, we can see that, after assuming a new time X-axis, the oscillation of fixed beam nearly follows the same pattern as for cantilever beam shown in Figure 5.21. Although, result for frame model, shown in Figure 5.28, do not completely oscillate like the fixed beam model but, the results are better than previous results. The new bending moment results shown in Figures 5.28 and 5.21 are now compared with frequency domain results by conducting equivalent frequency analysis. This is done to check whether the introduction of a trend-line has been useful. The input acceleration PSD load for frequency analysis of frame and fixed beam models is shown in Figure 5.30.



(a) Input acceleration versus frequency - Frame model

(b) Input acceleration versus frequency - Fixed beam

Figure 5.30: Input PSD loads

The bending moment result shown in Figures 5.28 and 5.29 for frame and fixed beam model are converted to frequency domain using Fast Fourier transform and compared to results obtained from frequency analysis, similar procedure as done on cantilever beam. The comparison of the results are shown in Figures 5.31 and 5.32 for frame and fixed beam models respectively.

The results for frame and fixed beam models in Figures 5.31 and 5.32 are now more comparable than previous results. The results obtained using the trend-line more comparable than the results without trend-line. A check can now be performed by calculating the area under the bending moment PSD results for frame and fixed beam models, the results are listed in Table 5.11.

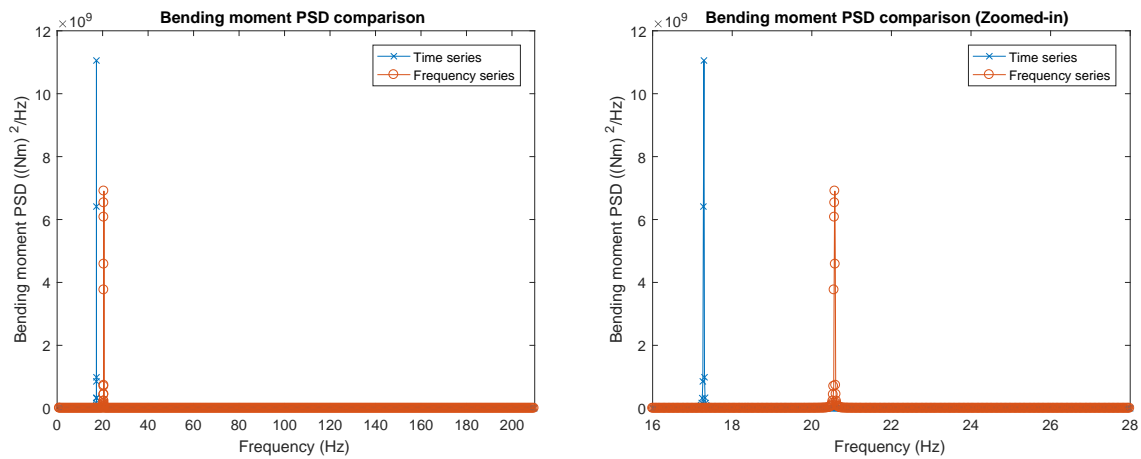


Figure 5.31: Bending moment result comparison - Frame model

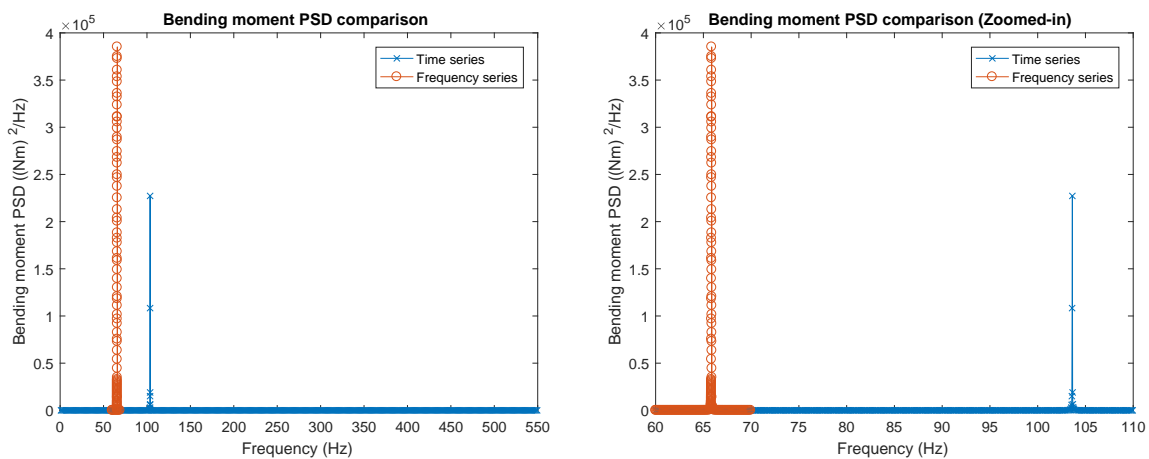


Figure 5.32: Bending moment result comparison - Fixed beam

Table 5.11: Bending moment PSD with trend-line (Single sine load) - Area calculation

Sub-case	Area under PSD $(Nm)^2$	
	Time series	Frequency series
Frame model	$2.96 * 10^{08}$	$2.55 * 10^{08}$
Fixed beam	$1.06 * 10^{04}$	$1.15 * 10^{04}$

From the results in Table 5.11 the area under PSD are comparable for frame model, which earlier had a huge difference. However, when the fatigue damage results are calculated using nominal stress approach for time domain and compared to frequency domain as shown in Table 5.12, the difference is very large.

The results obtained in Table 5.12 are not nearly as close as the results obtained for cantilever beam. Also, result for frame model is highly under predicted by frequency analysis when compared to equivalent time analysis. With this we can conclude, that the trend-line does not fully solve the issue of double integration. Moreover, when the same linear trend-line is implemented for random loads, and bending moment results are compared for frame and fixed beam shown in Appendix E.4, there is no periodicity achieved in the results. This proves that trend-line is not the universal solution to the problem. For fixed beam, linear trend-line provided comparable bending moment and slightly higher fatigue damage results, shown in Tables 5.11 and 5.12. However, from Figure 5.32, results show high discrepancy with respect to the peak frequency achieved

for time and frequency analysis. The expected frequency of peak occurrence is 65.87 Hz but, the bending moment peak occurs at 103.62 Hz for fixed beam. One of the main reasons for this discrepancy could be the total analysis time. This is based on the understanding that maybe 60 seconds is not enough for the models to reach steady state. Thus, in the next section, the total time of the analysis is increased to check its effect on the bending moment results for time and frequency analysis on both the models.

Table 5.12: Damage calculation – Single sine load

Analysis	Damage	% error (RF)
Single Sine load-Frame model		
Time domain analysis	$6.3 * 10^{-06}$	-
Frequency domain analysis	$3.3 * 10^{-11}$	100
Single Sine load-Fixed beam		
Time domain analysis	$1.01 * 10^{-09}$	-
Frequency domain analysis	$1.59 * 10^{-09}$	56.59

5.3.2. INCREASING ANALYSIS TIME

To check if the total analysis time has any effect on the bending moment result, total analysis time is increased from 60 seconds to 120 seconds. The periodic acceleration loads for frame and fixed beam are shown in Figures 5.33 and 5.34 respectively.

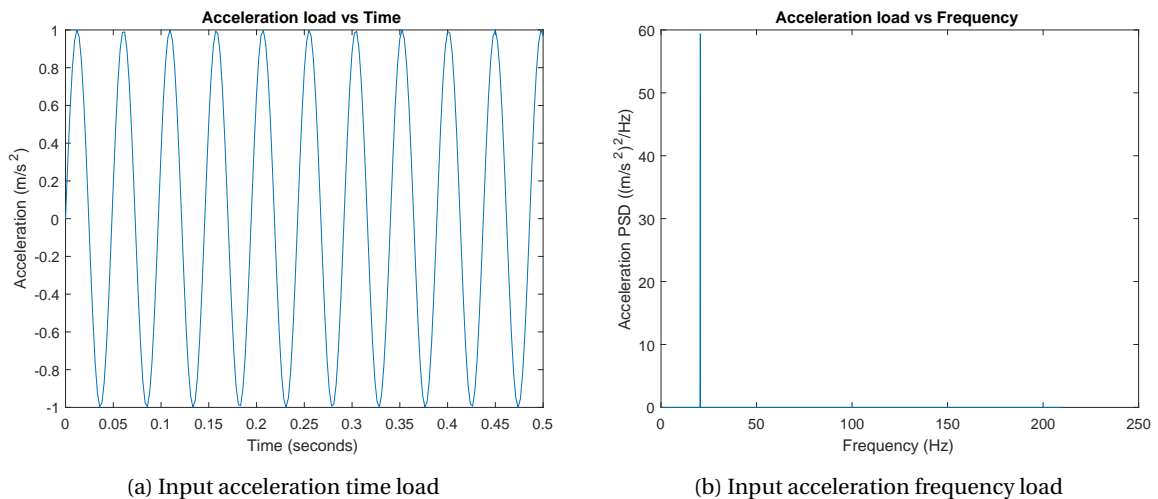


Figure 5.33: Input periodic load (120 seconds) - Frame model

Using the loads, both models were analyzed in time and frequency domain and the bending moment results are compared, shown in Figures 5.35 and 5.36. It should be noted that, in this analysis, all the assumptions and suggestions used in the previous sections have already been implemented. This means, linear trend-line has been used before comparing bending moment results.

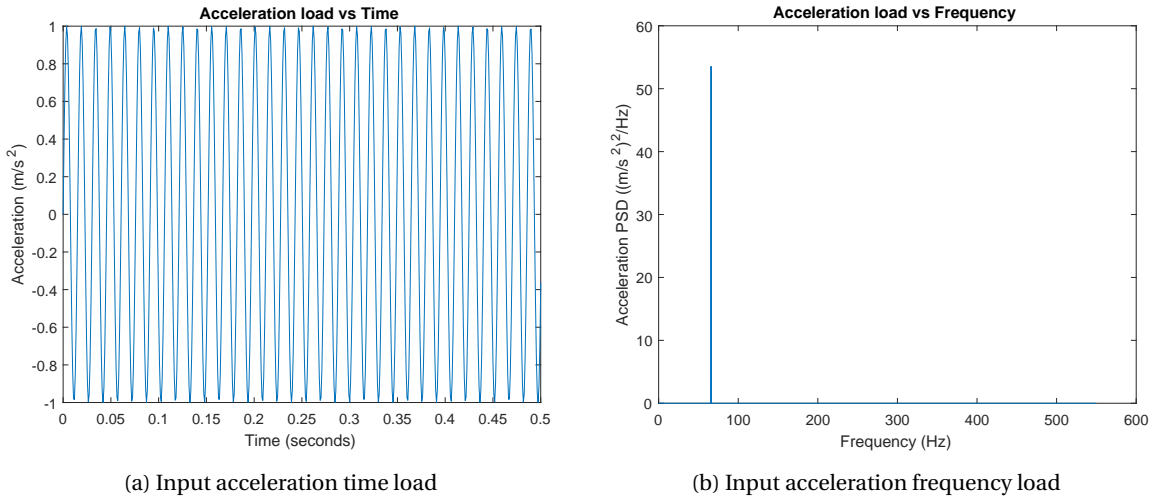


Figure 5.34: Input periodic load (120 seconds) - Fixed beam

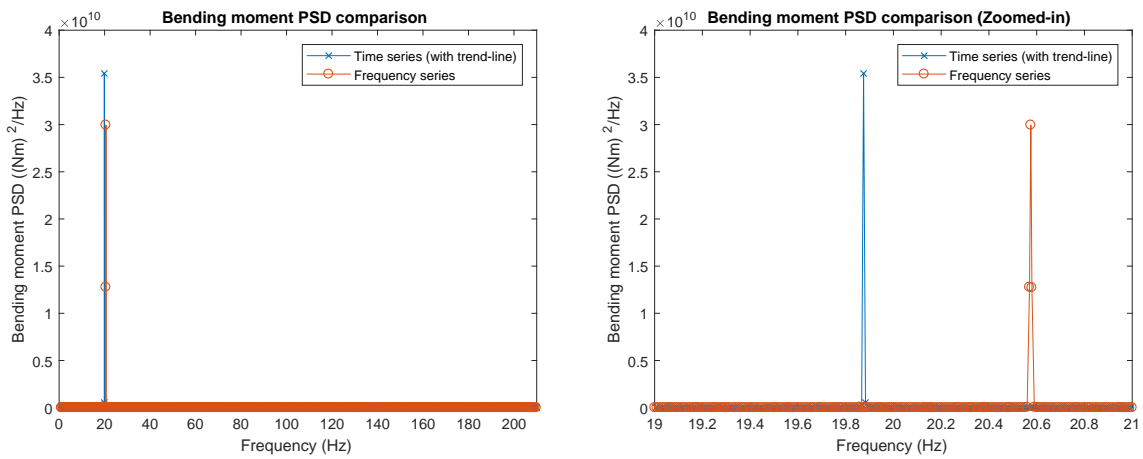


Figure 5.35: Bending moment result comparison (120 seconds) - Frame model

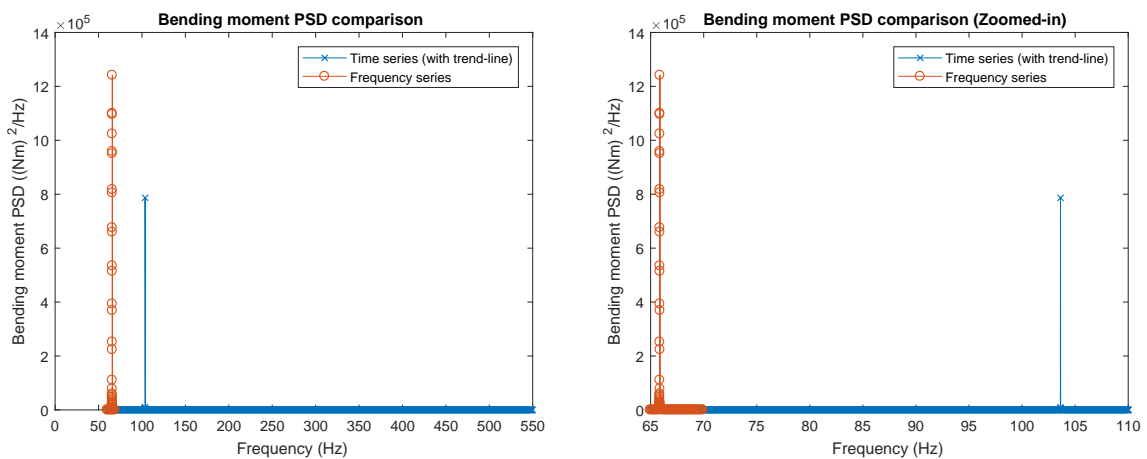


Figure 5.36: Bending moment result comparison (120 seconds) - Fixed beam

Increasing the total time of the analysis has offer some improvement for the frame model in terms of the

frequency of peak excitation (19.87 Hz) which is much closer to the applied frequency (20.57 Hz). However, there is no improvement for fixed beam as the frequency of peak excitation is still at 103.62 Hz. With this information, the area under the bending moment PSD results is calculated along with the fatigue damage for both the models, listed in Tables 5.13 and 5.14.

Table 5.13: Bending moment PSD with trend-line (Single sine load 120 seconds) - Area calculation

Sub-case	Area under PSD $(Nm)^2$	
	Time series	Frequency series
Frame model	$2.97 * 10^{08}$	$3.5 * 10^{08}$
Fixed beam	$1.06 * 10^{04}$	$1.15 * 10^{04}$

Table 5.14: Damage calculation (120 seconds) – Single sine load

Analysis	Damage	% error (RF)
Single Sine load-Frame model		
Time domain analysis	$1.26 * 10^{-05}$	-
Frequency domain analysis	$8.63 * 10^{-11}$	100
Single Sine load-Fixed beam		
Time domain analysis	$2.07 * 10^{-09}$	-
Frequency domain analysis	$3.29 * 10^{-09}$	58.55

The increase in total analysis time has made no impact in the damage results as confirmed by the comparison shown in Table 5.14. Only periodic loads are analyzed in this section because it is easy to predict the response of the structure. Also, since there is no appreciable improvement, it is decided not to carry out analysis for random loads. From the results in this section we can conclude that, increase in analysis time will not affect the bending moment results.

In Subsection 5.3.1, we concluded that the unusual bending moment results for frame and fixed beam could be due to double integration done in FEMAP and it may also be due to the influence of boundary condition of the models. In the next subsection we will analyze a model which has similar boundary conditions as cantilever beam but, it is a frame.

5.3.3. CANTILEVER FRAME MODEL

In the research, the proposed methodology of frequency domain analysis has been proven to work on cantilever beam, however, its application on frame model has been inconclusive. An additional model, cantilever frame, is analyzed in this section with two acceleration loads. The model, the location and direction of loads is shown in Figure 5.37.

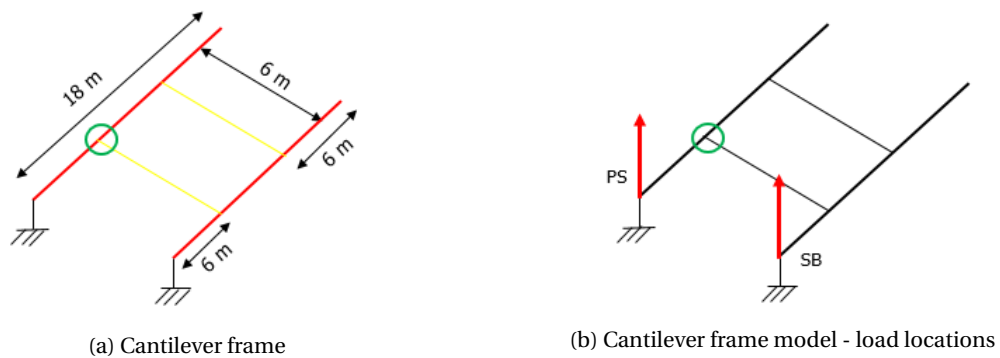


Figure 5.37: Cantilever frame model

This particular model is chosen because of its similarity with the cantilever beam. Because of its frame structure and cantilever-like boundary condition, it is called as ‘Cantilever Frame’. Two loads will be applied on both the fixed locations as shown in Figure 5.37b. Initial analysis will be done assuming periodic loads. In Figure 5.37a, the red lines represent chord and the yellow lines represent brace for the model. The material and geometrical properties is the same as frame model given in Tables 4.1 and 5.9, however, as the boundary conditions are different, modal analysis is conducted and results are shown in Figure 5.38.

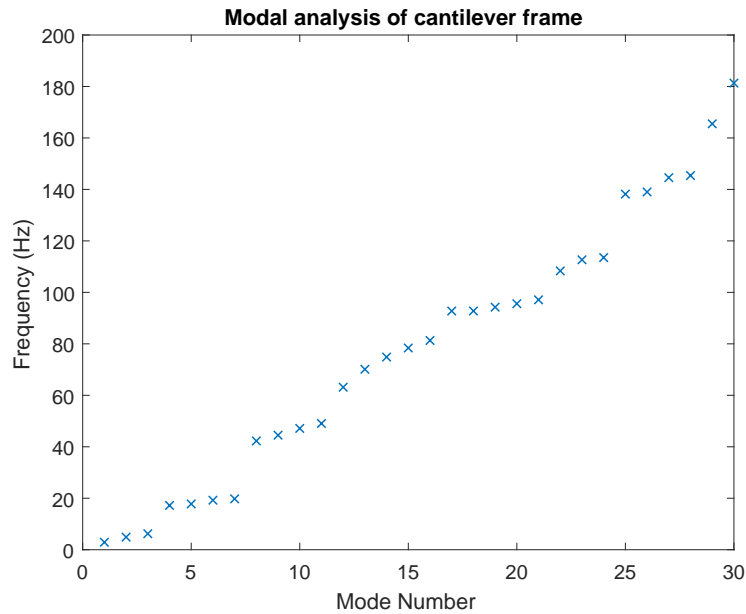


Figure 5.38: Modal analysis for cantilever frame model

From modal analysis, total frequency range from 0 Hz to 200 Hz is selected for application of periodic loads in time and frequency domain. To keep the analysis simple, both loads are the same in amplitude and frequency. The excitation frequency is selected as 2.9 Hz, which is the first mode of the model and the total time of the analysis is 60 seconds. The acceleration loads for time and frequency domain analyses are shown in Figure 5.39.

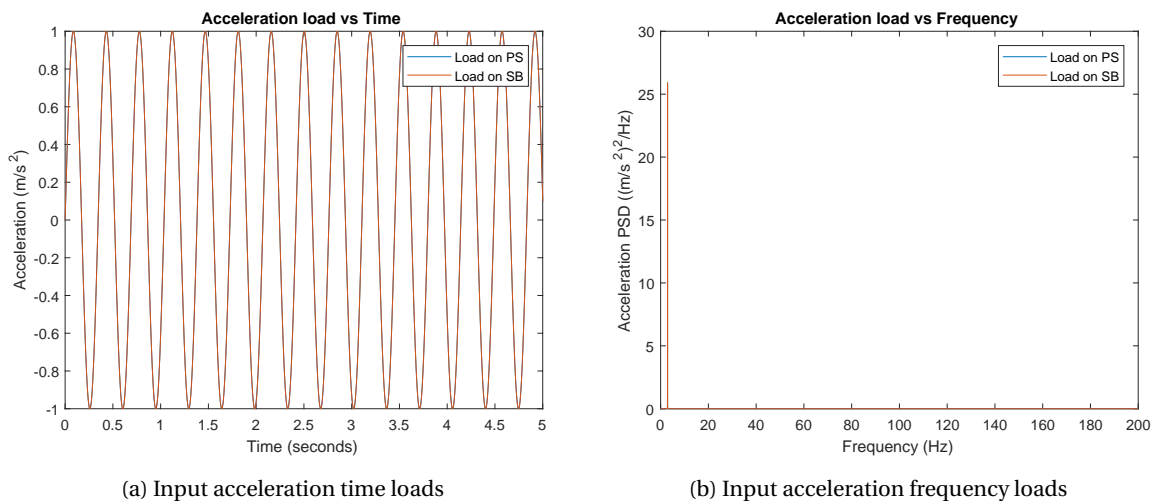


Figure 5.39: Input loads for cantilever frame model

When two loads are applied in case of frequency analysis, it is important to provide an additional input to

FEMAP as a cross power spectral density, discussed in Subsection 4.2.3. For two acceleration loads shown in Figure 5.39, the cross power spectral density is calculated in MATLAB using code attached in Appendix D.3. The results of cross power spectral density is shown in Figure 5.40.

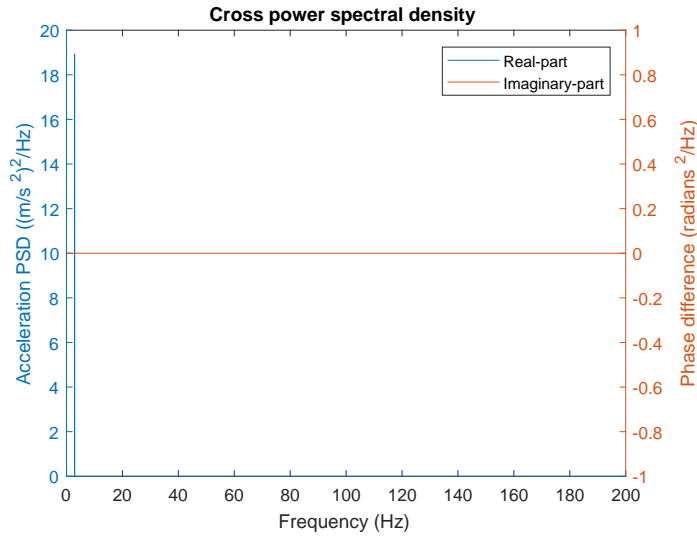


Figure 5.40: Cross power spectral density input

Using the input loads shown in Figures 5.39 and 5.40 along with a constant damping ratio of 0.02 throughout the frequency range, analysis of cantilever frame model is carried out in time and frequency domain. The bending moment results are calculated at the brace of the pre-selected joint shown in Figure 5.37a and the out of plane bending moment PSD results are compared as shown in Figure 5.41.

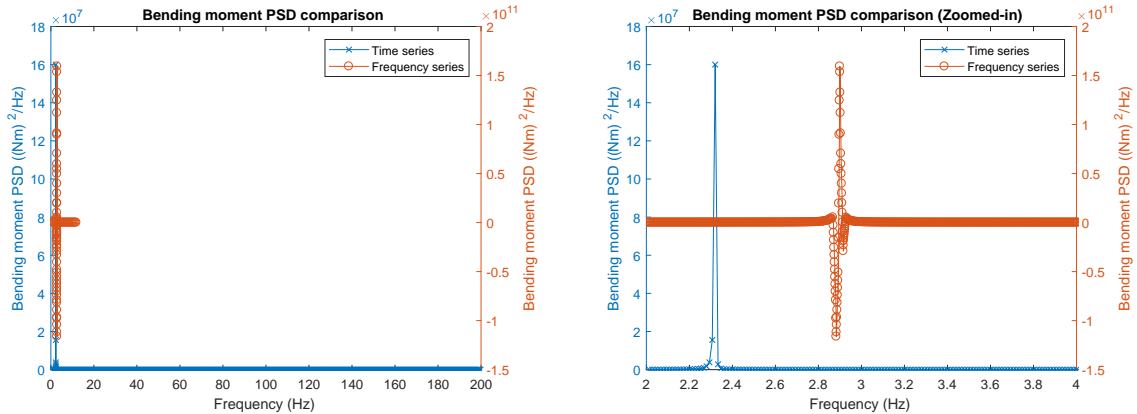


Figure 5.41: Bending moment result comparison - Cantilever frame

Results of frequency analysis of cantilever frame model shows negative bending PSD moment PSD results, whereas the time series analysis is calculating only positive results. Comparing these results will not give us any valuable information. We now see that here, the frequency analysis is calculating incorrect results. We can make this conclusion because, all PSD loads applied to the model are positive which can never lead to negative result [24]. Similar procedure was conducted on cantilever beam model with two periodic loads in Subsection 5.1.2, which showed comparable results, however, for cantilever frame model, the results could not be compared.

Additional analysis using periodic loads at different natural frequencies of the cantilever frame model were also conducted shown in Appendix E.4. In Appendix E.4, analysis has been conducted on third and seventh

modes having frequencies 6.21 Hz and 19.76 Hz respectively. These two modes are chosen after conducting a frequency analysis with random loads on first 10 modes of model. Peak amplitudes were achieved at first, third and seventh mode for bending moment result. Analyses conducted with different periodic loads on cantilever frame model resulted in similar pattern of bending moment PSD result for frequency analysis. This was communicated to the support group [44] and no helpful suggestion was provided by them. According to the author, the reason behind this could be interpretation of PSD loads at two different locations in FEMAP. Having conducted the analysis on different models with different loading condition, we can now conclude the research. In the next section, we will discuss about the main conclusion and learning's from this chapter.

5.4. CONCLUSION

In this chapter, fatigue damage calculation is conducted on cantilever beam and frame models using frequency domain analysis. Verification of fatigue damage results is done by conducting an equivalent time domain analysis. For cantilever beam model, fatigue damage results from frequency analysis showed good comparison with equivalent time domain results but, for the frame model, similar results are not achieved. An extensive research is conducted with the main focus on trying to locate the root cause of the problem. After conducting analysis on different models using different load cases, it can be concluded that, the two reasons for the incorrect results in time analysis are the effect of boundary conditions and the method used for integration of acceleration in FEMAP.

The method used for integration of acceleration inputs in FEMAP adds two constants to the displacement output, which passes on to bending moment giving incorrect results for the frame model. Similar observation was made for cantilever beam but, the final bending moment result remains unaffected. As discussed earlier, one of the reasons could be the boundary conditions of the frame model, where every free end is fixed. For frame model, only one of the four constraint points are loaded, unlike cantilever beam, where there is only one constrain point. The bending moment result for frame model calculated in time domain analysis in FEMAP may include static bending moment induced due to the remaining three constraint points, which is why the results are diagonally increasing. There is no theoretically explanation for the previous statement, as it is an observation of the author. To understand this behavior, fixed beam is considered and analyzed in time domain in FEMAP. Fixed beam is a statistically undetermined system, which showed similar pattern of bending moment result as shown by the frame model. One of the conclusions could be that, for statistically undetermined systems, time analysis as base excitation gives incorrect results in FEMAP. This conclusion maybe far fetched, as only two models are analyzed and the conclusion may not be completely true.

To remove the effect of additional constraints on the frame model, a cantilever frame model is introduced with two periodic loads. Immediate effect on the bending moment results in time domain analysis is seen, as the results are once again periodic. However, no significance conclusion on the results could be made, as for cantilever frame, frequency domain started to give incorrect results. For cantilever frame model it was concluded that, the interpretation of two PSD loads at two different locations in FEMAP had to be studied in detail. With this, we conclude the research and in the next chapter we discuss on the main conclusion for the overall research with respect to the objectives mentioned in Chapter 1 and also provide recommendations for future research in this subject.

6

CONCLUSION AND RECOMMENDATIONS

CONCLUSION

Design of fatigue resistant structures in the offshore industry is an evolving area of study and the introduction of frequency analysis for fatigue damage estimation using Dirlik's method has proven to have certain advantages over conventional time domain analysis. With this research, an attempt is made to understand the the procedure for fatigue damage estimation in frequency domain using Dirlik's method and verify its application on simple models using equivalent time domain analysis. Cantilever beam and a simple frame are selected as verification models used in this research to verify the frequency analysis subjected to single and two periodic and random loads. The reason behind their selection is discussed in Chapter 4. The software used for conducting analyses in this research is FEMAP which uses Nastran as the main solver. FEMAP is extensively used at Allseas Engineering for conducting structural analysis on various components of the vessel and related offshore structures.

The research begins with identifying the main research question, which is to conduct a feasibility study on the application of frequency analysis to estimate fatigue damage using Dirlik's method. With the research objective in mind, literature study is done to understand the basis of frequency analysis and base excitation problems. A detailed study on fatigue analysis in frequency domain is done and its relation with Dirlik's method is also studied. Fatigue estimation using Dirlik's method was verified by conducting equivalent time domain analysis with rainflow counting by comparing the fatigue damage values. For cantilever beam, frequency analysis give comparable results with respect to time domain analysis for different types of periodic and random loads. For periodic loads, errors slightly over 30% is observed for all sub-cases. This, as concluded, is in-line with the results presented in paper [34], establishing that Dirlik's method will always give conservative results for periodic loads. From industrial point of view, a 30% error is not very high and can be used during the early stages of development which could be helpful to further optimize the design. For random loads, the fatigue damage results for cantilever beam give good comparison (less than 10% difference) with the equivalent time domain analysis. Similar results are presented in paper [34] for Gaussian distributed random loads, successfully verifying the frequency analysis for cantilever beam.

Similar analysis is also conducted on the frame model, however, the results obtained from time and frequency analysis could not compared due to large differences between the results. Detailed research is conducted to find the source of the problem. After conducting different analyses with different models and load cases, it is concluded that, there are two places where the problems could exist. First is the integration method used in FEMAP and the second is the influence of boundary conditions of the frame model. Both of these problems are related to time domain analysis. Influence of the boundary condition on the analysis is proven by analyzing cantilever frame model for time domain analysis, towards the ending of Chapter 5. However, bending moment PSD results could not be verified with equivalent frequency analysis due to the anomalies involving application of two PSD loads at different locations. The various reasons for the deviations of results are discussed in Section 5.4.

Having conducted a feasibility study, the research is concluded by saying that the proposed frequency domain analysis is verified for cantilever beam model. Unfortunately, similar verification could not be achieved for frame model and the reasons for this are already mentioned above. Effort is put into finding the root causes which are affecting the results of frame model. As only one of the selected models is verified using the proposed method, we can conclude that the research objective is not fully completed. However, this does not mean that the proposed method is incorrect, as it is giving comparable results for cantilever beam. The author feels that, additional simulations with modified strategy would be needed for better understanding of the results. Even though the research objectives set at the start are not fully completed, a good basis for the proposed method is formed by conducting this research and results can be useful for conducting further investigation by the company or the university.

One of the additional objectives of the research is to incorporate fatigue damage calculated using Dirlik's method into the overall fatigue analysis procedure of *Pioneering Spirit's* stinger. In this research, stinger is not considered, but suggestions are given, assuming that the bow deflection loads can be calculated in frequency domain. According to Allseas, the main reason for conducting fatigue analysis on stinger for bow deflection loads is to check the percentage increase in damage values on each tubular joints of the stinger. If this percentage increase is significant, according to the company, suitable measures will be taken to maintain the reliability of the stinger. Stinger tubular joints are analyzed for different load cases like, hydrodynamic and roller box loads, at different positions of the stinger and for different environment conditions (wave height, wave period, wave spreading), which together contribute to the fatigue damage. Bow deflection loads mainly depend upon the environmental conditions surrounding the vessel. Fatigue analysis excluding bow deflection loads, for pipelaying operation are divided into different load cases depending mainly upon the significant wave height, time period and the position of the stinger. Hence, fatigue damage due to bow deflection loads based on environmental conditions can be calculated separately, using frequency analysis. To check the fatigue damage increase in a tubular joint, simply adding the damage value calculated by Dirlik's method to the damage value obtained for other load cases would lead to incorrect results. This is because, damage value due to a single load case would be negligible in comparison to the damage value calculated by combining all other load cases. To effectively quantify the increase, stress ranges calculated using Dirlik's method should be added to the stress ranges calculated for all the other load cases. With the addition of stress ranges from all load cases, including bow deflection, fatigue damage should be calculated using DNVGL recommendations. This damage value can now be compared with the damage value excluding bow deflection load case, to give the increase in damage. Using these steps, we can quantify the increase in damage due to bow deflection loads.

RECOMMENDATIONS

For future recommendation, the most important task is the verification of proposed methodology on the frame model. Enough ground work has been conducted in this research which will be helpful in providing a strong basis. Below, few points are recommended which can be used to conduct further investigation.

1. For single load application on frame model, either periodic or random, additional analysis can be carried out using a different type of load, for example, using displacement instead of acceleration. However, the author could not find any substantial literature which could provide information on the theoretical background of using displacement as a load for vibrational analysis. For acceleration loads, the author is able to find enough information and has also conducted a theoretical verification in Chapter 4. If displacement are to be used as loads, it is recommended to collect suitable information and perform theoretical verification before proceeding with fatigue analysis.
2. For two load application on frame model, background information on analyzing suspension components for automobiles may provide a good starting point. For automobiles, loads on vehicles during operation on the road are considered as random and critical components, mostly suspension components are analyzed for vibrational loading using frequency analysis. As the input loads is applied at all four wheels, which may differ in magnitude and/or phase, this provides a good basis for analyzing frame model with multiple loads applied at different locations. A technical article was found [45], which

implements multiple random excitations to estimate fatigue damage on the chassis of trucks. The main context of the paper is that, it uses a PSD matrix which consists of individual PSD loads applied on all wheels along the diagonal to the matrix. The remaining matrix elements are filled by cross power spectral densities giving relation between two PSDs. This PSD matrix is then used to calculate the stress response PSD using the transfer function of the chassis. Further investigation has to be conducted on the overall procedure described in the paper.

If the proposed research methodology is verified for single and multiple loads on the frame model, the method then can be applied on the main stinger model with available bow measurement data, to calculate fatigue damage.

BIBLIOGRAPHY

- [1] D. AS, *Fatigue design of offshore steel structures*, Tech. Rep. (DNVGL AS, 2016) rP-C203.
- [2] D. A. Halfpenny, *A frequency domain approach for fatigue life estimation from finite element analysis*, International Conference on Damage Assessment of Structures **167-1**, 401 (1999).
- [3] M. B. Matjaž Mršnik, Janko Slavič, *Frequency-domain methods for a vibration-fatigue-life estimation - application to real data*, International Journal of Fatigue **47**, 8 (2013).
- [4] Y. Eldoğan and E. Cigeroglu, *Vibration fatigue analysis of a cantilever beam using different fatigue theories*, in *Topics in Modal Analysis, Volume:7* (The Society for Experimental Mechanics, 2004) Chap. 45, pp. 471–478.
- [5] Allseas, *Allseas / company / about*, <http://allseas.com/company/about/> (2017), [Online; 07/02/2017].
- [6] Allseas, *Allseas / equipment / Pioneering Spirit*, <https://allseas.com/equipment/pioneering-spirit/> (2017), [Online; 02/03/2017].
- [7] Allseas, *Pioneering spirit - photo gallery*, <https://allseas.com/equipment/pioneering-spirit/> (2017), [Online; 02/03/2017].
- [8] Y. Yu, *Pieter schelte – stinger & stf basis of design, rev.a*, (2013), document number - PI-929X1-001-M-F-001.
- [9] DrillingFormulas.Com, *Pipe line s-lay method*, <http://www.drillingformulas.com/pipe-line-s-lay-method/> (2016), [Online; 01/06/2017].
- [10] askIITians.com, *Wave motion*, <http://www.askiitians.com/iit-jee-wave-motion/> (2017), [Online; 02/03/2017].
- [11] I. Wikimedia Foundation, *Ship motions*, https://en.wikipedia.org/wiki/Ship_motions (2017), [Online; 02/03/2017].
- [12] J.-Q. Sun, *Stochastic Dynamics and Control* (Elsevier, 2006).
- [13] W. Fricke, *Fatigue analysis of welded joints: state of development*, Marine Structures **16**, 185 (2003).
- [14] W. F. Dieter Radaj, C M Sonsino, *Fatigue Assessment of Welded Joints by Local Approaches* (Woodhead Publishing Ltd., 2006).
- [15] M. AYGÜL, *Fatigue Analysis of Welded Structures Using the Finite Element Method*, Master thesis, CHALMERS UNIVERSITY OF TECHNOLOGY, Gothenburg (2012).
- [16] M. G. Backstrom M, *Evaluation of interaction equations for multiaxial loaded welded structures*, European Structural Integrity Society **1**, 65 (2001).
- [17] S. J. M. E. Niemi, W Fricke, *Fatigue Analysis of Welded Components: Designer's Guide to the Structural hot spot stress* (Woodhead Publishing Ltd., 2006).
- [18] C. M. Wooryong Park, *Fatigue assessment of large-size welded joints based on the effective notch stress approach*, International institute of welding **55**, 30 (2011).
- [19] N. R. Tom Lassen, *Fatigue Life Analyses of Welded Structures: Flaws* (ISTE Ltd., 2006).
- [20] M. M. Georgios Savaidis, *Advanced notch strain approach for fatigue calculation of welded components*, International Colloquium on Mechanical Fatigue of Metals **74**, 397 (2014).

- [21] W. F. P. L. Claas Fischer, Olav Feltz, *Application of the notch stress intensity and crack propagation approaches to weld toe and root fatigue*, International Journal of Fatigue **30**, 1556 (2008).
- [22] J. Wægter, *Stress concentrations in simple tubular joints*, Civil & Structural engineering course material, P8 (2009).
- [23] M. P. S. Halil Karadeniz, Vedat Togan, *Stochastic Analysis of Offshore Steel Structures* (Springer-Verlag, 2013).
- [24] D. N. B. . D. F. Sherratt, *Vibration fatigue analysis*, in *Finite Element Based Fatigue Calculations* (The International Association of Engineering Analysis community, 2000) Chap. 8, pp. 93–112.
- [25] C. research institute, *What the power spectral density function is and how the customer can use it*, <http://www.cygres.com/OcnPageE/Glosry/SpecE.html> (2017), [Online; 06/06/2017].
- [26] V. research institute, *What is the psd?* <http://www.vibrationresearch.com/university/lesson/what-is-the-psd/> (2015), [Online; 06/06/2017].
- [27] S. Chandrasekaran, *Damping in offshore structures*, in *Dynamic Analysis and Design of Offshore Structures*, Vol. 5 (Springer India, 2005) Chap. 4, pp. 155–171.
- [28] F. S. M. Priestley, *Methods of analysis*, in *Seismic Design and Retrofit of Bridges* (John Wiley & Sons Inc, 1996) Chap. 4.
- [29] N. Svensson, *Fatigue Analysis with Loads from MBS*, Master thesis, KTH Industrial Engineering and Management, STOCKHOLM (2015).
- [30] D. S. Steinberg, *VIBRATION ANALYSIS FOR ELECTRONIC EQUIPMENT - Third edition* (John Wiley & Sons, Inc., 2000).
- [31] D. A. Halfpenny and M. F. Kihm, *Rainflow cycle counting and acoustic fatigue analysis techniques for random loading*, 10th International Conference on Recent Advances in Structural Dynamics (2010).
- [32] T. Dirlik, *Application of computers in fatigue analysis*, Department of Engineering, University of Warwick (1985).
- [33] N. Bishop and F. Sherratt, *Theoretical solution for the estimation of 'rainflow' ranges from power spectral density data*, Fatigue & Fracture of engineering material and structures **13**, 311 (1990).
- [34] P. Ragan and L. Manuel, *Comparing estimates of wind turbine fatigue loads using time domain and spectral methods*, Wind Engineering **31**, 83 (2007).
- [35] Y. Yu, *Stinger structural design report, rev.a*, (2013), document number - PI-929-X1-001-S-R-001.
- [36] SteelConstruction, *Steel material properties*, https://www.steelconstruction.info/Steel_material_properties#cite_ref-BSEN1993-1-3_5-0 (2017), [Online; 03/11/2017].
- [37] G. Maymon, *Dynamic response of a structure to random excitation*, in *Structural Dynamics and Probabilistic Analyses for Engineers* (Elsevier, Butterworth-Heinemann, 2008) Chap. 3, pp. 70–145.
- [38] P. J. T. Broch, *Response of mechanical systems to vibrations and shocks*, in *Mechanical Vibration and Shock Measurements* (Brüel & Kjaer, 1984) Chap. 3, pp. 40–71.
- [39] R. E. T. C. L. A. G. of the Scalefour Society, *Deflection of beams*, <http://www.clag.org.uk/beam.html> (2010), [Online; 14/07/2017].
- [40] B. C. N. G. S. F. C. RYAN SIMMONS, SCOTT GORDON, *Finite element modeling continuous improvement*, https://femci.gsfc.nasa.gov/workshop/2001/posters/simmons/Simmons_MilesEquation.pdf (2001), [Online; 14/07/2017].
- [41] T. V. Irvine, *Steady-state vibration response of a cantilever beam due to base excitation*, https://pdfs.semanticscholar.org/8181/3053aca55c6172d73934fec236f4bcadc819.pdf?_ga=2.136381744.1829486450.1499341936-1287349595.1499341936 (2013), [Online; 19/07/2017].

- [42] A. G. P. Julius S. Bendat, *Engineering applications of correlation and spectral analysis* (John Wiley & sons, Inc., 1993).
- [43] T. E. Union, *Eurocode 3: Design of steel structures - Part 1-9: Fatigue*, Tech. Rep. (The European Union, 2005).
- [44] F. Engineering, *Femto engineering - homepage*, <https://www.femto.nl/> (2017), [Online; 05/11/2017].
- [45] R. L. M.H.A. Bonte, A. de Boer, *Prediction of mechanical fatigue caused by multiple random excitations*, PROCEEDINGS OF ISMA , 697 (2004).
- [46] S. S. Rao, *Harmonically excited vibration*, in *Mechanical Vbrations - Fifth Edition* (Pearson Education, Inc., 2011) Chap. 3, pp. 259–362.
- [47] W. T. V. B. P. F. William H. Press, Saul A. Teukolsky, *NUMERICAL RECIPES IN FORTRAN 77: THE ART OF SCIENTIFIC COMPUTING - Chapter 12* (Cambridge University Press, 1992).
- [48] R. M. Gray, *Probability, Random Processes, and Ergodic Properties* (Springer Verlag, 1987).
- [49] J. Engineering, *J-rain - free rainflow counting software*, <https://jesmondengineering.com/engineering-software/j-rain-free-rainflow-counting-software/> (2017), [Online; 24/10/2017].
- [50] J. Engineering, *J-rain v2.0, user guide*, (2013), document Number: JRP-13-024-1.

A

RESEARCH PAPER

Fatigue assessment of offshore tubular structures using Dirlik's method

Pankaj Dheer, Dr. Ir. Xiaoli Jiang, Dr. Ir. Yanrong Yu and Dr. Ir. Dingen Schott

Abstract Fatigue assessment for offshore structures has always been important, owing to the nature of dynamic loading caused by waves and wind. To effectively quantify the fatigue damage and design fatigue resistant structures, various recommendation practices developed by classification societies, like DNV-GL [1], are used. For tubular structures, fatigue assessment is conducted using hot spot stress approach, using stress concentration factors (SCF) formulae for simple joints and finite element method for multi-planar joints [1]. Traditionally, time domain analysis is conducted to calculate stresses at critical locations of the structure and fatigue damage is calculated using a suitable counting algorithm, mostly rainflow counting. Time domain analysis is computationally expensive, because at every time step, entire model has to be analyzed to calculate response [2]. Computational time can be reduce by conducting frequency domain analysis for bigger models and higher periods. Moreover, fatigue damage can be calculated with good accuracy using Dirlik's semi-empirical counting method [3].

Keywords: Fatigue, Tubular joints, FEM, PSD, Frequency analysis, Dirlik.

1 Introduction

Structures for offshore application are typically constructed using tubular frames fabricated from steel. To stiffen the structure, tubular members are joined together, forming tubular joints. A tubular joint consists of two main parts, 'chord' and 'brace', among them chord has the larger diameter of the two and there can be more than one brace attached to the chord. Fatigue analysis of tubular joints is conducted using hot spot stress life approach and fatigue damage is estimated using specified S-N curve and Miner's rule [1]. Depending upon the method of calculation of hot spot stress, tubular joints can be broadly classified as simple and complex joints. For simple tubular joints, hot spot stress is calculated using stress concentration factors depending upon the type of joint, formulae are available in [1]. For complex joints, hot spot stress is calculated using FEM and extrapolation methods.

Fatigue analysis of offshore structure is predominately conducted in time domain analysis with rainflow counting method, as the procedure is well established. However, for random loads like wave, wind and earthquakes, time based analysis can be computationally more expensive as the total analysis time is very high. This issue

Pankaj Dhher
3ME, Delft University of Technology, Delft, Netherlands e-mail: p.dheer@student.tudelft.nl

Dr. Ir. Xiaoli Jiang
3ME, Delft University of Technology, Delft, Netherlands e-mail: X.Jiang@tudelft.nl

Dr. Ir. Yanrong Yu
Allseas Engineering B.V, Delft, Netherlands e-mail: YY@allseas.com

Dr. Ir. Dingen Schott
3ME, Delft University of Technology, Delft, Netherlands e-mail: D.L.Schott@tudelft.nl

can be addressed by implementing frequency based analysis using Dirlik's method to estimate fatigue damage. Dirlik's method has been proven to offer good accuracy in estimating fatigue damage results compared to rain-flow counting [3, 4, 5, 6, 7]. In this study, feasibility of frequency analysis with Dirlik's method is checked on simple models like cantilever beam and a simple frame, by conducting simulations in FEMAP. Fatigue damage results calculated using Dirlik's method are verified by conducting equivalent time based analysis with rain-flow counting method. First, the theory behind frequency analysis including loads in power spectral density are discussed, which is followed by explaining important steps involved in the frequency analysis on the selected models. Next, the results for verification models are discussed followed by the conclusion.

2 Methodology

Structural response due to environmental loads like wave, wind and earthquake are random in nature and hence, analysis in frequency domain provides better understanding on the structural behavior [8]. We start with a brief description of the basic principles of frequency analysis, followed by discussion on the input loads for frequency analysis in FEM and conclude with the verification procedure for the selected models.

2.1 Frequency domain analysis

Frequency analysis is used to calculate structural response of a system due to oscillating excitations. There are two ways in which frequency response analysis can be conducted in FEM, Direct frequency response analysis (DFRA) and Modal frequency response analysis (MFRA). Modal frequency response analysis is used in this research due to its ability to reduce the size of the problem by analyzing only the relevant frequencies of the structure. Accuracy of MFRA is comparable with DFRA for larger models and can be increased by considering more mode shapes during the analysis. The equilibrium equation for a linear structural system in terms of frequency (ω) is given below in Equation 1 [8].

$$\{P(\omega)\} = ([K] + i\omega[C] - \omega^2[M])\{D(\omega)\} \quad (1)$$

where 'K', 'C' and 'M' are stiffness, damping and mass matrix of the structure and 'D' and 'P' are representing displacement and load vectors in terms of frequency ' ω '. Frequency analysis in FEM is conducted using loads represented as power spectral density functions which uses the relationship shown in Equation 2 to calculate the response of structure [2].

$$|P(\omega)| = |H(\omega)|^2 \times |D(\omega)| \quad (2)$$

In Equation 2, $|P(\omega)|$ is the structural response, $|D(\omega)|$ is the input load and $|H(\omega)|$ is the complex transfer function. A transfer function can be defined as the response per unit input frequency of interest [2]. The concept of transfer function arises from the fact that any increase in amplitude of the input for a linear structure will have a proportional effect on the amplitude of the output. Transfer function only depends upon the structure and can be calculated separately, the response can then be easily calculated by multiplying the input with the transfer function, saving computational time [2]. It should be noted that the terms in Equation 2 are represented as power spectral density. In the next section, power spectral density is explained along with the description of loads used for verification.

2.2 Power Spectral Density

Loads in frequency domain analysis in FEM is represented in the form of a *Power spectral density*, which gives information about the normalized power of the input or load at different frequencies. Power Spectral density (PSD) is calculated from the Fourier transform ($f(\omega)$) obtained from a time series using Equation 3 [8].

$$f(\omega) = \frac{1}{2\pi} \int_{-\infty}^{\infty} f(t)e^{-i\omega t} dt$$

$$PSD = \frac{|f(\omega)|^2}{\omega} \quad (3)$$

where ω is the frequency in Hz and 't' is the total time. To get PSD (normalized power), the output of the Fourier transform has to be squared and divided by the frequency to get $units^2/Hz$ as shown in Equation 3. The simulation is conducted in FEMAP under "Random response analysis", which calculates the dynamic response of the structure in terms of response power spectral density. In this research, output responses are calculated as axial force PSD (N^2/Hz) and bending moment PSD (N^2m^2/Hz) in the pre-selected elements of the models. Two types of loads are used for verifying frequency analysis, which are, periodic (sine and cosine) loads and random (consisting of Gaussian distributed numbers) loads. The inputs required for the analysis are listed below:

1. **Damping:** Analysis of practical model should always include damping to completely consider the effects of loads on the structure and to get accurate results. In this paper, structural and viscous damping are considered for the models and a constant damping ratio (ζ) of 2% is used for both the models [9].
2. **Frequency range:** The models are analyzed within a frequency range which is selected based on the natural frequencies. For cantilever beam, frequency range from 0 Hz to 350 Hz is selected and for the frame 0 Hz to 210 Hz is selected. Enough frequencies should be used so that at-least 90% of the mass of the structures in the loading direction should be included [10].
3. **Input loads:** In this paper, acceleration is used as the main input load. For periodic and random loads, values of acceleration are assumed. The loads in time domain are converted to PSD using Fast Fourier Transform algorithm in MATLAB within the specified frequency range.

The procedure of fatigue estimation using the output response PSD calculated in FEM is explained in the next section.

2.3 Fatigue estimation using Power Spectral Density

Figure 1 highlights the important steps involved in a frequency domain fatigue estimation process.

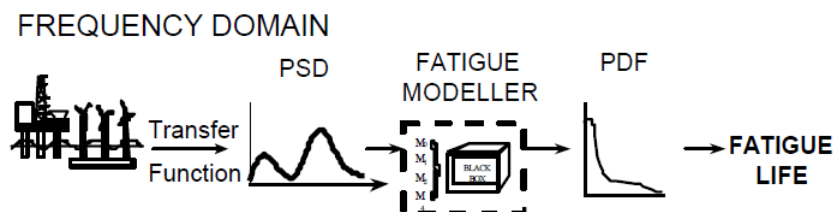


Fig. 1: Typical frequency domain fatigue life estimation process [2]

The response PSD is in terms of stress in the pre-selected element of the model, it is calculated from axial force PSD and bending moment PSD calculated from FEMAP. Dirlik's method is used as the fatigue modeller to calculate probability density function (PDF) of the stress ranges. From PDF, fatigue is calculated using S-N curve and Miner's rule. Two models are considered for verifying the frequency analysis, are shown in Figures

2 and 3. In Figures 2 and 3, we can see the location and direction of load, the material and geometric properties of the model and the pre-selected element at output response is calculated in FEMAP. For frame model, the hot spot stress PSD will be calculated using the recommendations provided in DNVGL-RP-C203:2016 [1]. As there are no tubular joints in cantilever beam, nominal stress will be calculated instead of hot spot stress.

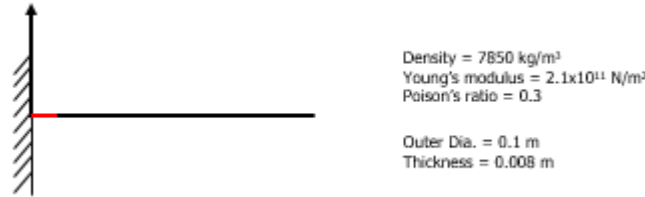


Fig. 2: Cantilever beam

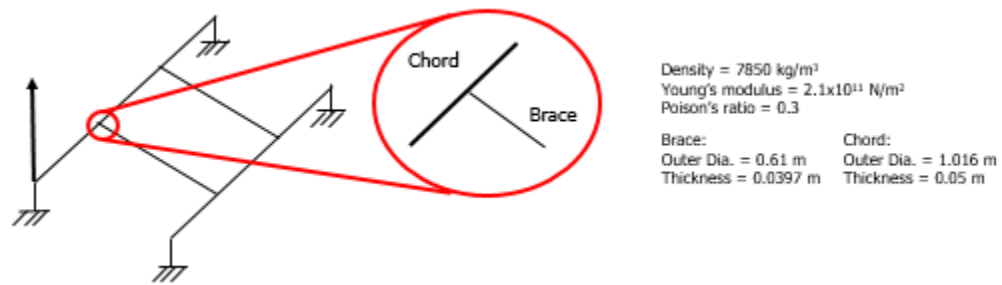


Fig. 3: Simple frame model

For verification of frequency analysis, fatigue damage values will be compared with equivalent time analysis with rainflow counting. The algorithm used for rainflow counting is available as an open-source software called as 'J-rain' [11], which is verified using hand calculations. The output of 'J-Rain' is the number of cycles and stress ranges, which can be used to calculate fatigue damage using Equation 4 (D_{time}) [12]. Dirlik's method calculates the probability density function of stress range which can be used to calculate fatigue damage using Equation 4 ($D_{frequency}$) [12]. The two damage values will be compared.

$$D_{time} = \frac{1}{C} \sum_{i=1}^k NS^m \quad D_{frequency} = \frac{E[P] T}{C} \sum_{i=1}^k p(S_i) S_i^m ds \quad (4)$$

In Equation 4, k is the number of divisions of stress range S , N is the number of cycles of stress ranges calculated using counting methods. m is the Basquin exponent and C is the Basquin constant, both the values can be found from S-N curve. $E[P]$ is the expected number of peaks calculated using spectral moments (m_n) shown in Equation 5 [3] and T is the total time in seconds.

$$E[P] = \sqrt{\frac{m_4}{m_2}} \quad (5)$$

$$m_n = \int f^n G(f) df \quad (6)$$

Spectral moments (m_n) are inherent properties of Power spectral density and can be used to calculated using Equation 6, where f is the frequency and $G(f)$ is the value of the stress PSD calculated from FEMAP output. For Dirlik's method, four spectral moments are calculated namely, m_0 , m_1 , m_2 and m_4 . These can be used to

calculate all the parameters in Equation 8 [3], and then calculate $p(S)$, probability density function and number of cycles $N(S)$ using Equation 7 [3].

$$N(S) = E[P] T p(S), \quad p(S) = \frac{D_1 e^{-Z/Q} + \frac{D_2 Z e^{-Z^2/2R^2}}{R^2} + D_3 Z e^{-Z^2/2}}{2\sqrt{m_0}} \quad (7)$$

$$\begin{aligned} D_1 &= \frac{2(x_m - \gamma^2)}{1 + \gamma^2} & R &= \frac{\gamma - x_m - D_1^2}{1 - \gamma - D_1 + D_1^2} & D_2 &= \frac{1 - \gamma - D_1 + D_1^2}{1 - R} \\ D_3 &= 1 - D_1 - D_2 & Q &= \frac{1.25(\gamma - D_3 - D_2 - R)}{D_1} & Q &= \frac{1.25(\gamma - D_3 - D_2 - R)}{D_1} \\ Z &= \frac{S}{2\sqrt{m_0}} & x_m &= \frac{m_1}{m_0} \sqrt{\frac{m_2}{m_4}} & \gamma &= \frac{m_2}{\sqrt{m_0 m_4}} \end{aligned} \quad (8)$$

x_m is the mean frequency, γ is the irregularity factor and Z is the normalized stress range. The method for calculating $p(S)$ and $N(S)$ was given by Dirlik in 1985 after conducting Monte-Carlo simulations to find the best-fit values of all the parameters using thousands of test data [13]. Using these steps, fatigue damage is calculated in both time and frequency domain for both the models and the results are discussed in the next section.

3 Results & Discussion

Figure 4 shows the comparison of fatigue damage values calculated from time and frequency analysis for cantilever beam. Fatigue damage is calculated according to Equation 4 considering a single slope S-N curve for steel with Basquin exponent (m) equal to '3' and Basquin constant (C) equal to $10^{14.88}$, according to Eurocode [14] and assumed analysis time of 60 seconds. Considering results of time analysis as the basis, percentage error is calculated to calculate the difference in the result of frequency analysis. In total, six different load cases are considered depending on the nature and quantity of loads. These six cases can be broadly classified as periodic (sine) and random loads. For periodic loads, different cases evaluated are harmonic (single frequency), non-harmonic (three frequency) and two different loads at the same time. For random loads, only two cases with single and two loads are implemented.

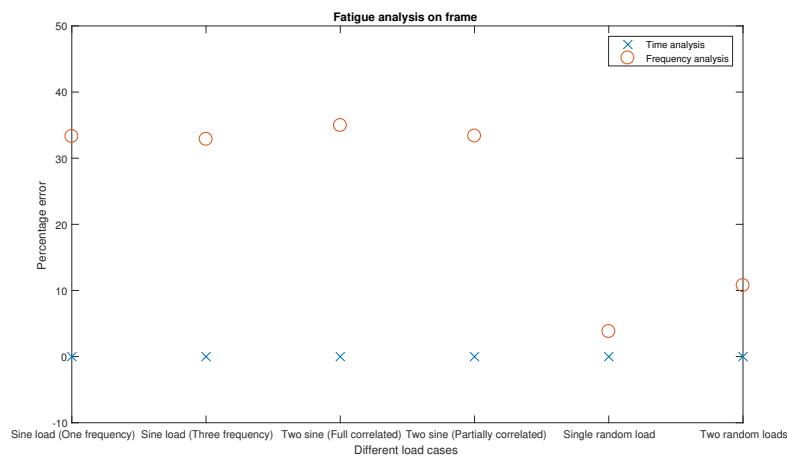


Fig. 4: Fatigue damage results - Cantilever beam

Comparison of fatigue damage results for cantilever beam reveals that for random loads (both cases), the values calculated using frequency analysis are within 10% of the values calculated using time analysis. Results are in-line with the results presented in the paper [12], verifying the frequency analysis procedure for random loads. For periodic loads, a constant difference of more than 30% is observed for all the different cases. These results are also in-line with the results presented in paper [12], where for periodic loads, fatigue damage value calculated for different combinations of sine loads consistently had more than 30% difference.

Similar analysis is conducted for frame model, starting with single periodic and single random load. Figure 5 shows the comparison of fatigue damages values calculated using time and frequency analysis. From the results, it is observed that the difference in the damage values is large. An extensive study is conducted using different models and different loading conditions to determine the probable causes for the deviation in the observed results. The summary of this study is given below:

1. **Increase analysis time:** To evaluate the effect of the analysis time, it is extended to 120 seconds, which is the case for both periodic and random loads. Similar difference in the damage results were observed for both types of load. Main issue is found in the FEMAP output of time domain analysis. Frequency analysis is giving expected results for both loading type.
2. **Using different model:** A different model with similar boundary conditions is analyzed for periodic and random loads. Again, similar differences in fatigue damage results are found for this new model. Similar to previous analysis, the issue is related to the FEMAP output of time domain analysis. Frequency analysis is giving expected results for both the loads.
3. **Change in boundary condition:** Boundary conditions similar to cantilever beam are applied to the frame model. Also, instead of a single load, two periodic loads are applied at the same time. Expected results are observed for time domain analysis with two periodic loads, attaining peak response around the natural frequency of the model. For frequency analysis, results also achieve peak response around the natural frequency, but the response also contained negative values. For frequency analysis, as all applied PSD loads are positive, only positive response values should be achieved [2]. Using this argument, the results of frequency analysis were concluded as incorrect.

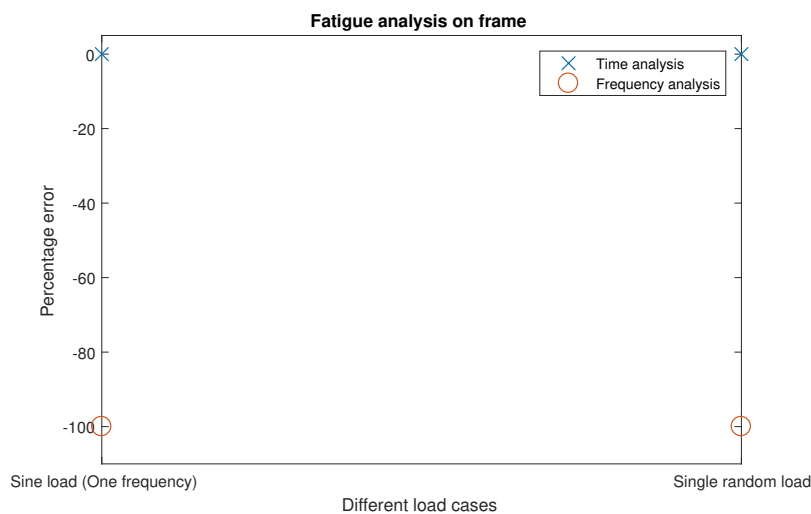


Fig. 5: Fatigue damage results - Frame

As seen from the above description of results, a detailed study was conducted to find the main issue in the analysis of frame. From the results of the analyses, we arrive at the following conclusion.

4 Conclusion

In this paper, a feasibility study is conducted on using Dirlik's method for fatigue assessment. Two models are chosen to verify the application of frequency analysis with Dirlik's method to calculate fatigue damage by comparing the results obtained from equivalent time domain analysis. For cantilever beam, comparable fatigue damage results are calculated using Dirlik's method for six different loading cases. However, similar results could not be achieved for frame model. Detail analysis is conducted to find the major reasons for the deviations in the results. After conducting analysis on different models with different boundary conditions and loads, the conclusion are:

1. For application with single loads, it is observed that, time domain analysis is giving unexpected results. The main reason for this could be the boundary conditions of the frame model. When the boundary conditions were changed, results obtained from time domain analysis are according to expectation. However, the core reason for this could not be further explored as it is mainly related with the internal workings of the solver.
2. Another deviation found in time domain analysis with single loads on frame and related models are, the conversation of applied acceleration loads into displacements. In FEMAP, acceleration is integrated twice to convert to equivalent displacement, adding two constants of integration. The addition of two constants may be one of the reasons for deviations in time domain results.
3. For applications of two loads, analysis is conducted on cantilever beam and the fatigue damage results are found to be comparable. Using the same analysis procedure, frame model is analyzed, but negative bending moment PSD results are calculated for frequency analysis in FEMAP, even though there are no negative inputs given to the analysis. Because of this, further damage calculation could not be conducted. As the method works for cantilever beam, definitive reasons for deviation in the results for frame model cannot be given until further study is conducted.

From the research conducted in this study, we can conclude that additional simulations with modified strategy are needed to better understand the issue involving the frame model. One of the recommendation would be to use displacement at the load to avoid errors due to double integration in FEMAP. The analysis procedure works well for the cantilever beam for periodic as well as random loads. For periodic load, conservative results are calculated using Dirlik's method, however, from the industrial point of view, these results can be used in the early stages of design to understand the effect of different types of loads and modifications.

References

- [1] Det Norske Veritas-Germanischer Lloyd SE (2016) Fatigue design of offshore steel structures. Recommended practice, DNVGL-RP-C203.
- [2] Dr. NWM Bishop & Dr. F Sherratt (2000) Finite Element Based Fatigue Calculations. Chapter '8', Vibration Fatigue Analysis. The International Association of Engineering Analysis community 93–112.
- [3] Dr. Andrew Halfpenny (1999) A frequency domain approach for fatigue life estimation from Finite Element Analysis. International Conference on Damage Assessment of Structures 167-1:401–410.
- [4] Dr. Andrew Halfpenny and Mr. Frédéric Kihm (2010) RAINFLOW CYCLE COUNTING AND ACOUSTIC FATIGUE ANALYSIS TECHNIQUES FOR RANDOM LOADING. 10th International Conference on Recent Advances in Structural Dynamics.
- [5] Niklas Svensson (2015) Fatigue Analysis with Loads from MBS. Master Thesis, KTH Industrial Engineering and Management, STOCKHOLM.
- [6] Yusuf Eldoğan and Ender Cigeroglu (2004) Vibration Fatigue Analysis of a Cantilever Beam Using Different Fatigue Theories. Chapter "45", 471–478, Topics in Modal Analysis, Volume:7, The Society for Experimental Mechanics.
- [7] Matjaž Mršnik, Janko Slavič, Miha Boltežar (2013) Frequency-domain methods for a vibration-fatigue-life estimation - Application to real data. International Journal of Fatigue, Vol: 47, 8–17, DOI:

10.1016/j.ijfatigue.2012.07.005.

- [8] Halil Karadeniz, Vedat Togan, Mehmet Polat Saka (2013) Stochastic Analysis of Offshore Steel Structures. Springer-Verlag, London.
- [9] Chandrasekaran, Srinivasan (2005) Damping in Offshore Structures. Chapter "4", 155–171, Dynamic Analysis and Design of Offshore Structures, Volume:5, Springer New Delhi, India, DOI: 10.1007/978-81-322-2277-4.
- [10] F. S. M. Priestley (1996) Methods of analysis in Seismic Design and Retrofit of Bridges. Chapter "4", John Wiley & Sons Inc.,
- [11] Jesmond Engineering (2017) J-Rain – Free Rainflow Counting Software
<https://jesmondengineering.com/engineering-software/j-rain-free-rainflow-counting-software/>. Cited 24 October 2017
- [12] Patrick Ragan and Lance Manuel (2007) Comparing estimates of wind turbine fatigue loads using time domain and spectral methods. Wind Engineering, Vol: 31, 83–99.
- [13] Dr. Turan Dirlik (1985) Application of computers in fatigue analysis. PhD thesis, Department of Engineering, University of Warwick.
- [14] The European Union (2005) Eurocode 3: Design of steel structures - Part 1-9: Fatigue. The European Union, Brussels.

B

RESEARCH FLOWCHARTS

B.1. DETAIL RESEARCH FLOW

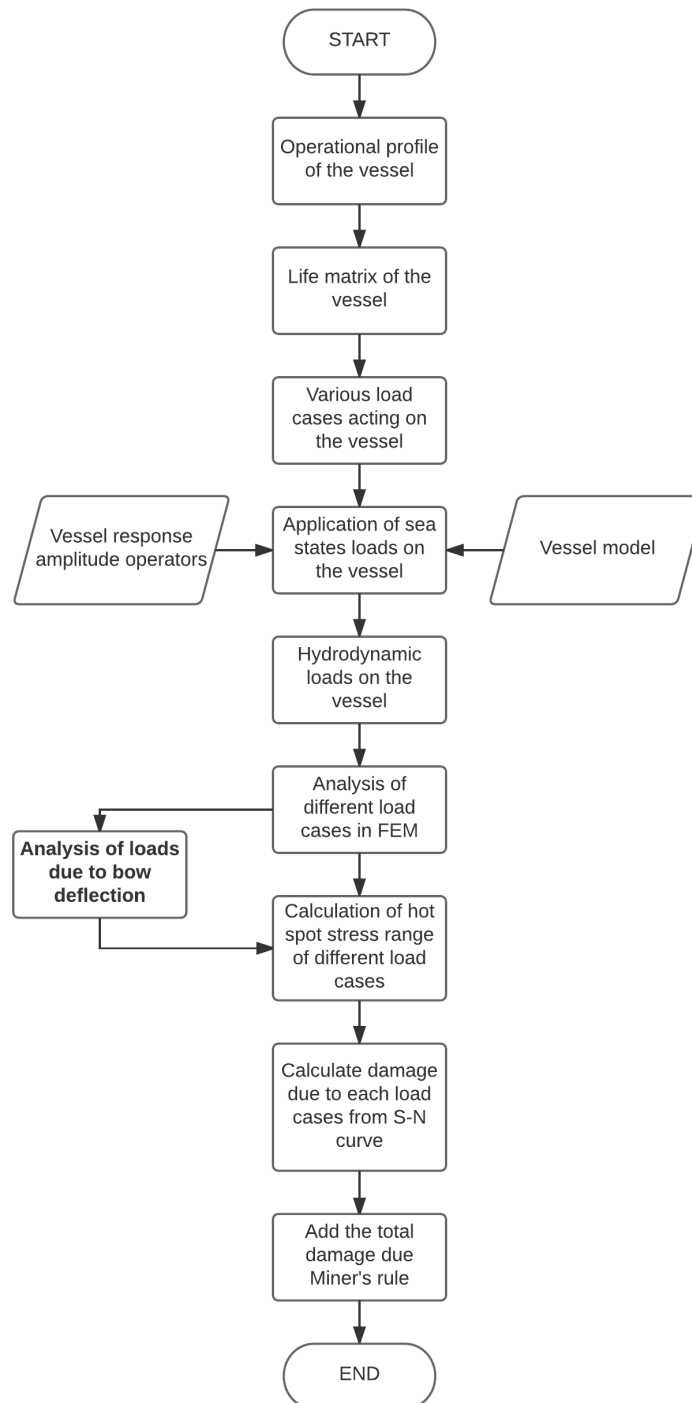


Figure B.1: Overview of Fatigue analysis of stinger

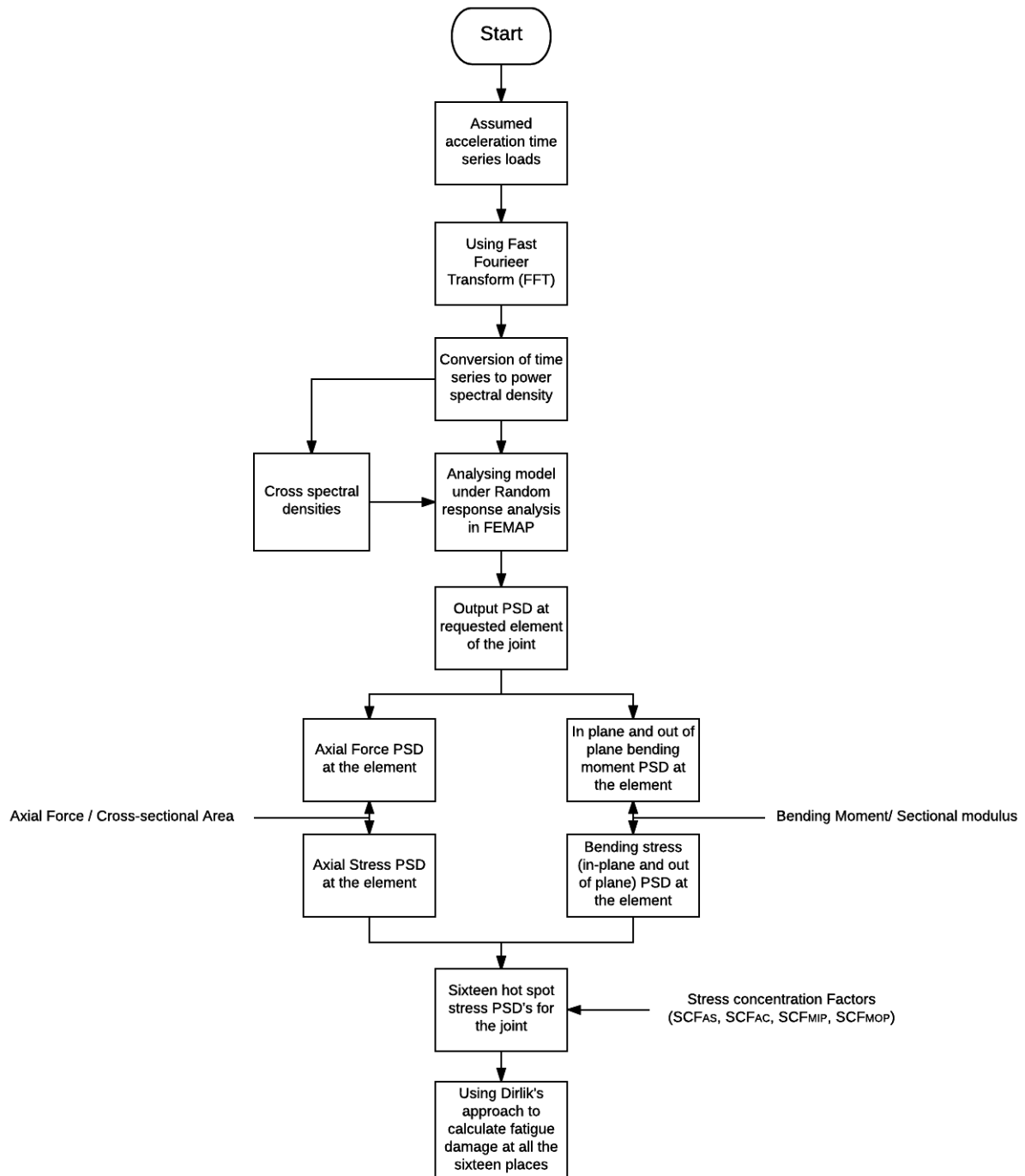


Figure B.2: Research flow - Part 1

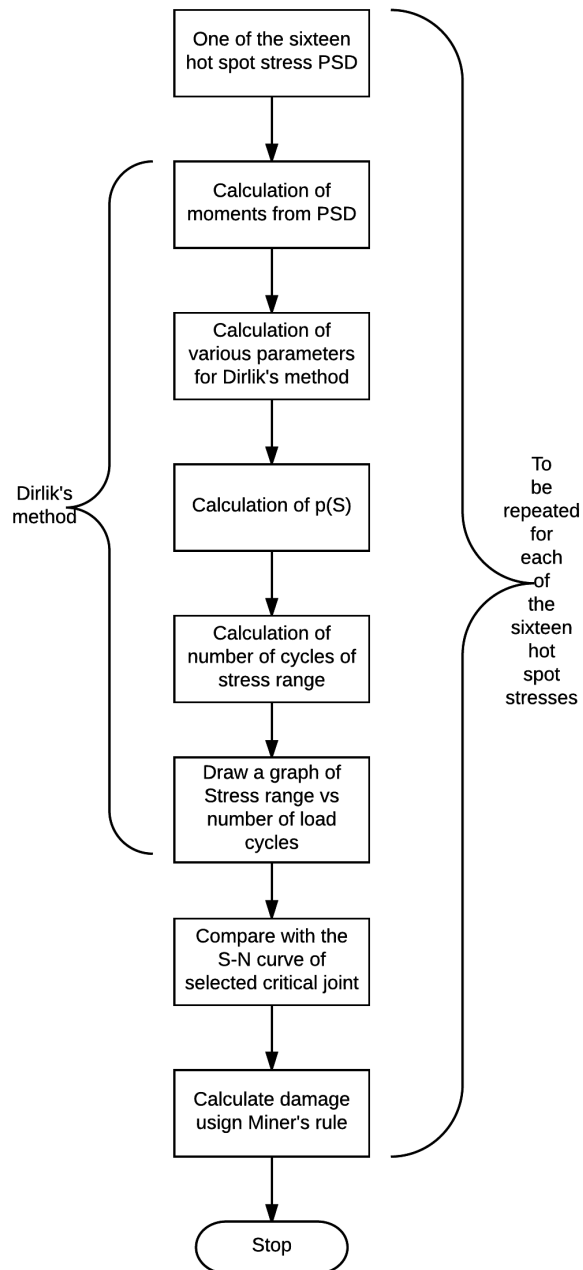


Figure B.3: Research flow - Part 2

C

ADDITIONAL THEORY

C.1. VIBRATION DUE TO BASE EXCITATION

Base excitation systems are often related with vibrational analysis. Most commonly, suspensions of automobiles are analyzed due to base excitation at the wheels of the vehicles due to rough loads. Fatigue analysis on the suspension supports and its components are conducted to make sure they are safe during operations on rough roads. Figure C.1 shows a mass attached to a spring-damper system which is displaced by a base motion $y(t)$ which in turn displaces mass m with a motion of $x(t)$.

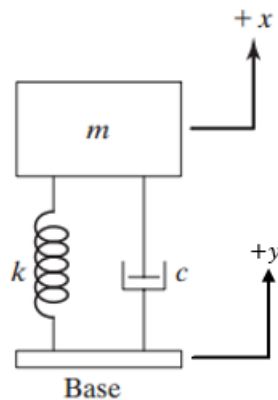


Figure C.1: Mass with spring-damper system [46]

If we assume $y(t)$ to be a simple harmonic motion which causes displacement of the base by a function $y(t) = Y \sin \omega t$, where Y is the amplitude, ω is the frequency of oscillation and t is the total time, the equation of motion for displacement of mass m is given by the Equation C.1 [46].

$$m\ddot{x} + c(\dot{x} - \dot{y}) + k(x - y) = 0 \quad (\text{C.1})$$

where c is the damping coefficient and k is the stiffness of spring, $x - y$ is the net elongation and $\dot{x} - \dot{y}$ is the relative velocity at two ends of the damper. If we substitute the value of $y(t)$ in Equation C.1 we can get Equation C.2 [46].

$$m\ddot{x} + c\dot{x} + kx = c\dot{y} + ky = A \sin(\omega t - \alpha) \quad (\text{C.2})$$

where $A = Y\sqrt{k^2 + (c\omega)^2}$ and $\alpha = \tan^{-1}\left(\frac{-c\omega}{k}\right)$, from this we can conclude that base excitation due to harmonic motion can be treated as an equivalent to a system where mass m is excited by a harmonic force with an amplitude A . Thus, the steady state response of the mass subjected to base excitation can be calculated using Equation C.3 [46].

$$x_{ss} = \frac{Y\sqrt{k^2 + (c\omega)^2}}{[(k - m\omega^2)^2 + (c\omega)^2]^{1/2}} \sin(\omega t - \phi_1 - \alpha) \quad (C.3)$$

where x_{ss} is the steady state displacement response of mass m and ϕ_1 is given by Equation C.4 [46].

$$\phi_1 = \tan^{-1}\left(\frac{c\omega}{k - m\omega^2}\right) \quad (C.4)$$

In a more general form, the steady state response x_{ss} can be represented as, $x_{ss} = X\sin(\omega t - \phi)$. For this research, we are interested in the relative motion with respect to the base. The equation of motion is expressed in Equation C.5 [46].

$$m\ddot{z} + c\dot{z} + kz = -m\ddot{y} = m\omega^2 Y \sin\omega t \quad (C.5)$$

where $z = x - y$, and the steady state displacement response is given by Equation C.6 [46].

$$z_{ss} = \frac{mY\omega^2 \sin(\omega t - \phi_1)}{[(k - m\omega^2)^2 + (c\omega)^2]^{1/2}} \quad (C.6)$$

In this way, the steady state response of a mass attached to a simple spring-damper system can be calculated.

C.2. RANDOM PROCESS

A physical phenomenon and data representing it are considered random when a future time history record from the experiment cannot be predicted within reasonable error [42]. To fully understand the data it is important to conceptually think in terms of all time signals that could have been occurred. The Dirlik's method is only applicable for stationary ergodic random processes. A stationary random process can be defined as the random process in which the mean and variance of the process does not change during the whole time record. An ergodic process is a stationary process whose properties computed from time averages over individual records will be the same from one time record to another and it will be equal to the properties of the stationary process calculated at average time records [47]. In terms of a dynamic system, an ergodic system has a property of a system with respect to measurement frequency 'f' if the sample average (f_n) converges almost everywhere along Equation C.7 [48].

$$f_n = n^{-1} \sum_{i=1}^{n-1} f(T^i x) \quad (C.7)$$

C.3. FAST FOURIER TRANSFORM

Fourier transform is a simple and efficient computational tool for accomplishing certain common manipulation of data [47]. A physical process can be represented either in time domain by some quantity 'h' which is a function of time 't' ($h(t)$), or can be represented in frequency domain where the amplitude of the quantity 'H' is a function of frequency 'f' ($H(f)$). $h(t)$ and $H(f)$ are merely two different ways of representing the same quantity and Fourier transform equations are used to switch between these two representations. Equations C.8 and C.9 gives the Fourier transform equations for switching between time domain and frequency domain [47].

$$H(f) = \int_{-\infty}^{\infty} h(t)e^{2\pi i f t} dt \quad (C.8)$$

$$h(t) = \int_{-\infty}^{\infty} H(f)e^{-2\pi ift} df \quad (\text{C.9})$$

Our main focus is to calculate power of the signal using the Fourier transform equations. There are mainly two types of algorithms which help in the calculation of power of a signal namely, Discrete Fourier transform (DFT) and Fast Fourier transform (FFT). As the number of computations for FFT is smaller when compared to DFT for a same signal, it is preferred method to convert time domain data to frequency domain and vice versa. Mathematically, DFT requires N^2 number of operations to perform Fourier transform, where N is the number of samples of the signal. On the other hand, FFT requires $N \log_2 N$ operations to perform the same transformation. For example, of $N = 10^6$, the calculation time for DFT was roughly about 2 weeks compared to around 30 seconds by FFT [47]. The theory of FFT was developed in the mid-1960s by J.W. Cooley and J.W. Tukey [47] and this will be explained below.

In 1942, Danielson and Lanczos provided the algorithm of FFT by showing that the Fourier transform of a signal of length N can be divided into two signals, one containing the even numbered points of N and the other containing odd number of points as shown in Figure C.2.

$$\begin{aligned} F_k &= \sum_{j=0}^{N-1} e^{2\pi ijk/N} f_j \\ &= \sum_{j=0}^{N/2-1} e^{2\pi ik(2j)/N} f_{2j} + \sum_{j=0}^{N/2-1} e^{2\pi ik(2j+1)/N} f_{2j+1} \\ &= \sum_{j=0}^{N/2-1} e^{2\pi ikj/(N/2)} f_{2j} + W^k \sum_{j=0}^{N/2-1} e^{2\pi ikj/(N/2)} f_{2j+1} \\ &= F_k^e + W^k F_k^o \end{aligned}$$

Figure C.2: Dividing a single signal into two [47]

where F_k is the original signal and it has been divided into two signals each of length $N/2$, F_k^e containing all the even numbered points and F_k^o containing all the odd numbered points. W^k is given by equation C.10

$$W \equiv e^{2\pi i/N} \quad (\text{C.10})$$

The most important advantage of the algorithm is that you can still divide the signals F_k^e and F_k^o into two parts each making four signals each with a length of $N/4$. This step is carried out till the length of the signal becomes 1. Then the individual Fourier transformation is done and then these are combined according together. This is done in two different sections, the first section is responsible to sort the data into bit-reversed order and then the second sections transforms has an outer loop which performs $\log_2 N$ transformations. The sorting of data according to bit-reversals does not take up any additional memory which leads to completion of the algorithm in $N \log_2 N$ operations. Since the length of the signal helps to increase the efficiency of the operations, it is important to convert a signal which has a signal length of 2^N , this is help in an effective division of signal [47]. If the length is not a integer power of 2, then it is suggested to add zero value data to increase the length of the signal.

C.4. CROSS POWER SPECTRAL DENSITY

Cross power spectral density (CSD) gives relation between any two power spectral density functions. It is also the Fourier transform of cross correlation function [42]. When two or more power spectral densities act on a system at the same time, it is important to understand the relation between the amplitudes and phase information between these spectral densities. The process for calculating cross spectral density is shown in Figure C.3.

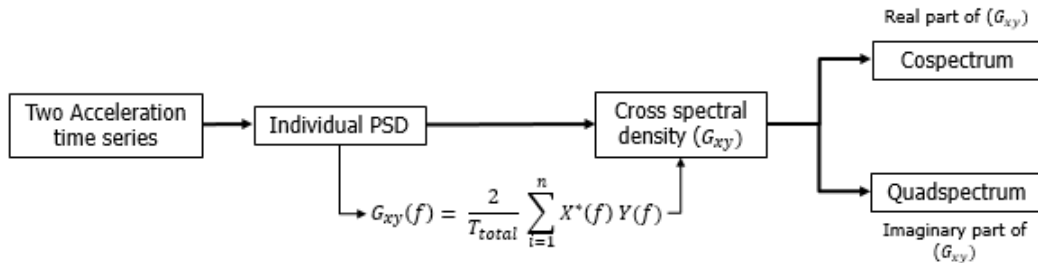


Figure C.3: Process of calculating Cross spectral density function

There are broadly two methods to calculate CSD, one by calculating the cross correlation function between the two time series and then using Fourier transformation or the second and the preferred method is to calculate power spectral densities of both the time series and then using the equation given in Figure C.3 to calculate the single sided spectrum of cross power density [42]. Multiplication of '2' is needed to convert two sided power spectral density to single sided spectrum to avoid use of negative frequencies. The CSD calculated is a complex signal and has to be divided into real and imaginary part. The real part gives relation between amplitudes of the two time series and imaginary part gives information on the phase differences between the time series.

The power spectral density and cross spectral density are given as inputs in the FEM model along with the natural frequencies of the model. Depending upon the number of time series loads act on a model, the number of cross spectral densities changes. For example, if there are two time series acting on the model, like in our case of simple frame model with two nodes excitation, the number of cross spectral density is one (one real part and one imaginary part). However, if we consider our simple frame model with four nodes excitation, the number of cross spectral density increase to six (six real part and six imaginary part). The six spectral density and their relations are shown in Figure C.4.

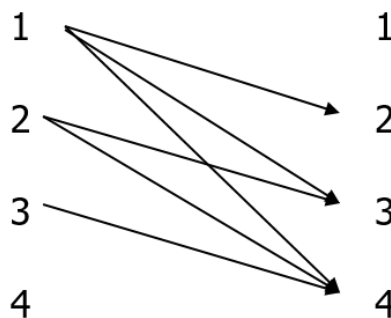


Figure C.4: Six cross spectral density for four time series input

The cross spectral density between four time series is shown in the above figure, it is important to understand that CSD between a signal 'X' and signal 'Y' is the same as the CSD between signal 'Y' and signal 'X'. For example, the CSD between signals '1' and '2' is same as CSD between '2' and '1', hence it is calculated only once. This brings the total to six CSD's for four time series.

D

MATLAB CODES

D.1. DYNAMIC RESPONSE OF SDOF MODEL

```
1 clear;
2 clc;
3 % This MATLAB file is coded to calculate the RMS response of displacement
4 % and acceleration for a SDOF mass spring damper system according to
5 % John Mile's equation for flat acceleration power spectral density
6
7 %% SDOF input variable
8 E = input('Enter Youngs modulus of the material in N/m^2: '); % Youngs modulus in N/
   m^2
9 L = input('Enter total length of the cantilever beam in meters: '); % Length of beam
   in m
10 OD = input('Enter the outer diameter in meters: '); % Outer diameter of beam in m
11 T = input('Enter the thickness in meters: '); % Thickness of beam in m
12 Rho = input('Enter density of material in kg/m^3: '); % Density of the beam in kg/m
   ^3
13 Damp = input('Enter a constant damping ratio for the system: '); % Critical damping
   ratio
14 Mass = input('Enter the mass attached at the end in kg: '); % Mass at the end of the
   beam in kg
15 PSD_in = input('Enter a constant acceleration PSD in m^2/s^4/Hz: '); % Input
   acceleration PSD in m^2/s^4/Hz
16 g = 9.81; % Acceleration due to gravity in m/s^2
17
18 %% SDOF calculations
19 ID = OD-(2*T); % Inner diameter of beam
20 Area = (OD^2-ID^2)*pi/4; % Cross sectional area
21 Iner = (OD^4-ID^4)*pi/64; % Area moment of inertia
22
23 PSD_in_g = PSD_in/(g*g); % Input PSD in g^2/Hz
24 delta = (Mass*g*L^3)/(3*E*Iner); % Deflection at the free end due to weight in m
25 freq = ((g/delta)^(1/2))*((2*pi)^(-1)); % First Natural frequency of the beam in Hz
26 Q = 1/(2*Damp); % Transmissibility
27
28 G_rms = ((pi*Q*freq*PSD_in_g)/2)^(1/2); % RMS value of acceleration in g
29 Yrms = ((Q*PSD_in)/(32*pi^3*freq^3))^(1/2); % RMS value of displacement in m
30 Grms = G_rms*g; % RMS value of acceleration in m/s^2
31
```

```

32 %% Display output
33
34 fprintf('RMS displacement of mass = %0.2f m\n', Yrms);
35 fprintf('RMS acceleration of mass = %0.2f m/s^2', Grms)

```

D.2. DYNAMIC RESPONSE OF MDOF MODEL

The following MATLAB code can be used to calculate dynamic displacement response at the free end of the cantilever beam subjected to either single or two PSDs.

```

1  clear;
2  clc;
3
4  % This MATLAB code is used to calculate the dynamic frequency response of a
5  % cantilever beam subjected to input excitation acceleration PSD with units
6  % (m/s^2)^2/Hz. The output calculated is the displacement response in units
7  % m^2/Hz at the free end of the beam.
8  % For single PSD excitation, input is an external ASCII file having two
9  % columns 'Frequency (Hz) and Acceleration PSD ((m/s^2)^2/Hz)
10 % For two PSD excitation, three inputs should be provided as three
11 % different external ASCII files. Two of the files should contain the input
12 % PSD's and third should contain ABSOLUTE Cross spectral density (CSD)
13 % values.
14 % The code also calculates the first four natural frequencies of the
15 % cantilever beam and in order to do that it requires below mentioned
16 % inputs. The code also considers a constant damping of 0.02 throughout the
17 % frequency range and it applicable for circular and square cross-sections
18 % only.
19 %% Inputs
20
21 E = input('Enter Youngs modulus of the material in N/m^2: '); % Youngs modulus in N/
    m^2
22 L = input('Enter total length of the cantilever beam in meters: '); % Length of beam
    in m
23 Rho = input('Enter density of material in kg/m^3: '); % Density of the beam in kg/m
    ^3
24 cs = input('Select cross sectional area, 1 = Circular tube, 2 = Square tube: ');
25 Damp = 0.02; % Critical damping ratio
26
27 % Constant for calculating natural frequency
28 A1 = 1.875;
29 A2 = 4.694;
30 A3 = 7.854;
31 A4 = 10.995;
32
33 %% Natural frequency calculation
34
35 if cs == 1
36     OD = input('Enter the outer diameter in meters: ');
37     T = input('Enter the thickness in meters: ');
38     ID = OD-2*T; % Inner diameter of beam
39     Area = (OD^2-ID^2)*pi/4; % Cross sectional area
40     Iner = (OD^4-ID^4)*pi/64; % Area moment of inertia
41 elseif cs == 2
42     OD = input('Enter the outer length in meters: ');
43     T = input('Enter the thickness in meters: ');
44     ID = OD-2*T; % Inner diameter of beam

```

```

45     Area = OD^2-ID^2; % Cross sectional area
46     Iner = (OD^4-ID^4)/12; % Area moment of inertia
47     else
48         disp('Please enter either 1 or 2 as input');
49         return
50     end
51
52     Mass = L*Rho*Area; % Mass of the beam in kg
53     Rho_L = Rho*Area; % Mass per length in kg/m
54
55     % Constants for natural frequency
56     B1 = A1/L;
57     B2 = A2/L;
58     B3 = A3/L;
59     B4 = A4/L;
60
61     % First four natural frequencies of the beam
62     omega_n_1 = B1^2*((E*Iner)/Rho_L)^(1/2);
63     omega_n_2 = B2^2*((E*Iner)/Rho_L)^(1/2);
64     omega_n_3 = B3^2*((E*Iner)/Rho_L)^(1/2);
65     omega_n_4 = B4^2*((E*Iner)/Rho_L)^(1/2);
66
67     % Eigenvectors
68     Yn_1 = ((cosh(A1)-cos(A1))-0.7341*(sinh(A1)-sin(A1)))*(Rho_L*L)^(-1/2);
69     Yn_2 = ((cosh(A2)-cos(A2))-0.7341*(sinh(A2)-sin(A2)))*(Rho_L*L)^(-1/2);
70     Yn_3 = ((cosh(A3)-cos(A3))-0.7341*(sinh(A3)-sin(A3)))*(Rho_L*L)^(-1/2);
71     Yn_4 = ((cosh(A4)-cos(A4))-0.7341*(sinh(A4)-sin(A4)))*(Rho_L*L)^(-1/2);
72
73     % Participation factors
74     Tn_1 = 0.783*(Rho_L*L)^(1/2);
75     Tn_2 = 0.4339*(Rho_L*L)^(1/2);
76     Tn_3 = 0.2544*(Rho_L*L)^(1/2);
77     Tn_4 = 0.1818*(Rho_L*L)^(1/2);
78
79     %% Inputs for dynamic response calculation
80     % PSD1 file
81     [filename, pathname] = uigetfile('*.');
82     filename = fullfile(pathname, filename);
83     fid = fopen(filename, 'r');
84     A = fscanf(fid, '%g %g', [2 inf]);
85     A = A';
86
87     ch = input('Do you want to analyze one more acceleration PSD, 1 = Yes and 2 = No: ');
88     ;
89     if ch == 1
90         % PSD2 file
91         [filename, pathname] = uigetfile('*.');
92         filename = fullfile(pathname, filename);
93         fid = fopen(filename, 'r');
94         B = fscanf(fid, '%g %g', [2 inf]);
95         B = B';
96
97         % CSD file
98         [filename, pathname] = uigetfile('*.');
99         filename = fullfile(pathname, filename);
100        fid = fopen(filename, 'r');

```

```

100     C = fscanf(fid, '%g %g', [2 inf]);
101     C = C';
102 end
103
104 %% Calculation of displacement response
105
106 in_freq1 = A(:,1); % Input frequency in rad/sec
107 in_omegal = (2*pi).*in_freq1; % Input frequency in Hz
108 in1 = A(:,2); % Input acceleration PSD in m^2/s^4/Hz
109 Hrd1 = (-(Yn_1*Tn_1) ./ ((omega_n_1^2-in_omegal.^2)+1i*2*Damp*omega_n_1*in_omegal))
        +(-(Yn_2*Tn_2) ./ ((omega_n_2^2-in_omegal.^2)+1i*2*Damp*omega_n_2*in_omegal)) +(-(
        Yn_3*Tn_3) ./ ((omega_n_3^2-in_omegal.^2)+1i*2*Damp*omega_n_3*in_omegal)) +(-(Yn_4*
        Tn_4) ./ ((omega_n_4^2-in_omegal.^2)+1i*2*Damp*omega_n_4*in_omegal)); % Complex
        Transfer function
110 Hrd1 = Hrd1.^2; % square of transfer function
111 out_1 = Hrd1.*in1; % Complex displacement response output at the free end in m^2/Hz
112 out1_abs = abs(out_1); % Absolute displacement response output at the free end in m
        ^2/Hz
113
114 if ch == 1
115     in_freq2 = B(:,1); % Input frequency in rad/sec
116     in_omega2 = (2*pi).*in_freq2; % Input frequency in Hz
117     in2 = B(:,2); % Input acceleration PSD in m^2/s^4/Hz
118     Hrd2 = (-(Yn_1*Tn_1) ./ ((omega_n_1^2-in_omega2.^2)+1i*2*Damp*omega_n_1*in_omega2))
            +(-(Yn_2*Tn_2) ./ ((omega_n_2^2-in_omega2.^2)+1i*2*Damp*omega_n_2*in_omega2))
            +(-(Yn_3*Tn_3) ./ ((omega_n_3^2-in_omega2.^2)+1i*2*Damp*omega_n_3*in_omega2))
            +(-(Yn_4*Tn_4) ./ ((omega_n_4^2-in_omega2.^2)+1i*2*Damp*omega_n_4*in_omega2));
            % Complex Transfer function
119     Hrd2 = Hrd2.^2; % square of transfer function
120     out_2 = Hrd2.*in2; % Complex displacement response output at the free end in m
            ^2/Hz
121     out2_abs = abs(out_2); % Absolute displacement response output at the free end
            in m^2/Hz
122
123     in_freq3 = C(:,1); % Input frequency in rad/sec
124     in_omega3 = (2*pi).*in_freq3; % Input frequency in Hz
125     in3 = C(:,2); % Input acceleration PSD in m^2/s^4/Hz
126     Hrd3 = (-(Yn_1*Tn_1) ./ ((omega_n_1^2-in_omega3.^2)+1i*2*Damp*omega_n_1*in_omega3))
            +(-(Yn_2*Tn_2) ./ ((omega_n_2^2-in_omega3.^2)+1i*2*Damp*omega_n_2*in_omega3))
            +(-(Yn_3*Tn_3) ./ ((omega_n_3^2-in_omega3.^2)+1i*2*Damp*omega_n_3*in_omega3))
            +(-(Yn_4*Tn_4) ./ ((omega_n_4^2-in_omega3.^2)+1i*2*Damp*omega_n_4*in_omega3));
            % Complex Transfer function
127     Hrd3 = Hrd3.^2; % square of transfer function
128     out_3 = Hrd3.*in3; % Complex displacement response output at the free end in m
            ^2/Hz
129     out3_abs = abs(out_3); % Absolute displacement response output at the free end
            in m^2/Hz
130 end
131 %% Different plots
132
133 omega = [omega_n_1;omega_n_2;omega_n_3;omega_n_4];
134 if ch == 1
135     output = out1_abs + out2_abs + 2*out3_abs;
136 else
137     output = out1_abs;
138 end

```

```

139
140 x = 1:4;
141 figure(1)
142 plot(x,omega, 'x')
143 xticks([1 2 3 4])
144 xticklabels({'First mode', 'Second mode', 'Third mode', 'Fourth mode'})
145 title('Modal Analysis');
146 xlabel('Mode number');
147 ylabel('Frequency (Hz)');
148
149 if ch == 1
150     figure(2)
151     plot(in_freq1, in1, 'r')
152     title('Input PSD for analysis');
153     xlabel('Frequency (Hz)');
154     ylabel('Acceleration PSD ((m/s^2)^2/Hz)');
155     hold on
156     plot(in_freq2, in2, 'b')
157     plot(in_freq3, in3, 'k')
158     hold off
159     legend('PSD 1', 'PSD 2', 'CSD')
160 end
161
162 if ch == 2
163     figure(2)
164     plot(in_freq1, in1, 'r')
165     title('Input PSD for analysis');
166     xlabel('Frequency (Hz)');
167     ylabel('Acceleration PSD ((m/s^2)^2/Hz)');
168 end
169
170 figure(3)
171 plot(in_freq1, output)
172 title('Total displacement PSD at the free end');
173 xlabel('Frequency (Hz)');
174 ylabel('Displacement PSD (m^2/Hz)');

```

D.3. TIME DOMAIN TO POWER SPECTRAL DENSITY AND CROSS SPECTRAL DENSITY

Below code is used for converting one or two time series into frequency series. If two time series are used, the code also calculates the cross spectral density between the time series. More information on cross spectral density is given Section C.4.

```

1 clear;
2 clc;
3
4 % This MATLAB code is used to calculate power spectral density of a time
5 % domain periodic signal using Fast Fourier transform.
6 % The input file must be in a external ASCII file having two columns 'Time
7 % (seconds) vs Quantity (Units)'
8 % If two time series are to be converted, ensure that both of them are of
9 % same length. If not, add zeros.
10 %% Reading data
11 [filename, pathname] = uigetfile('*.');

```

```

12 filename = fullfile(pathname, filename);
13 fid = fopen(filename, 'r');
14 THF1 = fscanf(fid, '%g %g', [2 inf]);
15 THF1 = THF1';
16 t1 = THF1(:,1); % Time in seconds
17 x1 = THF1(:,2); % amplitude of quantity (units)
18 Fs = input('Enter the sampling frequency in Hz');
19 ch = input('Additional time series, 1 = Yes and 2 = No');
20 if ch == 1
21     [filename, pathname] = uigetfile('*.');
22     filename = fullfile(pathname, filename);
23     fid = fopen(filename, 'r');
24     THF2 = fscanf(fid, '%g %g', [2 inf]);
25     THF2 = THF2';
26     t2 = THF2(:,1); % Time in seconds
27     x2 = THF2(:,2); % amplitude of quantity (units)
28 end
29 %% Power spectral density calculation
30
31 % PSD1
32 N1 = length(x1);
33 freq1 = 1:Fs/N1:Fs/2; % frequency range
34 freq1 = freq1';
35 x1dft = fft(x1); % FFT of the time signal
36 x1dft = x1dft(1:floor(N1/2)+1);
37 psdx1 = (1/(Fs*N1)) * abs(x1dft).^2; % Converting spectrum into PSD
38 psdx1(2:end-1) = 2*psdx1(2:end-1); % Double side to single side
39 psdx1 = psdx1';
40
41 if ch == 1
42     % PSD2
43     N2 = length(x2);
44     freq2 = 1:Fs/N2:Fs/2; % frequency range
45     freq2 = freq2';
46     x2dft = fft(x2); % FFT of the time signal
47     x2dft = x2dft(1:floor(N2/2)+1);
48     psdx2 = (1/(Fs*N2)) * abs(x2dft).^2; % Converting spectrum into PSD
49     psdx2(2:end-1) = 2*psdx2(2:end-1); % Double side to single side
50     psdx2 = psdx2';
51 end
52
53 %% Cross spectral density calculation
54 if ch == 1
55     window = hanning(length(x1));
56     [csd, f] = cpsd(x1, x2, window, [], [], Fs); % Calculating the complex cross spectral
57         density function between two time signals
58     csd_r = real(csd); % Real part of cross spectral density
59     csd_i = imag(csd); % Imaginary part of cross spectral density
60     csd_abs = abs(csd); % Absolute part of cross spectral density
61 end
62 %% Plotting PSD graphs
63 if ch == 1
64     figure(1)
65     plot(t1, x1)
66     title('Acceleration vs Time')
67     xlabel('Time (seconds)')

```

```

67     ylabel('Acceleration (m/s^2)')
68     hold on
69     plot(t1,x2)
70     legend('Load - PS', 'Load - SB')
71
72     figure(2)
73     title('Acceleration PSD vs Frequency')
74     plot(freq1,psdx1)
75     xlabel('Frequency (Hz)')
76     ylabel('Acceleration PSD (m^2/s^4/Hz)')
77     hold on
78     plot(freq2,psdx2)
79     legend('Load - PS', 'Load - SB')
80
81     figure(3)
82     title('CSD')
83     xlabel('Frequency (Hz)')
84     ylabel('Acceleration PSD (m^2/s^4/Hz)')
85     plot(f,csd_r)
86     hold on
87     yyaxis right
88     plot(f,csd_i)
89     ylabel('Phase difference (radians)')
90     legend('Real', 'Imaginary')
91 end
92
93 if ch == 2
94     figure(1)
95     plot(t1,x1)
96     title('Acceleration vs Time')
97     xlabel('Time (seconds)')
98     ylabel('Acceleration (m/s^2)')
99
100    figure(2)
101    title('Acceleration PSD vs Frequency')
102    plot(freq1,psdx1)
103    xlabel('Frequency (Hz)')
104    ylabel('Acceleration PSD (m^2/s^4/Hz)')
105 end

```

Below code is used for conversion of random time series to frequency series. If two signals are used, the code also calculates the cross spectral density between the two time domain series.

```

1 clear;
2 clc;
3
4 % This MATLAB code is used to calculate power spectral density of a acceleration
   time
5 % domain random signal using Fast Fourier transform and converting to Gaussian white
   noise.
6 % This code can generate random number time series The input file must be in a
   external ASCII file having two columns 'Time
7 % (seconds) vs Amplitude (m/s^2)'
8 % If two time series are to be converted, ensure that both of them are of
9 % same length. If not, add zeros.
10 %% Reading data
11 Fs = input('Enter the sampling frequency in Hz'); % Sampling frequency, should be

```

```

    atleast twice the frequency range considered for analysis
12 choice = input('Would you like to generate time series or upload? 1 = Generate , 2 =
    Upload');
13 ch = input('Additional time series , 1 = Yes and 2 = No');
14 if choice == 1
15     mu1 = input('Enter the mean of the standard signal');
16     sigma1 = input('Enter the standard deviation of the random signal');
17     if ch == 1
18         mu2 = input('Enter the mean of the standard signal');
19         sigma2 = input('Enter the standard deviation of the random signal');
20     end
21 end
22
23 if choice == 2
24     [filename, pathname] = uigetfile('*.');
25     filename = fullfile(pathname, filename);
26     fid = fopen(filename, 'r');
27     THF1 = fscanf(fid, '%g %g', [2 inf]);
28     THF1 = THF1';
29     t1 = THF1(:,1); % Time in seconds
30     x1 = THF1(:,2); % amplitude of quantity (units)
31
32     if ch == 1
33         [filename, pathname] = uigetfile('*.');
34         filename = fullfile(pathname, filename);
35         fid = fopen(filename, 'r');
36         THF2 = fscanf(fid, '%g %g', [2 inf]);
37         THF2 = THF2';
38         t2 = THF2(:,1); % Time in seconds
39         x2 = THF2(:,2); % amplitude of quantity (units)
40     end
41 end
42
43 %% Generate random numbers
44 N = 16384; % Total sampling points for FFT, should be integer power of 2. Higher
    values gives smoother power spectral density of Gaussian white noise.
45 if choice == 1
46     N1 = input('Total time period of the signal');
47     t1 = 0:1/Fs:N1-1/Fs;
48     L = 1000;
49     MU = mu*ones(1,N);
50     C1 = (sigma1^2)*diag(ones(N,1));
51     R1 = chol(C1);
52     x1 = repmat(MU,L,1)+randn(L,N)*R1;
53     if ch == 1
54         N2 = input('Total time period of the signal');
55         t2 = 0:1/Fs:N2-1/Fs;
56         C2 = (sigma2^2)*diag(ones(N,1));
57         R2 = chol(C2);
58         x2 = repmat(MU,L,1)+randn(L,N)*R2;
59     end
60 end
61 %% Power spectral density calculation
62
63 % PSD1
64 Z1 = 1/sqrt(N*fs)*fft(x1,[],2); % Performing FFT

```

```

65 Pxx1 = mean(Z1.*conj(Z1)); % Taking square to calculate Power spectral density
66 Pxx1 = Pxx1(1:floor(length(Z1)/2)+1); % Considering only positive frequencies
67 Pxx1(2:end-1) = 2*Pxx1(2:end-1); % Converting two sided to single sided power
    spectral density
68 Pxx1 = Pxx1';
69 freq1 = 0:fs/length(Z1):fs/2;
70 freq1 = freq1';
71
72 if ch == 1
73     Z2 = 1/sqrt(N*fs)*fft(x2,[],2); % Performing FFT
74     Pxx2 = mean(Z2.*conj(Z2)); % Taking square to calculate Power spectral density
75     Pxx2 = Pxx2(1:floor(length(Z2)/2)+1); % Considering only positive frequencies
76     Pxx2(2:end-1) = 2*Pxx2(2:end-1); % Converting two sided to single sided power
    spectral density
77     Pxx2 = Pxx2';
78     freq2 = 0:fs/length(Z2):fs/2;
79     freq2 = freq2';
80 end
81
82 %% Cross spectral density calculation
83 if ch == 1
84     z3 = x1+x2; % Superpositioning both random signals
85     % Performing FFT as above for the superpositioned signal
86     Pxx3 = mean(Z3.*conj(Z3));
87     Pxx3 = Pxx3(1:floor(length(Z3)/2)+1);
88     Pxx3(2:end-1) = 2*Pxx3(2:end-1);
89     Pxx3 = Pxx3';
90     % Calculating the absolute cross spectral density using
91     % superpositioning rule
92     csd_r = (Pxx3 - Pxx1 - Pxx2)/2;
93     f = freq1;
94     csd_i = zeros(length(f),1);
95 end
96 %% Plotting PSD graphs
97 if ch == 1
98     figure(1)
99     plot(t1,x1)
100    title('Acceleration vs Time')
101    xlabel('Time (seconds)')
102    ylabel('Acceleration (m/s^2)')
103    hold on
104    plot(t1,x2)
105    legend('Load - PS', 'Load - SB')
106
107    figure(2)
108    title('Acceleration PSD vs Frequency')
109    plot(freq1,psdx1)
110    xlabel('Frequency (Hz)')
111    ylabel('Acceleration PSD (m^2/s^4/Hz)')
112    hold on
113    plot(freq2,psdx2)
114    legend('Load - PS', 'Load - SB')
115
116    figure(3)
117    title('CSD')
118    xlabel('Frequency (Hz)')

```

```

119     ylabel('Acceleration PSD (m^2/s^4/Hz)')
120     plot(f,csd_r)
121     hold on
122     yyaxis right
123     plot(f,csd_i)
124     ylabel('Phase difference (radians)')
125     legend('Real','Imaginary')
126 end
127
128 if ch == 2
129     figure(1)
130     plot(t1,x1)
131     title('Acceleration vs Time')
132     xlabel('Time (seconds)')
133     ylabel('Acceleration (m/s^2)')
134
135     figure(2)
136     title('Acceleration PSD vs Frequency')
137     plot(freq1,psdx1)
138     xlabel('Frequency (Hz)')
139     ylabel('Acceleration PSD (m^2/s^4/Hz)')
140 end

```

D.4. CALCULATION OF SCF AND HOT SPOT STRESS PSD FOR SIMPLE TUBULAR JOINT

```

1  clc;
2  clear;
3
4  % This code is used to calculate the stress concentration factor (SCF) and
5  % corresponding 16 hot spot stress PSD for a simple tubular T/Y joint
6  % having values theta (angle between chord and brace) between 20 and 90
7  % degrees.
8  % The formulae used to calculate SCF is according to Table B-1 (Appendix
9  % B) of recommended practice DNV-RP-C203, Oct. 2011 and is applicable for
10 % chords with fixed ends. In addition, the code can only be used in the
11 % validity range given in DNV for all geometrical parameters.
12 % There are two ASCII input files, one containing the output frequency and axial
13 % force PSD and the other containing the in-plane and out of plane bending
14 % moment PSD.
15 %% Inputs
16
17 [filename, pathname] = uigetfile('*.txt');
18 filename = fullfile(pathname, filename);
19 fid = fopen(filename, 'r');
20 THF1 = fscanf(fid, '%g %g', [2 inf]);
21 THF1 = THF1';
22 freq = THF1(:,1); % Frequency in Hz
23 ax_force = THF1(:,2); % Axial force in N^2/Hz
24
25 [filename, pathname] = uigetfile('*.txt');
26 filename = fullfile(pathname, filename);
27 fid = fopen(filename, 'r');
28 THF2 = fscanf(fid, '%g %g', [2 inf]);
29 THF2 = THF2';

```

```

30 ben_mom_ip = THF2(:,1); % In-Plane bending moment (Nm)^2/Hz
31 ben_mom_op = THF2(:,2); % Out of Plane bending moment (Nm)^2/Hz
32
33 d = input('Enter brace diameter in meters: '); % brace diameter in meter
34 t = input('Enter brace thickness in meters: '); % brace thickness in meter
35 D = input('Enter chord diameter in meters: '); % chord diameter in meter
36 T = input('Enter chord thickness in meters: '); % chord thickness in meter
37 theta = input('Enter brace to chord angle in degrees: '); % angle between chord and
    brace
38 L = input('Enter chord length in meters: '); % Length of the chord segment
39
40 %% Joint parameters
41
42 beta = d/D;
43 alpha = (2*L)/D;
44 gamma = D/(2*T);
45 tau = t/T;
46 di = d-2*t;
47 Di = D-2*T;
48 %% SCF calculation for T joint
49
50 % SCF for Axial load on chord
51
52 CS_1 = gamma*tau^(1.1)*(1.11-3*((beta-0.52)^2)*(sin(theta)^1.6));
53 CC_1 = gamma^0.2*tau*(2.65+5*(beta-0.65)^2)+tau*beta*sin(theta)*(0.25*alpha-3);
54
55 % SCF for Axial load on brace
56
57 BS_1 = 1.3+gamma*tau^0.52*alpha^0.1*(0.187-1.25*beta^1.1*(beta-0.96))*(sin(theta)
    ^2.7-0.01*alpha);
58 BC_1 = 3+gamma^1.2*(0.12*exp(-4*beta)+0.011*beta^2-0.045)+beta*tau*(0.1*alpha-1.2);
59
60 % SCF for In-plane bending
61
62 IBMCC_1 = 1.45*beta*tau^0.85*gamma^(1-0.68*beta)*(sin(theta)^0.7);
63 IBMBC_1 = 1+0.65*beta*tau^0.4*gamma^(1.09-0.77*beta)*(sin(theta)^(0.06*gamma-1.16));
64
65 % SCF for Out-plane bending
66
67 OBMCC_1 = beta*tau*gamma*(1.7-1.05*beta^3)*(sin(theta)^1.6);
68 OBMBC_1 = tau^(-0.54)*gamma^(-0.05)*(0.99-0.47*beta+0.08*beta^4)*OBMCC_1;
69
70 % Short cord correction factor
71
72 if alpha < 12
73
74     F1 = 1-(0.83*beta-0.56*beta^2-0.02)*gamma^0.23*exp(-0.21*gamma^1.16*alpha^2.5);
75     F2 = 1-(1.43*beta-0.97*beta^2-0.03)*gamma^0.04*exp(-0.71*gamma^(-1.38)*alpha
        ^2.5);
76     F3 = 1.-0.55*beta^1.8*gamma^0.16*exp(-0.49*gamma^(-0.89)*alpha^1.8);
77
78     CS = CS_1*F1;
79     CC = CC_1;
80     BS = BS_1*F1;
81     BC = BC_1;
82     IBMCC = IBMCC_1;

```

```

83     IBMBC = IBMBC_1;
84     OBMCC = OBMCC_1*F3;
85     OBMBC = OBMBC_1*F3;
86     else
87         CS = CS_1;
88         CC = CC_1;
89         BS = BS_1;
90         BC = BC_1;
91         IBMCC = IBMCC_1;
92         IBMBC = IBMBC_1;
93         OBMCC = OBMCC_1;
94         OBMBC = OBMBC_1;
95     end
96     %% Equivalent stresses
97
98     % At the brace
99     brace_area = pi/4*(d^2-di^2);
100    brace_modulus = (pi/(32*d))*(d^4-di^4);
101    ax_stress_B = ax_force./brace_area^2;
102    ben_stress_B_ip = ben_mom_ip./brace_modulus^2;
103    ben_stress_B_op = ben_mom_op./brace_modulus^2;
104
105    sigma_1_B = ax_stress_B.*BC + ben_stress_B_ip.*IBMBBC;
106    sigma_2_B = ax_stress_B.*(BC+BS)*0.5 + ben_stress_B_ip.*IBMBBC*(sqrt(2)/2) -
        ben_stress_B_op.*OBMBC*(sqrt(2)/2);
107    sigma_3_B = ax_stress_B.*BC - ben_stress_B_op.*OBMBC;
108    sigma_4_B = ax_stress_B.*(BC+BS)*0.5 - ben_stress_B_ip.*IBMBBC*(sqrt(2)/2) -
        ben_stress_B_op.*OBMBC*(sqrt(2)/2);
109    sigma_5_B = ax_stress_B.*BC - ben_stress_B_ip.*IBMBBC;
110    sigma_6_B = ax_stress_B.*(BC+BS)*0.5 - ben_stress_B_ip.*IBMBBC*(sqrt(2)/2) +
        ben_stress_B_op.*OBMBC*(sqrt(2)/2);
111    sigma_7_B = ax_stress_B.*BC + ben_stress_B_op.*OBMBC;
112    sigma_8_B = ax_stress_B.*(BC+BS)*0.5 + ben_stress_B_ip.*IBMBBC*(sqrt(2)/2) +
        ben_stress_B_op.*OBMBC*(sqrt(2)/2);
113
114    % At the chord
115    sigma_1_C = ax_stress_B.*CC + ben_stress_B_ip.*IBMCC;
116    sigma_2_C = ax_stress_B.*(CC+CS)*0.5 + ben_stress_B_ip.*IBMCC*(sqrt(2)/2) -
        ben_stress_B_op.*OBMCC*(sqrt(2)/2);
117    sigma_3_C = ax_stress_B.*CC - ben_stress_B_op.*OBMCC;
118    sigma_4_C = ax_stress_B.*(CC+CS)*0.5 - ben_stress_B_ip.*IBMCC*(sqrt(2)/2) -
        ben_stress_B_op.*OBMCC*(sqrt(2)/2);
119    sigma_5_C = ax_stress_B.*CC - ben_stress_B_ip.*IBMCC;
120    sigma_6_C = ax_stress_B.*(CC+CS)*0.5 - ben_stress_B_ip.*IBMCC*(sqrt(2)/2) +
        ben_stress_B_op.*OBMCC*(sqrt(2)/2);
121    sigma_7_C = ax_stress_B.*CC + ben_stress_B_op.*OBMCC;
122    sigma_8_C = ax_stress_B.*(CC+CS)*0.5 + ben_stress_B_ip.*IBMCC*(sqrt(2)/2) +
        ben_stress_B_op.*OBMCC*(sqrt(2)/2);
123    %% Plots
124
125    figure(1)
126    plot(freq, ax_force)
127    title('Axial Force PSD vs Frequency')
128    xlabel('Frequency (Hz)')
129    ylabel('Axial Force (N^2/Hz)')
130

```

```

131 figure (2)
132 plot(freq, ben_mom_ip)
133 title('Bending Moment PSD vs Frequency')
134 xlabel('Frequency (Hz)')
135 ylabel('Bending moment ((Nm)^2/Hz)')
136 hold on
137 plot(freq, ben_mom_op)
138 hold off
139 legend('In-plane', 'Out of plane')
140
141 figure (3)
142 plot(freq, sigma_1_B)
143 title('Hot spot stress at brace vs Frequency')
144 xlabel('Frequency (Hz)')
145 ylabel('Hot spot stress (Pa^2/Hz)')
146 hold on
147 plot(freq, sigma_2_B)
148 plot(freq, sigma_3_B)
149 plot(freq, sigma_4_B)
150 plot(freq, sigma_5_B)
151 plot(freq, sigma_6_B)
152 plot(freq, sigma_7_B)
153 plot(freq, sigma_8_B)
154 hold off
155 legend('Point-1', 'Point-2', 'Point-3', 'Point-4', 'Point-5', 'Point-6', 'Point-7', 'Point
    -8')
156
157 figure (4)
158 plot(freq, sigma_1_C)
159 title('Hot spot stress at chord vs Frequency')
160 xlabel('Frequency (Hz)')
161 ylabel('Hot spot stress (Pa^2/Hz)')
162 hold on
163 plot(freq, sigma_2_C)
164 plot(freq, sigma_3_C)
165 plot(freq, sigma_4_C)
166 plot(freq, sigma_5_C)
167 plot(freq, sigma_6_C)
168 plot(freq, sigma_7_C)
169 plot(freq, sigma_8_C)
170 hold off
171 legend('Point-1', 'Point-2', 'Point-3', 'Point-4', 'Point-5', 'Point-6', 'Point-7', 'Point
    -8')

```

D.5. DIRLIK'S APPROACH TO CALCULATE STRESS RANGE

```

1 clear;
2 clc;
3 % This MATLAB code is used to calculate probability density function of a
4 % stress range from stress range PSD using Dirlik's method.
5 % The input file should be an external ASCII file with two columns
6 % 'frequency(Hz) & psd(units^2/Hz)'
7
8 %% Reading stress PSD data
9 [filename, pathname] = uigetfile('*.');
10 filename = fullfile(pathname, filename);

```

```

11 fid = fopen(filename, 'r');
12 THF = fscanf(fid, '%g %g', [2 inf]);
13 THF = THF';
14 f = THF(:,1); % Frequency in Hz
15 a = THF(:,2); % amplitude of stress PSD in units^2/Hz
16 n = length(f); % Length of the signal
17 T = input('Enter total time in seconds = '); % Total time in second
18
19 %% Calculating spectral moments and constants according to Dirlik's method
20 df = zeros(n-1,1);
21 for i = 1:n-1
22     df(i) = f(i+1)-f(i); % Frequency increment step
23 end
24 m0=0;
25 m1=0;
26 m2=0;
27 m4=0;
28 for i = 1:n-1
29     m0=m0+s(i)*df(i); % Zeroth moment
30     m1=m1+s(i)*f(i)*df(i); % First moment
31     m2=m2+s(i)*f(i)^2*df(i); % Second moment
32     m4=m4+s(i)*f(i)^4*df(i); % Fourth moment
33 end
34 m0 = abs(m0);
35 m1 = abs(m1);
36 m2 = abs(m2);
37 m4 = abs(m4);
38 grms = sqrt(m0); % RMS value of the signal
39 EP = sqrt(m4/m2); % Expected number of positive peaks
40 x = (m1/m0)*sqrt(m2/m4);
41 ga = m2/(sqrt(m0*m4)); % Irregularity factor
42 D1 = 2*(x-ga^2)/(1+ga^2);
43 R = (ga-x-D1^2)/(1-ga-D1+D1^2);
44 D2 = (1-ga-D1+D1^2)/(1-R);
45 D3 = 1-D1-D2;
46 Q = 1.25*(ga-D3-D2*R)/D1;
47 srange_max = 10*grms; % Maximum stress range in Pa
48 b = 400; % Division of the stress range PDF curve
49 srange_step = srange_max/b;
50 s1 = zeros(b,1);
51 Z = zeros(b,1);
52 p = zeros(b,1);
53 for i = 1:b
54     s1(i) = i*srange_step; % Calculating stress ranges in MPa
55     Z(i) = s1(i)/(2*grms); % Normalized stress amplitude
56     p1 = (D1/Q)*exp(-Z(i)/Q);
57     p2 = ((Z(i)*D2)/(R^2))*exp(-Z(i)^2/(2*R^2));
58     p3 = (Z(i)*D3)*exp(-Z(i)^2/2);
59     t1 = 2*sqrt(m0);
60     p(i) = (p1+p2+p3)/t1; % Total PDF of stress range
61 end
62 N = T*EP; % Expected number of cycles corresponding to stress range
63 prompt('Calculating fatigue damage fraction')
64 m = input('Enter the Basquin exponent of the material');
65 dam_1 = p.*s1.^(m);
66 damage_frac = N*sum(dam_1.*srange_step); % Total damage fraction using Miner's rule

```

```
67
68 %% Plot stress range PDF as per Dirlik 's method
69
70 ch = input('Units of stress PSD is, 1 = Pa^2/Hz or 2 = MPa^2/Hz');
71 if ch == 1
72     s1 = s1.*10^(-6);
73 end
74
75 figure(1)
76 plot(s1,p)
77 title('PDF of stress range using Dirliks method')
78 xlabel('Stress range (MPa)')
79 ylabel('Probability density function')
80
81 printf('Damage fraction (D*C) = %0.2f\n', damage_frac);
```


E

ADDITIONAL RESULTS

E.1. EXAMPLE TO CALCULATE STRESS RANGES USING DIRLIK'S METHOD

This section we will calculate stress range and damage fraction of a assumed stress response PSD. Each parameter is calculated according to the formulae given in Section 3.3. Figure E.1 shows the assumed stress PSD. From Figure E.1, we can clearly see a peak around 10Hz, which is the first natural frequency of the structure, there is also a small peak around 65Hz. Having two distinct peaks means that the input load is a broad banded process and the value of irregularity factor Γ will be close to zero.

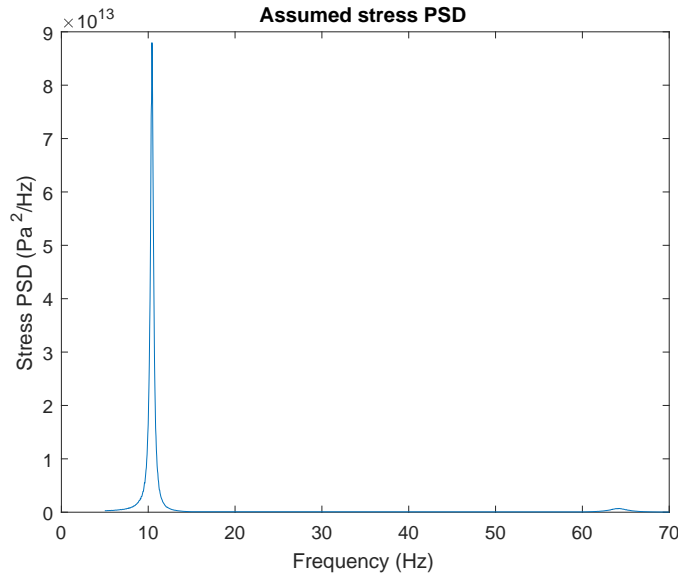


Figure E.1: Assumed hot spot stress PSD

The total time of the input signal is assumed to be 60 seconds, so $T = 60 s$. Using the MATLAB code given in Appendix D.5 the zeroth, first, second and fourth ($n = 0,1,2,4$) are calculated along the total length of PSD. $G(f)$ is the value of hot spot stress PSD (Y-axis of the above graph) and f is the frequency (X-axis of the above graph). The value of moments are given below.

$$m_0 = \int_1^p f^0 G(f) df = 6.17 * 10^{13} \quad (E.1)$$

$$m_1 = \int_1^p f^1 G(f) df = 7.80 * 10^{14} \quad (\text{E.2})$$

$$m_2 = \int_1^p f^2 G(f) df = 1.63 * 10^{16} \quad (\text{E.3})$$

$$m_4 = \int_1^p f^4 G(f) df = 4.00 * 10^{19} \quad (\text{E.4})$$

Using the values of all the moments, all the parameter of $p(S)$ except Z are calculated using Equations 3.17 to 3.23. The values are listed in Table E.1

Table E.1: Dirlik's parameters

Parameter	Value
x_m	0.255
γ	0.328
D_1	0.266
R	0.0048
D_2	0.478
D_3	0.255
Q	0.332
$E[P]$	49.54

In addition to the values calculated in Table E.1, the RMS (Root Mean Square) value of the PSD is also calculated. The RMS value is equal to the square root of zeroth moment m_0 and which is $7.85 * 10^{06}$. The RMS value is used to calculate the maximum stress range as discussed in Subsection 3.2.3 is never more than 8-10 times the RMS value. Assuming 10 times the RMS value, the maximum stress range is equal to $7.85 * 10^{07}$. The maximum stress range is then divided into small segments (S) and each of the segments is used to calculate normalized stress range Z using Equation 3.24. All parameters are now calculated and next we calculate value of $p(S)$ corresponding to each S and Z using Equation 3.16.

Damage fraction is calculated using Equation 5.2 for $m = 3$ (for steel). It should be noted that the stress used has units of Pa , but S-N curves are usually plotted in terms of MPa . Hence to calculate damage corresponding to Basquin constant ' C ', damage fraction ($D * C$) has to be converted in units of MPa . This is done dividing the damage fraction value by 10^{18} corresponding to S^m in Equation 5.2, where S is stress range. Table E.2 shows the damage fraction values in both the units and corresponding damage for $C = 10^{12.48}$, selected for tubular joints in air according to DNVGL [1], T-curve.

Table E.2: Damage fraction calculation

Damage fraction (Pa)	Damage fraction (terms of MPa)	Damage
$1.17 * 10^{25}$	$1.17 * 10^{07}$	$3.87 * 10^{-06}$

Also the probability density function versus stress range graph is also shown in Figure E.2 below.

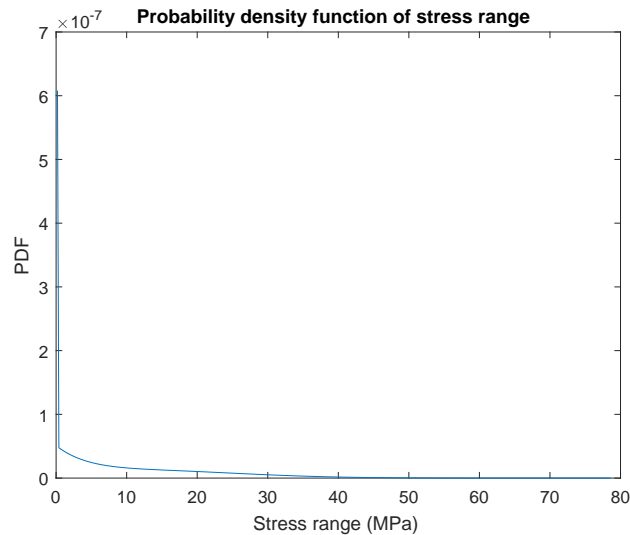


Figure E.2: Probability density function versus Stress range

This are the steps involved in calculating the damage fraction and eventually damage using Dirlik’s method.

E.2. J-RAIN VERIFICATION

J-Rain is an open source software which is used to count stress cycles and corresponding number of cycles using four point counting method [49]. The stress history is provided to the software in the form of a external ASCII file and its provides an output file containing rainflow stress ranges according to the algorithm. The number of cycles for each stress range is considered to be one. This assumption on number of cycles leads to conservative results, but since the software is essentially developed for industrial application, conservative results are accepted. The user interface of the software is shown in Figure E.3, the input file is uploaded using "Set input" tab and the output directory is set using "Set Output" tab. Any amount of input files can be uploaded and solved individually for calculating rainflow stress ranges.

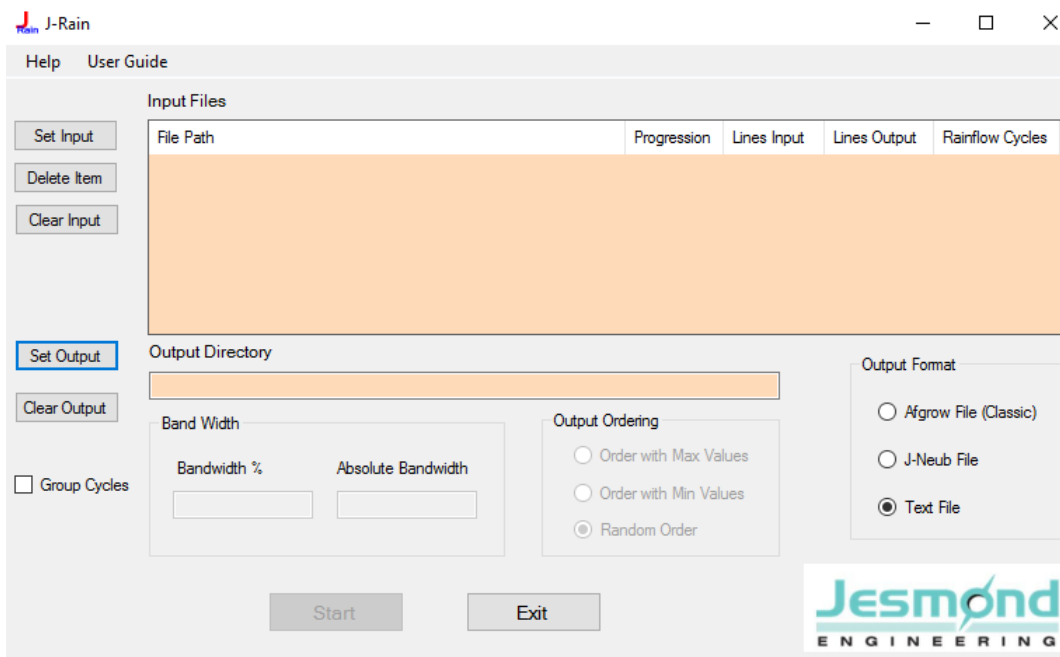


Figure E.3: Graphical User interface of J-Rain [50]

Additional option given by the software is to group the stress range using the "Group cycles" tab. In order to check whether J-Rain is providing correct results, a small stress history is assumed and the damage fraction results calculated using simple hand calculation is compared with the results from J-Rain. Figure E.4 shows the assumed stress cycle, a small time is considered so that it is quite easy to estimate damage fraction using hand calculation.

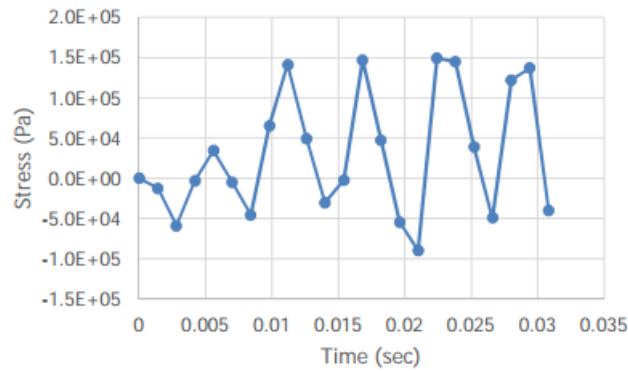


Figure E.4: Assumed stress cycle for J-Rain verification

First it is important to filter out the stress reversal amplitudes which are important in order to calculate stress ranges. Figure E.5 shows the filtered stress history of the stress cycle shown in Figure E.4

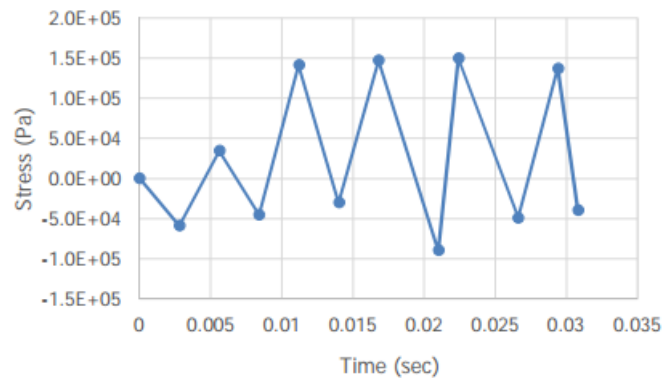


Figure E.5: Filtered stress cycle for J-Rain verification

From Figure E.5 it is now easy to find out the maximum and minimum stress. Figures E.6 and E.7 shows the stress range calculation done using hand calculations.

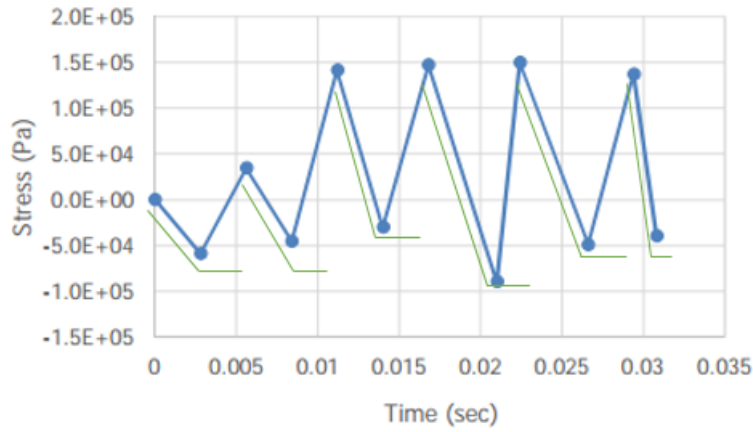


Figure E.6: Stress range calculation starting from peak

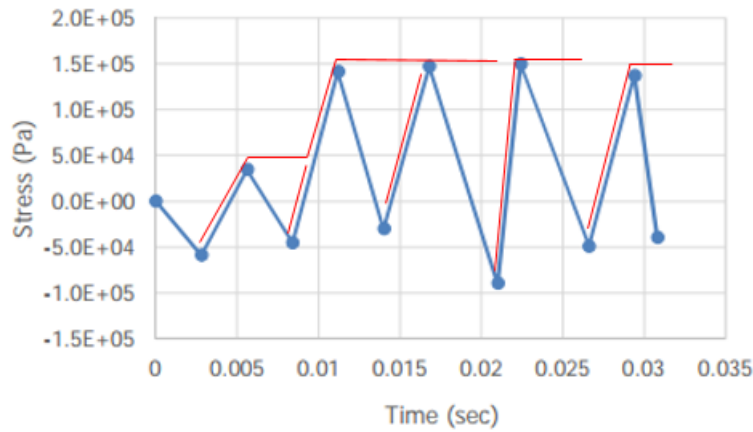


Figure E.7: Stress range calculation starting from valley

The stress ranges calculated are listed in Table E.3 below.

Table E.3: Stress range using hand calculations

Maximum	Minimum	Stress range	Number of cycle
0	-5.90×10^4	5.90×10^4	0.5
3.45×10^4	-4.55×10^4	8.00×10^4	0.5
1.41×10^5	-3.03×10^4	1.71×10^5	0.5
1.47×10^5	-8.97×10^4	2.37×10^5	0.5
1.50×10^5	-4.89×10^4	1.99×10^5	0.5
1.37×10^5	-3.98×10^4	1.77×10^5	0.5
1.47×10^5	-5.90×10^4	2.06×10^5	0.5
1.41×10^5	-4.55×10^4	1.87×10^5	0.5
1.47×10^5	-3.03×10^4	1.77×10^5	0.5
1.50×10^5	-8.97×10^4	2.40×10^5	0.5
1.37×10^5	-4.89×10^4	1.86×10^5	0.5

The filtered stress cycle shown in Figure E.5 is given as an input to the J-Rain software and Table E.4 shows

the output.

Table E.4: Stress range using J-Rain

Maximum	Minimum	Stress range	Number of cycle
$3.45 * 10^{04}$	$-4.55 * 10^{04}$	$8.00 * 10^{04}$	1
$1.41 * 10^{05}$	$-3.03 * 10^{04}$	$1.71 * 10^{05}$	1
0	$-3.98 * 10^{04}$	$3.98 * 10^{04}$	1
$1.37 * 10^{05}$	$-4.89 * 10^{04}$	$1.86 * 10^{05}$	1
$1.47 * 10^{05}$	$-5.90 * 10^{04}$	$2.06 * 10^{05}$	1
$1.50 * 10^{05}$	$-8.97 * 10^{04}$	$2.39 * 10^{05}$	1

Damage fraction for both the outputs shown in Tables E.3 and E.4 is calculated according to formula given in Equation 5.1. The relative error in damage fraction and number of cycles with hand calculation as the reference is shown in Table E.5.

Table E.5: Results of verification of J-Rain

Method	Damage fraction	Number of cycles	% error (damage fraction)	% error (Number of cycles)
Hand calculation	$3.45 * 10^{16}$	5.5	-	-
J-Rain	$3.67 * 10^{16}$	6	6.05	9.09

The percentage error for damage fraction is quite low but, for number of cycles the percentage error is a little higher. This is explained before, the software converts all half cycles to full cycles to provide conservative results hence we get higher number of cycles and because of that a slightly higher damage fraction result. The values are still within acceptable limits hence it can be concluded that the J-Rain is suitable for damage fraction calculation for time domain analysis.

E.3. ADDITIONAL RESULTS FOR VERIFICATION MODELS

CANTILEVER MODEL WITH SINGLE PSD

INPUT LOADS

Table E.6: Details of square cross-section cantilever beam model

Property	Value	Units
Length	$5 * 10^{-2}$	<i>m</i>
Thickness	$8 * 10^{-3}$	<i>m</i>
Cross-sectional Area	$1.3 * 10^{-3}$	<i>m</i> ²
Moment of inertia	$4.07 * 10^{-7}$	<i>m</i> ⁴
Length of beam	3	<i>m</i>
Mass of the beam	31.65	<i>kg</i>
Gravity	9.81	<i>m/s</i> ²
Mass per length	10.55	<i>kg/m</i>

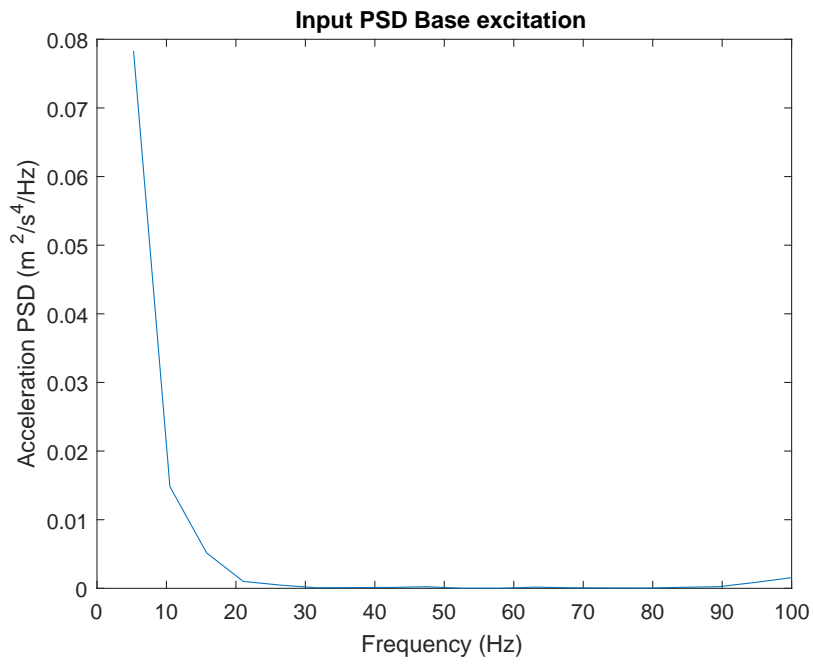


Figure E.8: Input load for Sub-case 2-Single PSD

RESULTS

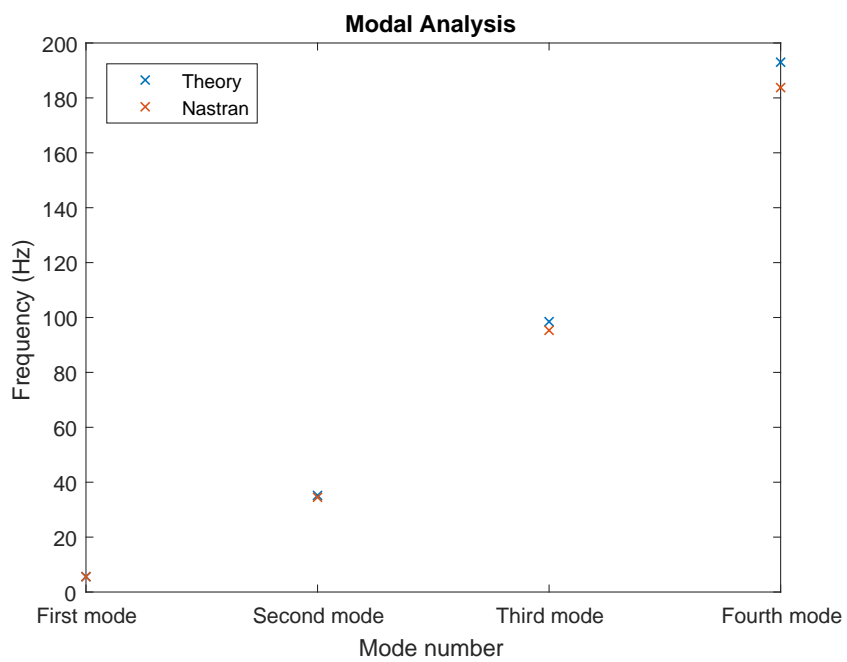


Figure E.9: Modal analysis - Sub case 3

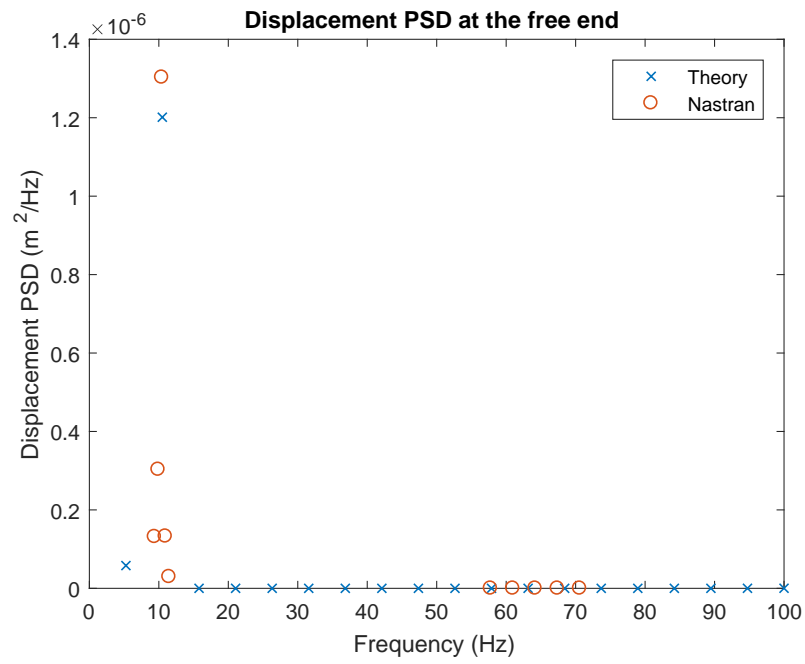


Figure E.10: Displacement response PSD for sub-case 2 - Single PSD

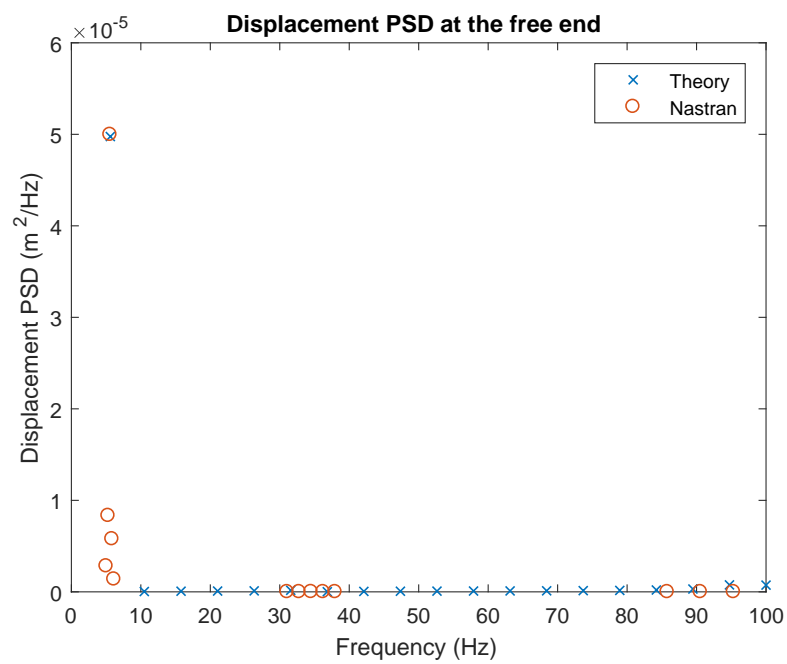


Figure E.11: Displacement response PSD for sub-case 3 - Single PSD

CANTILEVER MODEL WITH TWO PSD

INPUT LOADS

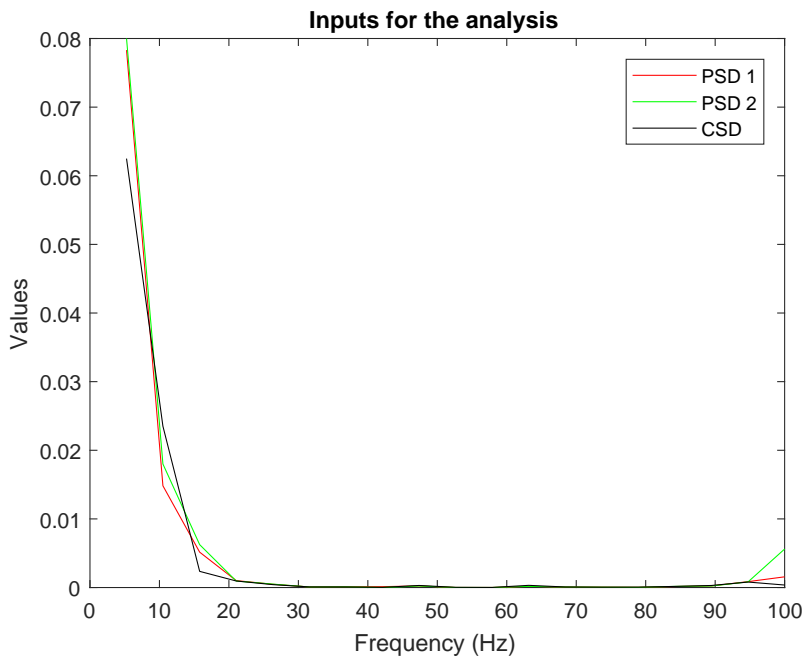


Figure E.12: Input load for Sub-case 2-Two PSD

DISPLACEMENT RESPONSE

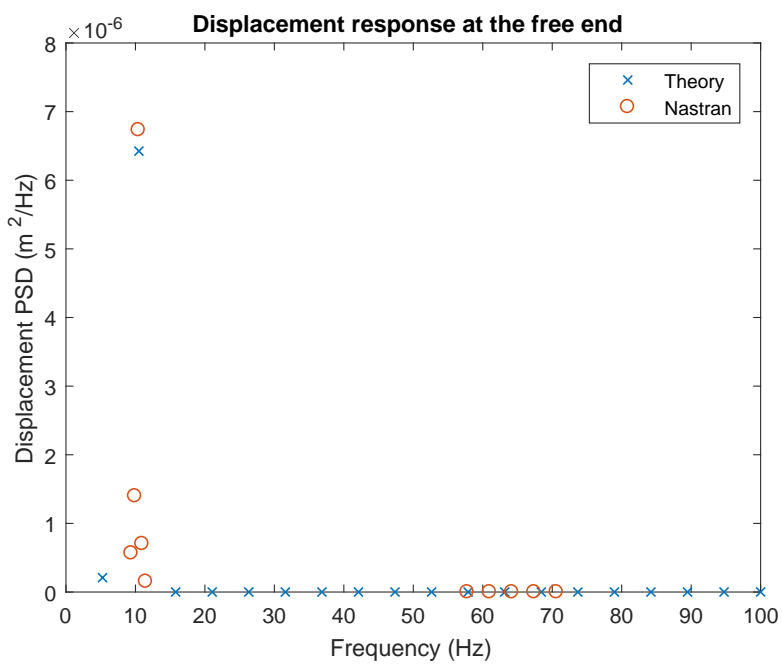


Figure E.13: Displacement response PSD for sub-case 2 - Two PSD

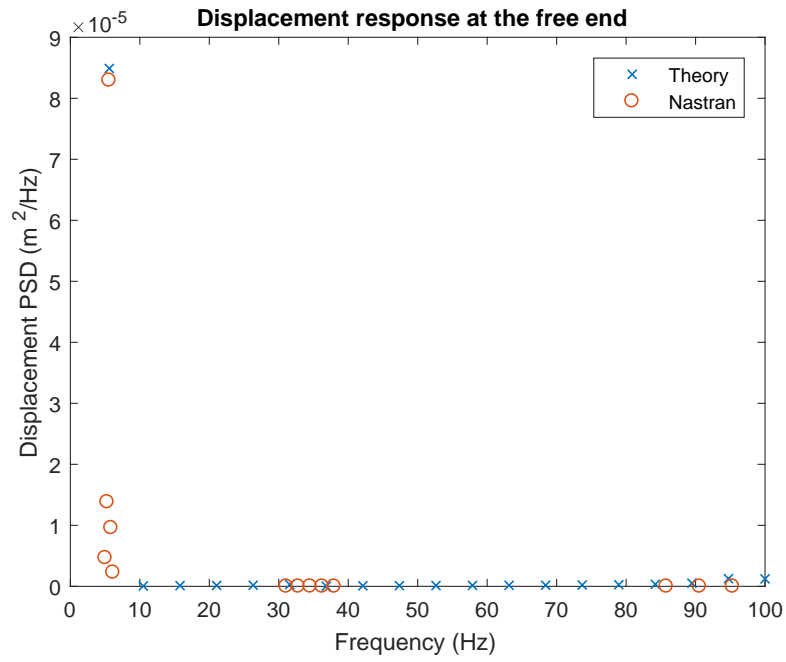
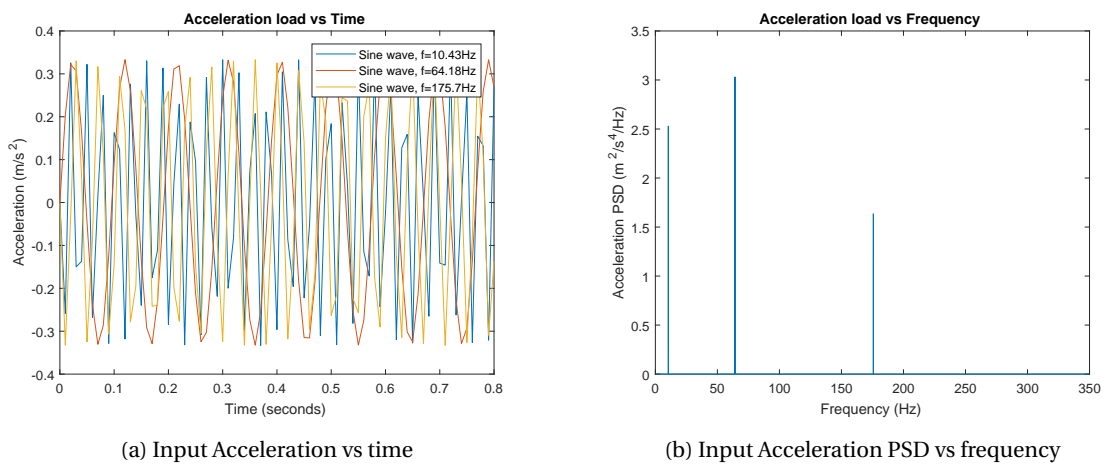


Figure E.14: Displacement response PSD for sub-case 3 - Two PSD

E.4. ADDITIONAL RESULTS OF COMPLETE ANALYSIS

CANTILEVER BEAM MODEL WITH SINGLE PSD

INPUT LOADS



(a) Input Acceleration vs time

(b) Input Acceleration PSD vs frequency

Figure E.15: Input acceleration load – Three frequency periodic load

RESULT

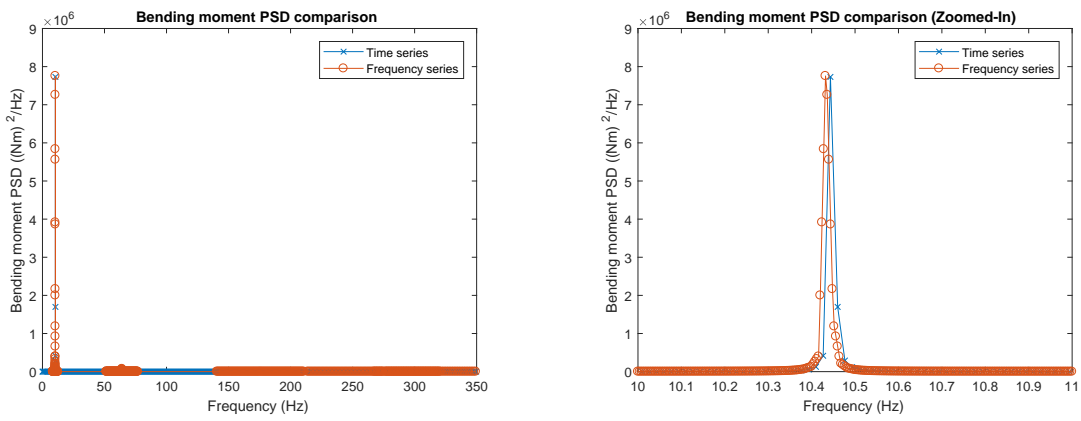


Figure E.16: Bending moment PSD – Three frequency periodic load

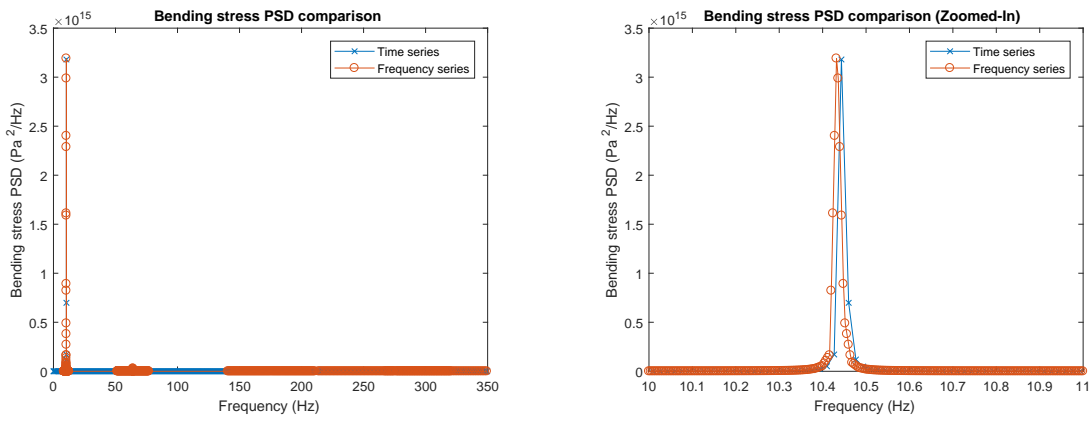
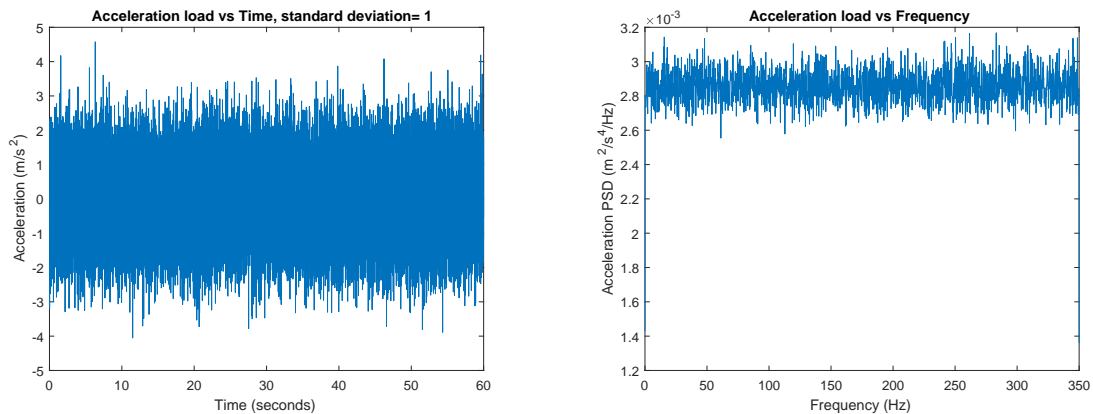


Figure E.17: Bending stress PSD – Three frequency periodic load

INPUT LOADS



(a) Input Acceleration vs time

(b) Input Acceleration vs frequency

Figure E.18: Input acceleration load – Standard Deviation = 1

RESULT

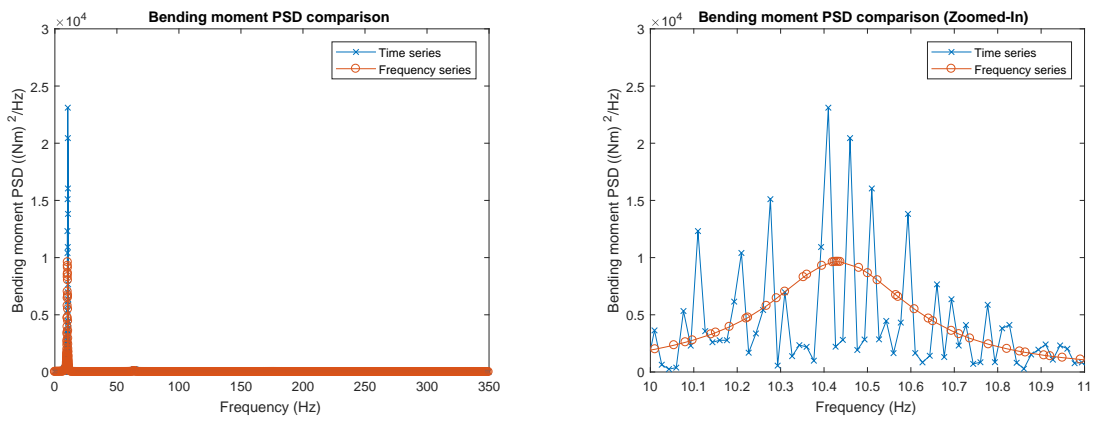


Figure E.19: Bending moment PSD – Standard Deviation = 1

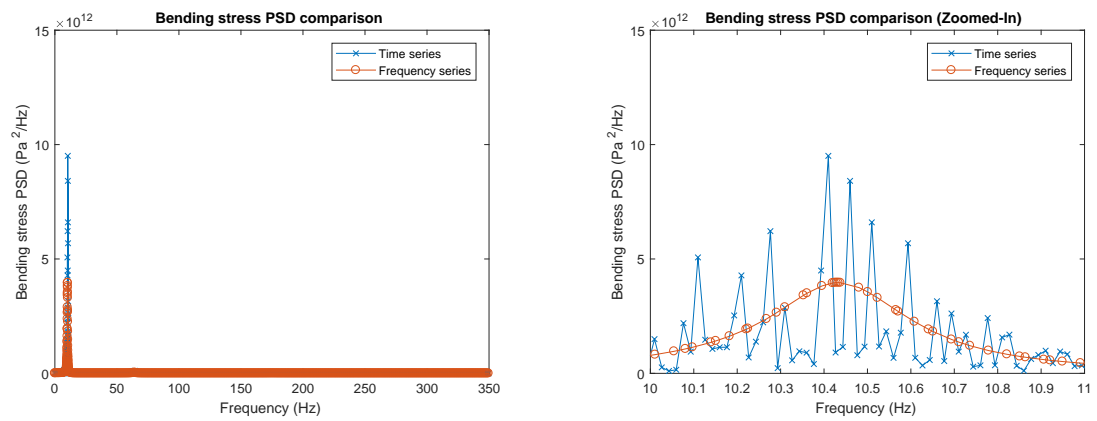


Figure E.20: Bending stress PSD – Standard Deviation = 1

CANTILEVER MODEL WITH TWO PSD

INPUT LOADS

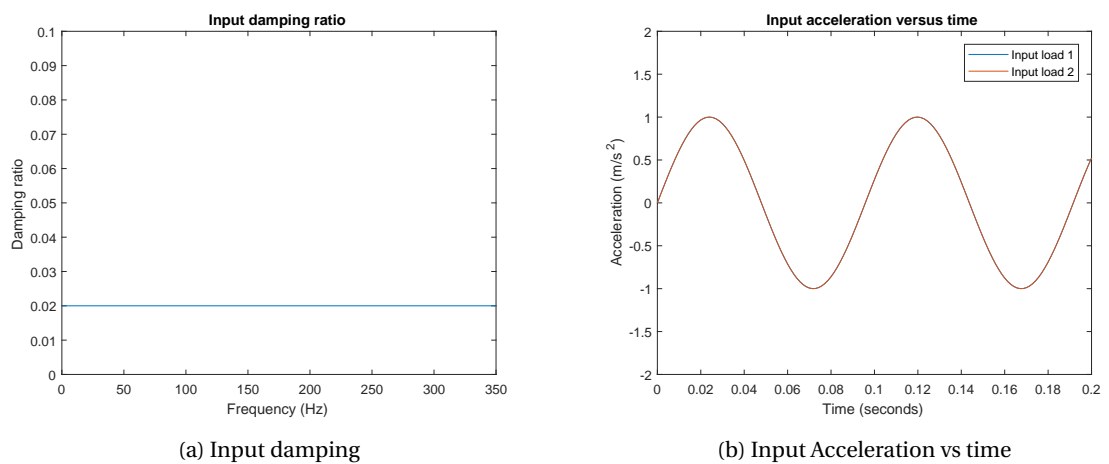
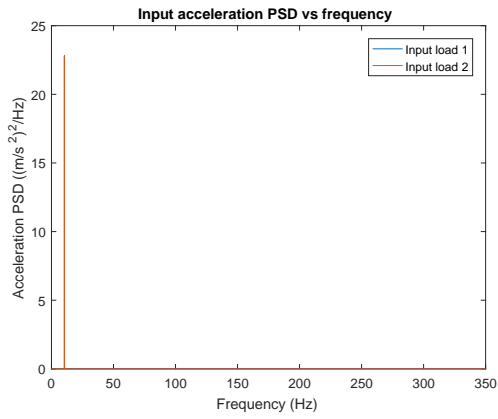
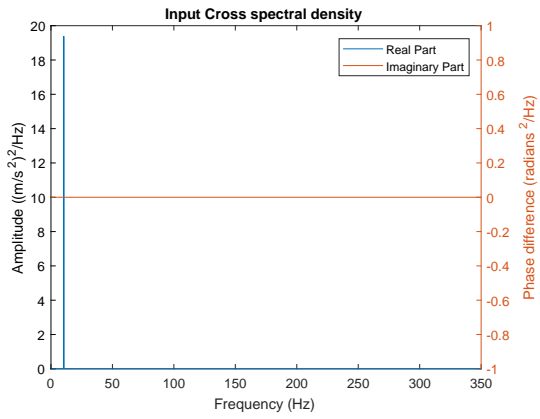


Figure E.21: Input loads for analysis - PSD (Periodic) - 1

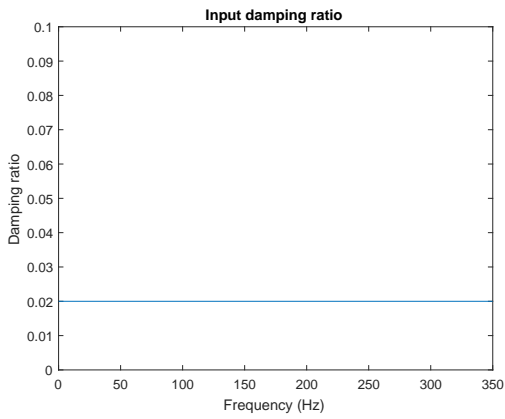


(a) Input acceleration PSD vs frequency

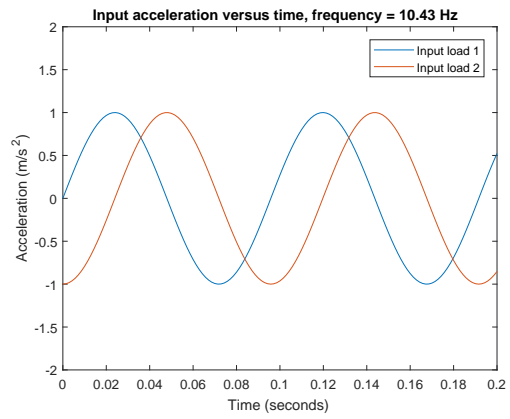


(b) Input cross spectral density

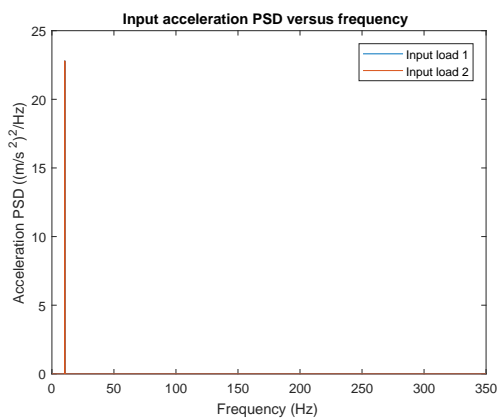
Figure E.22: Input loads for analysis - PSD (Periodic) - 2



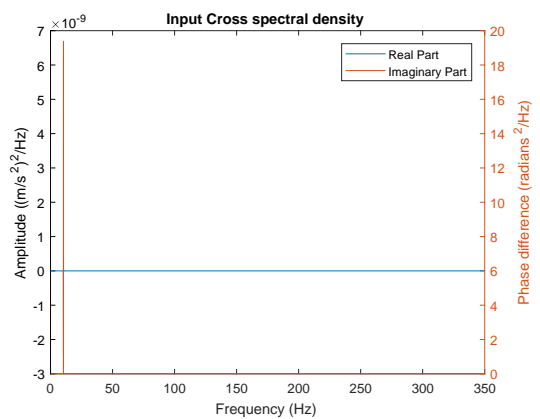
(a) Input damping



(b) Input Acceleration vs time



(c) Input acceleration PSD vs frequency



(d) Input cross spectral density

Figure E.23: Input loads for analysis - PSD (Periodic) with phase difference

RESULT

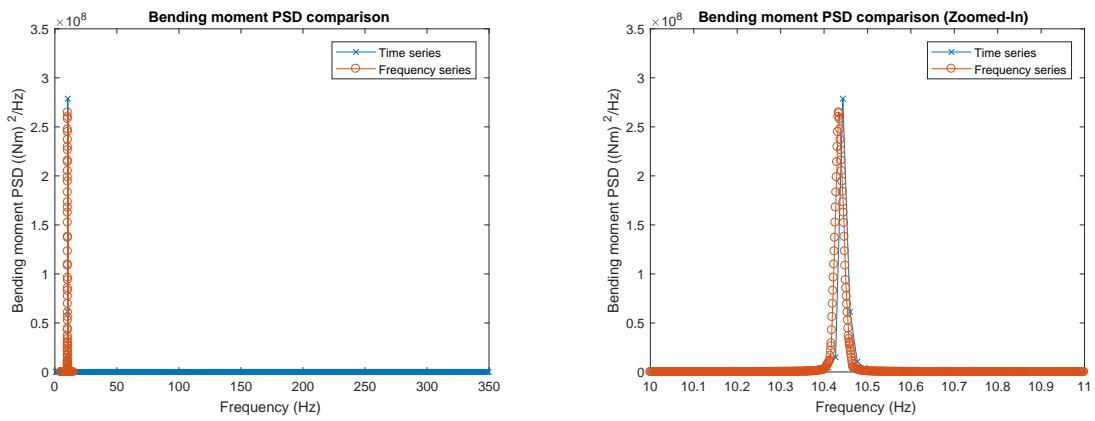


Figure E.24: Bending moment PSD comparison - 2 PSD (Periodic)

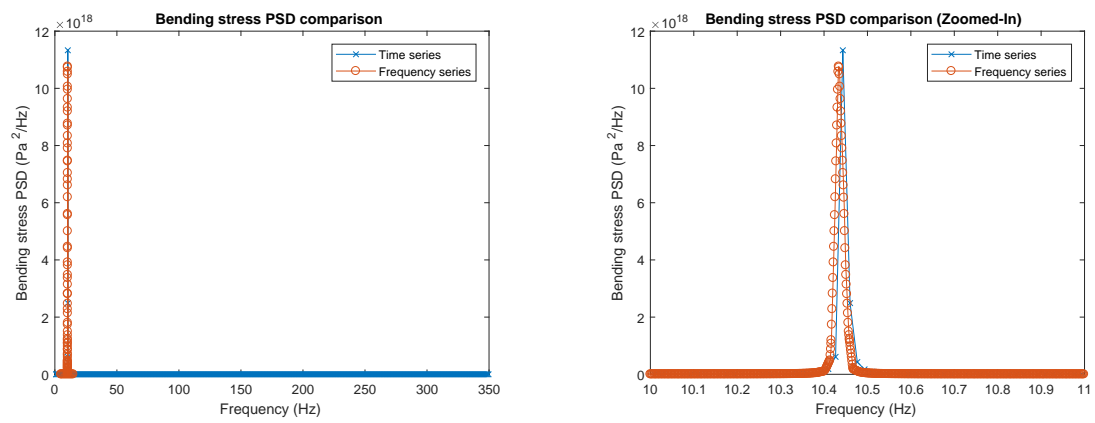


Figure E.25: Bending stress PSD comparison - 2 PSD (Periodic)

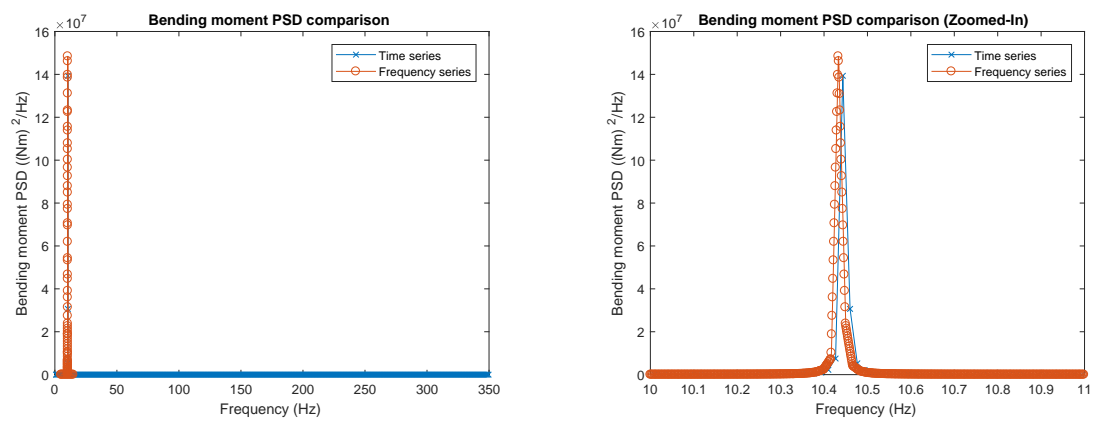


Figure E.26: Bending moment PSD comparison - 2 PSD (Periodic) with phase difference

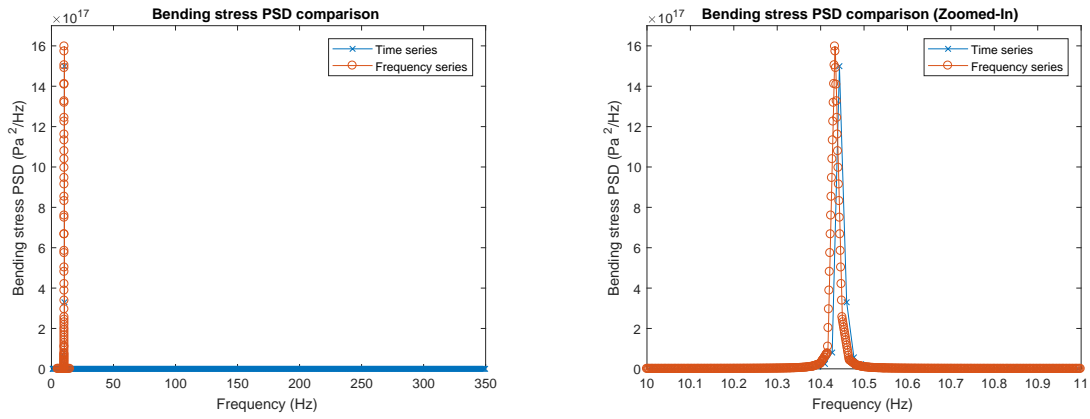
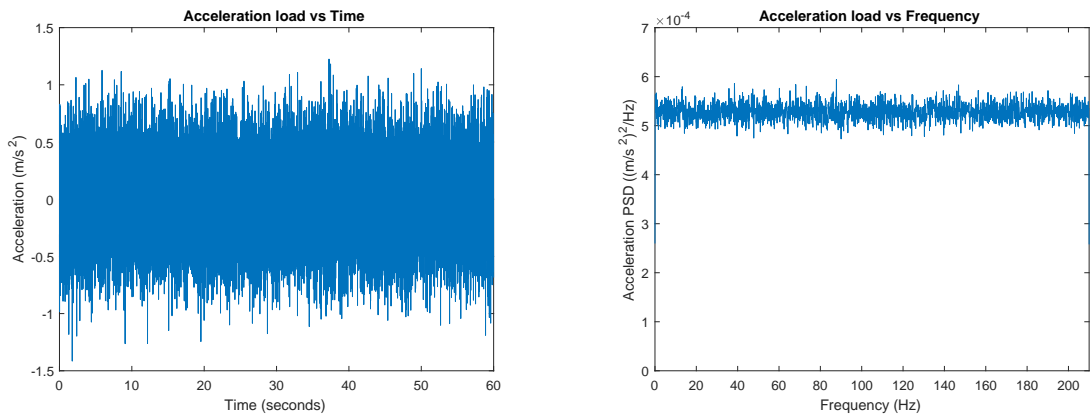


Figure E.27: Bending stress PSD comparison - 2 PSD (Periodic) with phase difference

FRAME MODEL WITH SINGLE PSD

INPUT LOAD AND RESULT FOR SINGLE RANDOM LOAD - FRAME MODEL



(a) Input acceleration versus time load

(b) Input acceleration PSD versus frequency load

Figure E.28: Input random load - Frame model

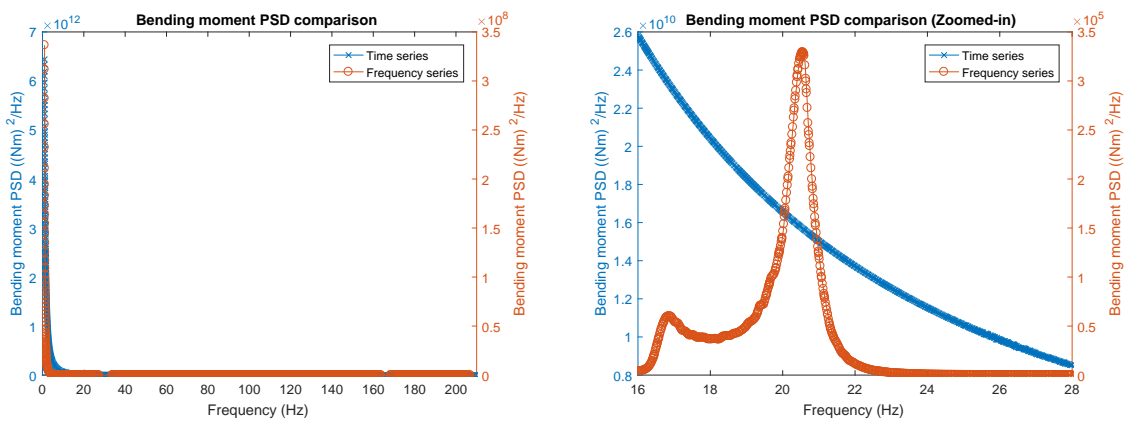
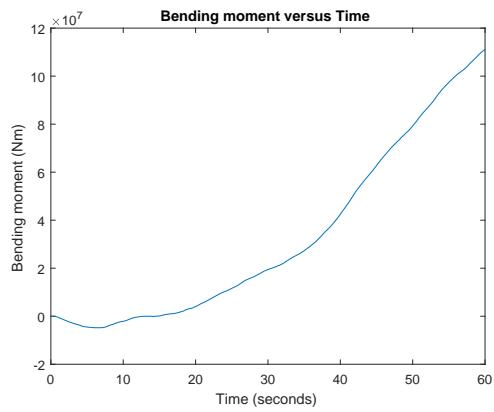


Figure E.29: Bending moment PSD comparison - Single random load - Frame model

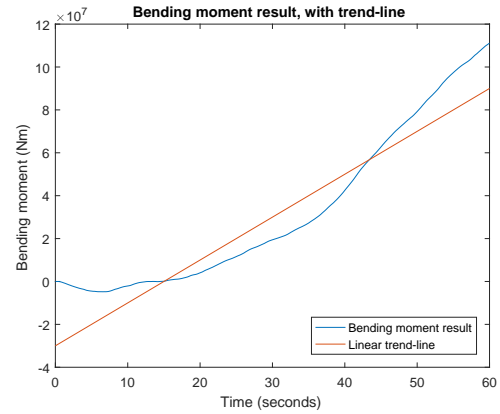
SINGLE RANDOM LOAD USING 'TREND-LINE'

INPUT LOAD AND RESULT - FRAME MODEL

Inputs are the same as shown in Figure E.28.



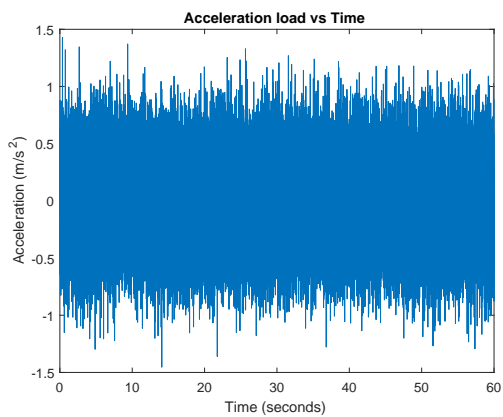
(a) Bending moment versus time - without trend-line



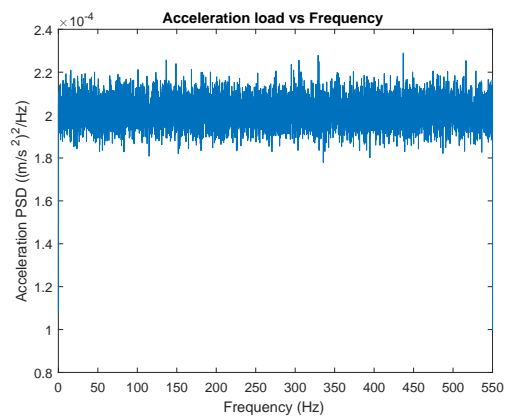
(b) Bending moment versus time - with trend-line

Figure E.30: Bending moment results - Frame model

INPUT LOAD AND RESULT - FIXED BEAM

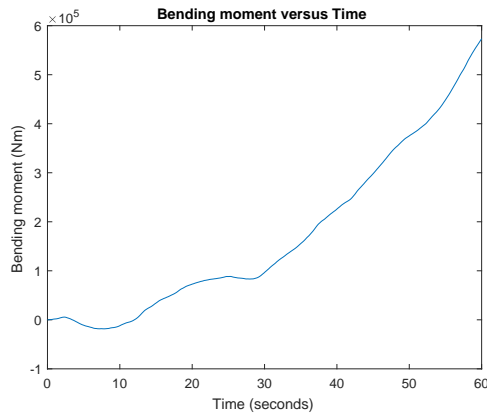


(a) Input acceleration time load

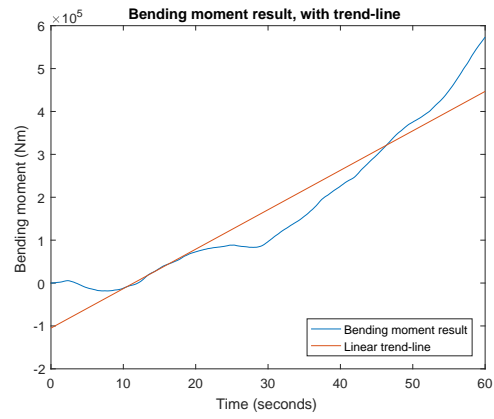


(b) Input acceleration PSD load

Figure E.31: Input loads - Fixed beam



(a) Bending moment versus time - without trend-line

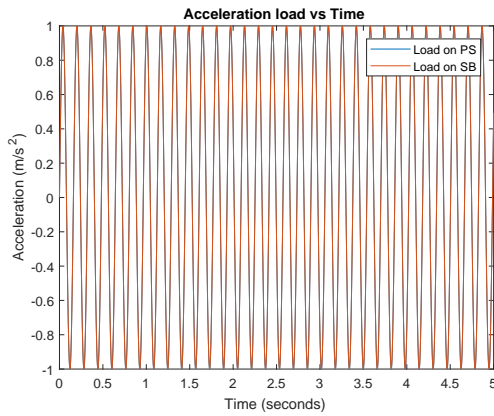


(b) Bending moment versus time - with trend-line

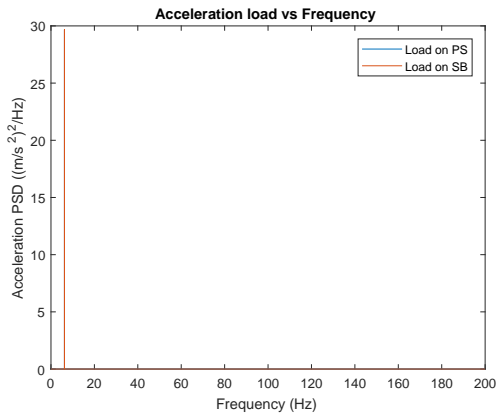
Figure E.32: Bending moment results - Fixed beam

ADDITIONAL ANALYSIS ON CANTILEVER FRAME MODEL

INPUT LOADS

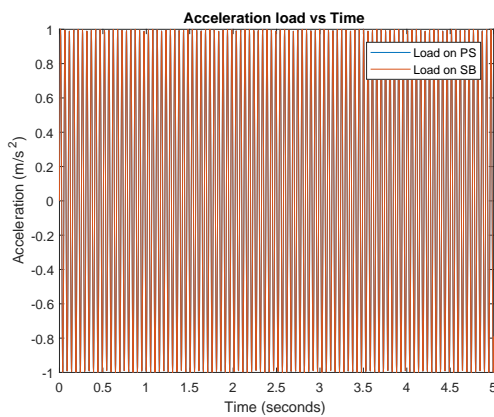


(a) Input acceleration time load

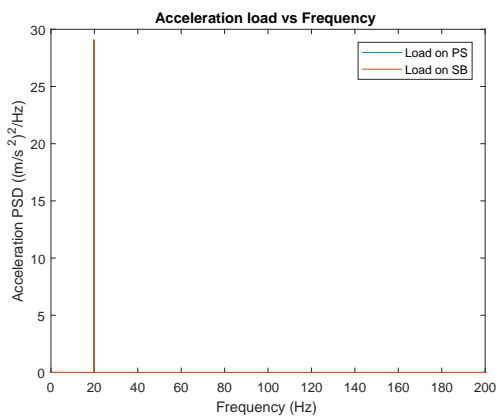


(b) Input acceleration PSD load

Figure E.33: Input loads (3rd mode) - Cantilever frame model

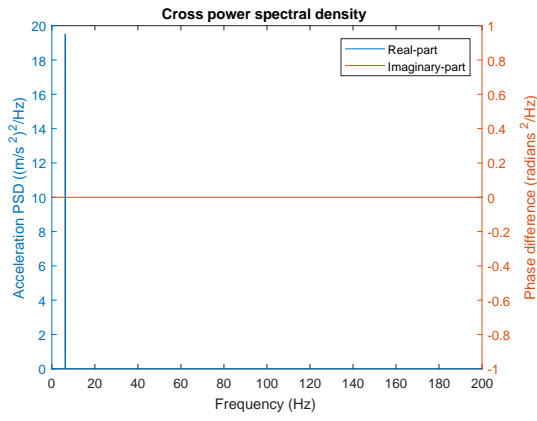


(a) Input acceleration time load

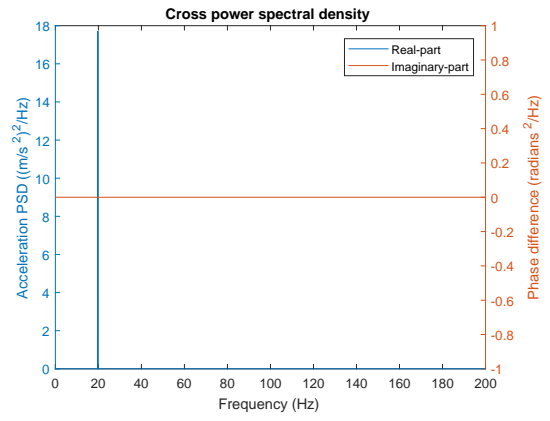


(b) Input acceleration PSD load

Figure E.34: Input loads (7th mode) - Cantilever frame model



(a) Input Cross power spectral density (3rd mode)



(b) Input Cross power spectral density (7th mode)

Figure E.35: Input Cross power spectral density - Cantilever frame model

OUTPUT BENDING MOMENT COMPARISON RESULTS

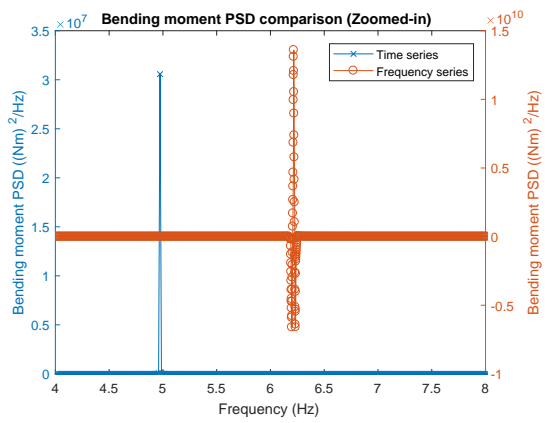
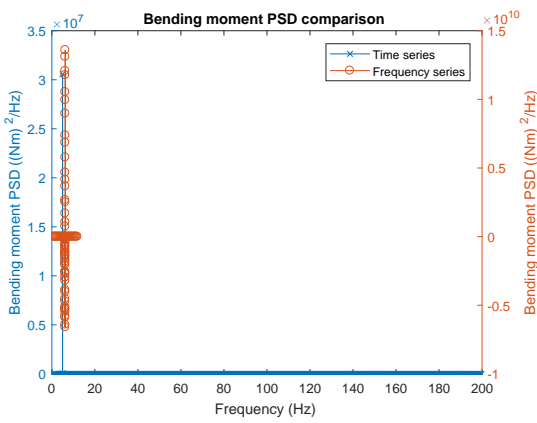


Figure E.36: Output bending moment PSD comparison (3rd mode) - Cantilever frame model

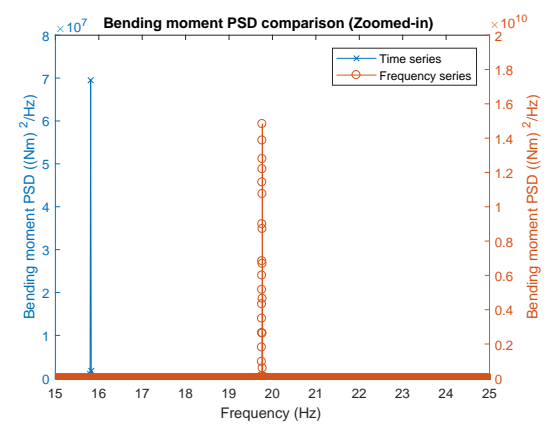
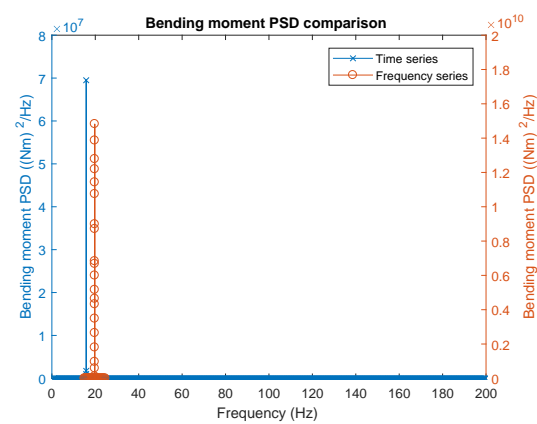


Figure E.37: Output bending moment PSD comparison (7th mode) - Cantilever frame model